The Ultra-filtration of Macromolecules with Different Conformations and Configurations through Nanopores

GE, Hui

A Thesis Submitted in Partial Fulfilment

of the Requirements for the Degree of

Doctor of Philosophy

in

Chemistry

The Chinese University of Hong Kong
August 2010

UMI Number: 3483834

UMI®

Dissertation Publishing

ProQuest®

Thesis / Assessment Committee

Professor LIU, Zhifeng (Chair)

Professor WU, Chi (Thesis Supervisor)

Professor CHAN, Man Chor (Committee Member)

Professor LIANG, Haojun (External Examiner)

摘　要

此篇博士論文闡述了用超微濾的方法研究不同質性和構象的高分子。儘管對於高分子鏈在拉伸流場的作用下穿過小孔的理論已經研究了很多年，但是實驗上的資料證明很少，這是因為對於此類的實驗研究有如下兩個難點：1）缺少能夠精確研究單分子鏈穿越單孔的方法；2）儘管很容易得到符合要求的高分子鏈，但是很難得到其他結構的具有單分散且規整結構的高分子。本文研究的中心是找出使不同種高分子鏈穿孔的臨界流速閾值（也是所需最小流速）。我們提出了一種新的測量方法，用靜態光散射與動態光散射來準確檢測高分子溶液在過膜前後的濃度改變$((C_0-C)/C_0)$，從而達到知道該高分子的閾值。通過對比理論臨界流速閾值與實驗測出的臨界流速閾值進行比較，可以更進一步準確理解不同形狀的高分子鏈是如何被拉伸變形穿越納米小孔。

第一章簡要的介紹了高分子過孔的一些理論背景研究及相關應用，同時列出了近期在此方面的研究進程。本章還介紹了不同構象和構造的高分子穿孔情況，例如高分子線性鏈，星狀高分子，枝化高分子以及高分子膠束。其中重點強調 de Gennes 和 Brochard-Wyart 提出的線性及星狀高分子過孔的理論。根據前人的理論，線性高分子的臨界閾值不隨穿越小孔的孔徑和高分子鏈長的改變而變化 $q_c \simeq k_BT/(3\pi\eta)$，其中 k_B 是玻爾茲曼常數，T 是絕對溫度，η 是溶劑的年度；而對於星狀高分子過孔，存在入孔最優模式，即以幾個臂進孔最佳。

第二章闡述了靜態光散射和動態光散射的基本原理及儀器裝置。本章還介紹了超微濾實驗的步驟及實驗裝置。

第三章介紹了超微濾實驗中所用樣品的陰離子製備方法。本章先簡單介紹了陰離子活性聚合方法的歷史及機理，接著運用自製的高真空系統合成了一系列不同長度的聚苯乙烯高分子鏈和不同臂長及臂數的星狀高分子。

第四章精確測量了不同長度的高分子線性鏈在不同孔徑的納米小孔中的臨界閾值，因為高分子的臨界閾值是與把高分子鏈拉過孔所需的水動力大小相關，通過測量相應的臨界閾值，可以得到克服高分子彈性熵從而把高分子蜷曲鏈拉直所需要的水動力大小，該方法非常靈敏（可以低到幾十飛牛）。這種超微濾

的方法與以往的光鑷以及原子力顯微鏡的方法完全不同，因爲以往的測量方法得出的是克服高分子線性鏈彈性焓所需的力，這種力要比克服彈性熵所需的力大的多。我們的實驗結果發現臨界閾值確實和高分子鏈長無關，但是隨著納米小孔的直徑減小而增加。且我們實驗測得的臨界閾值比理論臨界閾值 $k_B T/(3\pi\eta)$ 小～10 到 200 倍。這是由於 de Gennes 和他的同事錯誤的把高分子鏈滴近似爲實心球，而實際上受限於納米孔內的高分子鏈滴在流場方向上的投影長度要遠遠大於實心球直徑，也就是納米孔徑。最後，通過改變溶液溫度的方法來改變高分子鏈的構象以及測量相應構象下的的臨界閾值。結果顯示最小的臨界閾值位置點非常接近聚苯乙烯鏈的理論 Θ 溫度，這種用超微濾測量高分子鏈在不同構象下的臨界閾值的方法可以用來更好的測量高分子溶液的真實理想狀態，在此狀態不僅第二維裏係數爲零，所有的維裏係數都變爲零。

第五章配置了一系列不同組分的高分子星形及線形鏈的混合溶液，我們證明了在特定的流速下將這些高分子混合物通過納米小孔可以有效的分離星形同線形高分子鏈，這種分離方法与星形高分子和線形高分子的相對大小無關而只與各自的形狀相關。

第六章研究了星形聚苯乙烯高分子是如何在流場的作用下穿越給定納米小孔。我們通過測量了不同臂長，臂數的星形高分子在流場的作用下穿越納米小孔時的保留濃度$((C_0 - C)/C_0)$來研究其過孔的情況，其中 C_0 和 C 是高分子溶液在超微濾之前和之後的濃度。結果顯示對於給定臂長(L_A)的星形高分子，臨界閾值隨著高分子臂數(f)的增加而增大；但是對於給定臂數的星形高分子，閾值幾乎與臂長無關，這和之前 de Gennes 與 Brochard-Wyart 的預測不同。我們修正了前人在 $f_{in} < f_{out}$ (高分子進孔時，進孔臂數小於孔外臂數)這段區間內的理論以及考慮了每個鏈滴的實際有效長度。修正結果表明，星形高分子的臨界閾值與臂長無關但是與高分子總臂數及過孔時的進孔臂數有關，具體取決於進孔臂數是否大於總臂數的一半。通過比較星形高分子臨界閾值的實驗資料和理論計算資料，我們發現星形高分子趨向于以進孔臂數爲總臂數的一半的方式進孔。進一步研究聚苯乙烯星形高分子在環己烷中不同溫度下的保留濃度隨流速的變化表明，臨界閾值在～38 °C 有最小值，這與聚苯乙烯的Θ溫度非常接近(～ 34.5 °C)。

Abstract

This Ph. D. thesis presents our study on the ultrafiltration of polymers with different configurations and conformations; namly, theoretically, the passing of polymer chains through a nanopore under an elongational flow filed has been studied for years, but experimental studies are rare because of two following reasons: 1) lacks a precise method to investigate how individual single polymer chain pass through a nanopore; 2) it is difficult, if not impossible, to obtain a set of polymer samples with a narrow molar mass distribution and a uniform structures; except for linear chains. The central question in this study is to find the critical (minimum) flow rate (q_c) for each kind of chains, at which the chains can pass through a given nanopore. A comparison of the measured and calculated q_c leads to a better understanding how different chains are deformed, stretched and pulled through a nanopore. We have developed a novel method of combining static and dynamic laser light scattering (LLS) to precisely measure the relative retention concentration ((C_0-C)/C_0).

Chapter 1 briefly introduces the theoretical background of how applications and lists some of resent research progresses in this area. Polymer with various configurations and conformations pass through nanopores; including polymer linear chains, stars polymer, branched polymers, polymer micelles are introduced. Among them, the de Gennes and Brochard-Wyart's predictions of polymer linear and star chains passing through nanopores are emphasized, in which they predicted that q_c of linear chain is $q_c \simeq k_B T/(3\pi\eta)$, where k_B, T and η are the Boltzmann constant, the absolutely temperature, and the viscosity of solvent, respectively, independent of both the chain length and the pore size; and for star chains passing through nanopores, there exist a optimal entering arm numbers, namely, the star chains passing through nanopores.

Chapter 2 details basic theory of static and dynamic laser light scattering (LLS), including its instrumentation and our ultrafiltration setup.

Chapter 3 briefly introduces the sample preparation, including the history and mechanism of anionic living polymerization, as well as how we used a novel home-made set-up to prepare linear polystyrene with different chain lengths and star polystyrene with various arm numbers and lengths.

Chapter 4 Summarizes our measured critical flow rates (q_c) of linear polymer

chains with different lengths for nanopores with different sizes, since the flow rate is directly related to the hydrodynamic force, we have developed a sensitive method (down to tens fN) to directly assess how much the hydrodynamic force (F_h) is required to overcome the weak *entropy* elasticity and stretch individual coiled chains in solution. Our method is completely different from the using existing optical tweezers or AFM, because they measure the relatively stronger *enthalpy* elasticity. Our results confirm that q_c is indeed independent of the chain length, but decreases as the pore size increases. The value of q_c is ~10-200 times smaller than $k_B T/(3\pi\eta)$. Such a discrepancy has been attributed to the rough assumption made by de Gennes and his coworkers; namely, each chain segment "blob" confined inside the pore is not a hard sphere so that the effective length along the flow direction is much longer than the pore diameter. Finally, using the solution temperature, we varied the chain conformation, our result shows that q_c has a minimum which is near, but not exactly located at the theta temperature, might leading to a better way to determine the true ideal state of a polymer solution, at which all viral coefficients, not only the second vanish.

Chapter 5 uses polymer solutions made of different mixtures of linear and star chains, we have demonstrated that flushing these solution mixtures through a nanopore with a properly chosen flow rate can effectively and cleanly separate linear and star chains no matter whether linear chains are larger or smaller than star chains.

Chapter 6 further investigates how star-like polystyrene pass through a given nanopore under the flow field. Star polystyrene chains with different arm lengths (L_A) and numbers (f) passing through a nanopore (20 nm) under an elongational flow field was investigated in terms of the flow-rate dependent relative retention (($C_0 - C)/C_0$), where C_0 and C are the polymer concentrations before and after the ultrafiltration. Our results reveal that for a given arm length (L_A), the critical flow rate ($q_{c,star}$), below which star chains are blocked, dramatically increases with the total arm numbers (f); but for a given f, is nearly independent on L_A, contradictory to the previous prediction made by de Gennes and Brochard-Wyart. We have revised their theory in the region $f_{in} < f_{out}$ and also accounted for the effective length of each blob, where f_{in} and f_{out} are the numbers of arms inside and outside the pore, respectively. In the revision, we show that $q_{c,star}$ is indeed independent of L_A but related to f and f_{in} in two different ways, depending on whether $f_{in} \leq f/2$ or $\geq f/2$. A comparison of our experimental and calculated results reveals that most of star chains pass through the

nanopores with $f_{in} \sim f/2$. Further study of the temperature dependent $(C_0 - C)/C_0$ of polystyrene in cyclohexane reveals that there exists a minimum of $q_{c,star}$ at $\sim 38\ °C$, close to its theta temperature ($\sim 34.5\ °C$).

Table of Contents

List of Symbols and Abbreviations

a:	Monomer size
A:	Helmholtz free energy
A_2:	Second viral coefficient
b:	Monomer number between successive branch point
C:	Concentration after aultrafiltration
C_0:	Concentration before ultrafiltration
CONTIN:	A regularization program from Provencher
CMC:	Critical micelle concentration
CGC:	Critical gel concentration
D:	Diameter of nanopore
D_0:	Mutual translational diffusion coefficient
D_{min}:	The minimum diameter of branched polymer can be squeezed
D*:	A certain nanopores diameter at which the correlation length of one blob is equal to the length between two branched points.
DVB:	Divinylbenzene
dn/dC:	Refractive-index increment
E_s:	Scattered electric field
E_{conf}:	Confined energy
E_h:	Hydrodynamic energy
f:	Arm numbers of star polymer
f_{in}:	Forward arm numbers when star chains entering nanopores.
$f(\tau)$:	Characteristic decay time distribution
$f(R_h)$:	Hydrodynamic radius distribution
$f(q)$	Critical flow rate distribution of star chains pass through nanopores
F:	Restoring force of polymer chain
F_c:	Confined force
F_h:	Hydrodynamic force
$G^{(1)}(\tau)$:	Correlation function of electric field
g_ξ:	Monomer number in one correlation length
$g^{(1)}(\tau)$:	Normalized first-order electric field time correlation function

$g^{(2)}(\tau)$:	Base-line normalized intensity time correlation function
h:	Scattering vector
$G(\Gamma)$:	Normalized characteristic line-width distribution function of Γ
$G^{(2)}(\tau)$:	Correlation function of intensity
I:	Scattered intensity
$<I>_E$:	Ensemble-averaged scattered light intensity
I(h):	Averaged scattered light intensity at a finite scattering angle
I_0:	Intensity of the incident radiation
k:	Constant for a certain polymer solution in Flory scaling law.
k_{sp}:	Force constant
k_B:	Boltzmann constant
l:	The length of polymer squeezed into a nanopore
l_b:	Contour length for one blob
l_e:	Effective length of one blob along the flow field
$l*$:	The corresponding length of polymers squeezed into nanopores with the maximum energy barrier.
l_p:	Persistence length
l_s:	Average projection of each segment
L_e:	Effective length along flow rate
L_{max}:	Maximum squeezing length
$L^{-1}(t)$:	Inverse Langevin function
LLS:	Laser light scattering
M_0:	Molecular weight of one monomer
M_w:	Apparent weight average molar weight at a finite concentration
M_b:	Molecular weight of one blob
n:	Solvent refractive index
N:	Polymerization degree
N_A:	Avogadro's number
N_{arm}:	Polymerization degree of one arm
PS:	Polystyrene
$P(\theta)$:	Particle scattering factor
q:	Microscopic flow rate
q_c:	Critical microscopic flow rate

$q_{c,1}$:	Critical microscopic flow rate of linear chain
$q_{c,star}$:	Critical microscopic flow rate of star chain
$q_{c,star,s}$	Critical microscopic flow rate of star chain marked at start position
$q_{c,star,p}$	Critical microscopic flow rate of star chain marked at peak position
Q:	Macroscopic flow rate
Q_c:	Critical macroscopic flow rate
$Q_{c,1}$:	Critical macroscopic flow rate of linear chain
r:	Distance between the scatter and the observation point
R_0:	Unperturbed coil radius
R_F:	End-to-End distance
$\langle R_g \rangle$:	z-average radius of gyration
$\langle R_h \rangle$:	Average hydrodynamic radius
$R_{vv}(\theta)$:	Rayleigh ratio with vertically polarized incident and scattered light at scattering angle θ
S:	Entropy elasticity
S_r:	Shear rate
St:	Styrene
t:	Extension ratio of polymers
T:	Absolute temperature
U:	Potential energy
v:	Flow velocity
v_x:	Flow velocity along x-axis
v_y:	Flow velocity along y-axis
v_z:	Flow velocity along z-axis
W:	Weighting contribution
α:	polarizability; expansion factor; depth parameter of square well
β:	Coherence factor
ε:	dielectric constant
ϕ:	The optimal arm numbers enter into the nanopore
Φ:	Distribution function of end-to-end distance

η:	Viscosity of the solvent
λ_0:	Wavelength of light in vacuum
$\mu_2/<\Gamma>^2$:	Variance
υ:	Flory exponent
Π:	Osmotic pressure
θ:	Scattering angle
Θ:	Theta temperature
ρ:	Density
σ:	The internal concentration
τ:	Reduced temperature $= (T - \Theta)/\Theta$
Γ:	Characteristic linewidth
ξ:	correlation length of one blob

Acknowledgement

First of all, I would like to express my sincere gratitude to my supervisor, Prof. Wu Chi, for his insightful guidance and encouragement during the entire period of my study. I entered the *Polymer & Colloid Laboratory* in 2006 and during the last four years in the *Polymer & Colloid Laboratory*, I always feel warm and gratefulness since he has spent much time to give me his excellent guidance and considerations. I have not only learned a lot from him but also always been inspired by his dedicatory attitude to the scientific research. I believe the trainings and experiences I gained from him should be great helpful in my future.

I am also very grateful to Prof. Ngai To, Prof. Lu Zaijun, Prof. Zhang Mei, Prof. Zheng Bo, Prof. Xia Jiang, Prof. Chen Gaojian, Dr. So Ying H. for the springing up many illuminating discussions.

My sincere thanks are also given to my dear group members in *Polymer & Colloid Laboratory*, their friendship and assistance during the last four years left me many happy and unforgettable memories. They are Dr. Jin Fan, Dr. Hong Liangzhi, Dr. Ye Jing, Dr. Deng Rui, Dr. He Ning, Dr. Ye Xiaodong, Dr. Huo Hong, Dr. Li Junfang, Dr. Luo shizhong, Mr.Chen Qianjin, Mr. Zhao Hong, Mr. Ma Yongzheng, Mr. Wang Weimao, Mr. Li Zifu, Mr. Wei Xiaolin, Mr. Zhou XueChang, Ms. Diao Shu, Ms. Yue Yanan, Ms. Gong XiangJun, Ms Dai Zhuojun, Ms Cai Jinge, Ms. Xing Xiaocheng,

My sincerely thanks are also extended to all the staff members in the Department of Chemistry, the Chinese University of Hong Kong for the active academic atmosphere and the service they offered. The financial support of the Hong Kong Special Administration Region Earmarked Grants and the Special Funds for Major State Basic Research Projects are also gratefully acknowledged.

Finally, I am also indebted to my family and my husband Dr. Jiang Hai for their endless love and strong moral support during my pursuit of a higher degree.

Ge Hui

Hong Kong, June, 2010

Chapter 1

Introduction and background

1.1 Brief overview of polymer pass through nanopores under flow field.

The expansion of polymers with various conformations and configurations passing through nanopores under shear flow play an important role in studies of polymer physics and make a bettering understanding in transporting in cell membrane in vivo.[1,2] For dilute polymer solution under shear, Peterlin[3,4] brought forward a critical strain-rate should exist for polymer chain expansion under elongational flow in 1966. Later de Gennes[5,6] refined it as a so called "coil-stretching" transition and claimed such transition was a first-order transition. Then Pincus[7] described the transition was a process of stretching polymer chains into strings of blobs. Following these, various simulation studies on stretching of polymer chains under flow filed have been reported based on the development of computer technique and theoretical improvement.[1,8-25] Lots of experiments have been carried out to test and verify the former theories.[26-41] However, the "first order transition" of polymer chain under flow field only have been experimentally proved by our lab until recently.[38] Further more, based on the hydrodynamic models, semi-dilute solution with various of monomer concentration, velocity, and stress under elongational flows have also been studied.[42,43]

Compared with coil-stretching transition of polymer chains, the expansion of polymers with more complicated architectures are more intricate, only some of regular polymers have been studied theoretically, like stars,[1,44-47] comb-like polymers,[48] branch polymers, [1,49-53] micelles,[54] and microgels.[55] Most theories of these shaped monomers have no experimental data to support.

1.2 Polymer Chains pass through nanopores under flow field

1.2.1 Free energy of Polymer chains in solution

A linear Gaussian polymer chain can be seen as N beads connected by N-1 springs with a force constant k_{sp} as shown in figure 1.1.[56]
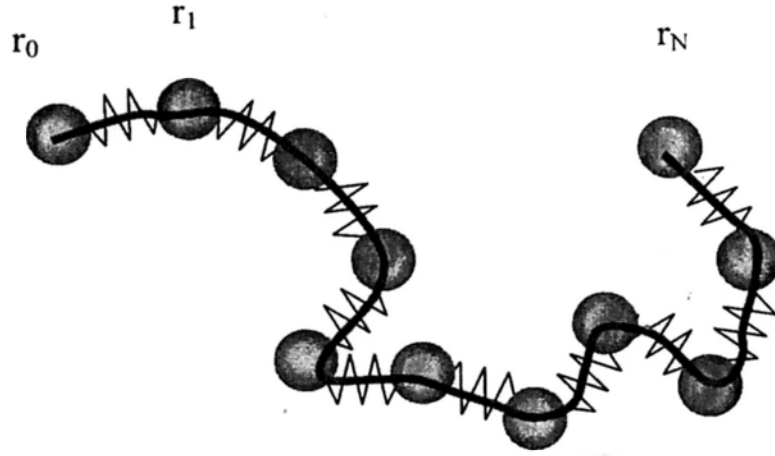
Figure 1.1 Gaussian chain of N segments is realized by a bead-spring model in which N springs are connected in series.[56]

The potential energy U of the chain is related to the elastic energy of the springs:

$$U(r_0,...r_N) = \frac{1}{2}k_{sp}\sum_{n=1}^{N}(r_n - r_{n-1})^2 \tag{1.1}$$

For a Gaussian distributed polymer chain, we have

$$a^2 = 3k_BT/k_{sp} \tag{1.2}$$

where k_B is the Boltzmann constant, T is the absolutely temperature and a is the monomer size respectively. If considered the whole polymer chain as a single spring. The force constant is given as:

$$k_{sp} = \frac{3k_BT}{R_F^2} = \frac{3k_BT}{Na^2} \tag{1.3}$$

where N is the monomer numbers and R_F is the end-to-end distance of a polymer chain.

The entropy elasticity of the Gaussian chain can be expressed as a function of the two ends at **r** and **r'** (G is here equal to U):

$$S = const. + k_B \ln G = const. - \frac{3k_B}{2R_F^2}(\mathbf{r} - \mathbf{r'})^2 \tag{1.4}$$

So the corresponding Helmholtz free energy A of the chain is calculated as:

$$A = const + SdT = const. + \frac{3k_BT}{2R_F^2}(\mathbf{r} - \mathbf{r'})^2 \tag{1.5}$$

On the other hand, the motion of polymer chain in solution can be viewed as self avoiding-random walks (SARW), in which model the key point is the excluded volume. As shown in figure 1.2, any two spheres are forbidden to overlap with each

other. So when considering a polymer chain as N spheres of diameter b, the free-energy change per chain is influenced by the excluded volume and is then

$$\Delta A / k_B T = N^2 a^3 / R^3 \qquad (1.6)$$

where R is the radius of gyration (R_g) and has the following relation with N

$$R_g \cong aN^\upsilon \qquad (1.7)$$

here υ is the flory exponent which is related with the solvent (for good solvent, $v = 0.6$, and theta solvent $v = 0.5$).
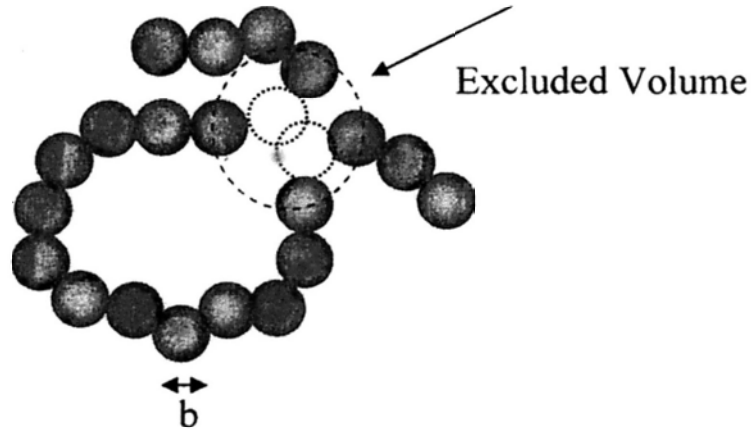
Figure 1.2 SFAW model of a polymer chain dilute in solution.[56]

In a word, there are two terms in the free energy of a polymer chain in solution, one is the entropy due to the freedom for chains with various conformations; the other is the interaction mostly due to the excluded volume. Finally, the free energy of the chain is shown as follow:

$$\frac{A}{k_B T} = \frac{R^2}{Na^2} + \frac{a^3 N^2}{R^3} \qquad (1.8)$$

Figure 1.3 shows a sketch of $A/k_B T$. The elasticity and interaction have the opposite R dependence. As a result, a minimum A exists.
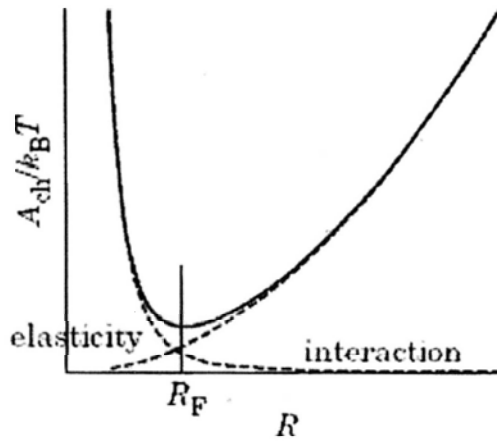
Figure 1.3 The chain dimension R dependency of free energy of a chain A in solution.[56]

1.2.2 Under a flow field

To decrease the complexity, polymer chains under homogeneous shear flow with a constant velocity gradient tensor are mainly discussed.

1.2.2.1 Weak shear rate

When polymer chains are under a weak shear rate, Janeshitz-Kriegl showed there was a linear relationship between distortions and reduced shear rate $\tau_z S_r$ (also know as Weissenberg number W_i) by birefringernce,[27] with S_r was the shear rate and τ_Z was the largest relaxation time of the unperturbed molecule based on zimm model,[57] respectively.

$$\tau_Z \cong 0.2\eta R_0^3/T \tag{1.9}$$

where η was the viscosity of solvent and R_0 is the unperturbed coil radius.

1.2.2.2 Strong shear rate

It is well known that a compact chain tries to remain its configuration when it is fully extended, namely, when under strong shear rate ($W_i > 1$). Using the "dumbbell model",[4] the restoring force F is written as:

$$F = - (3TR_F/R_0^3)E(t) \tag{1.10}$$

where $t = R_F/Na$ is the extension ratio, the factor $E(t) = L^{-1}(t)/3t$, here $L^{-1}(t)$ is the inverse Langevin function, $E(t)$ is unity at small t but diverges for $t \to 1$.[3,5] Besides the motion under restoring force F, the associated current q must contain other two factors, namely, drift in the external flow field $v = S_r r$, and a diffusion coefficient D term induced by Brownian motion.

$$q = \Phi S, \mathbf{r} + D[(\Phi/T)F - \nabla\Phi] \tag{1.11}$$

where Φ is the distribution function of end-to-end distance.

Considering a random coil under strong shear flow, only the outer segments are directly exposed to the flow field,[58] the exposure degree will increase as the increasing of the shear flow, then the chain will be more distorted and more monomers are exposed. More exposure leads to a further extension. Such a feedback process depends on the detailed structure of the flow field.[5] For a flow field of vorticity, namely, the flow field has a two dimensional flow (v_x, v_z) described as $\omega = \frac{1}{2}(\partial v_x/\partial z - \partial v_z/\partial x)$ and as shown in figure 1.4, the coil to stretch transition is continued and reputed as a second order transition, as shown in figure 1.5
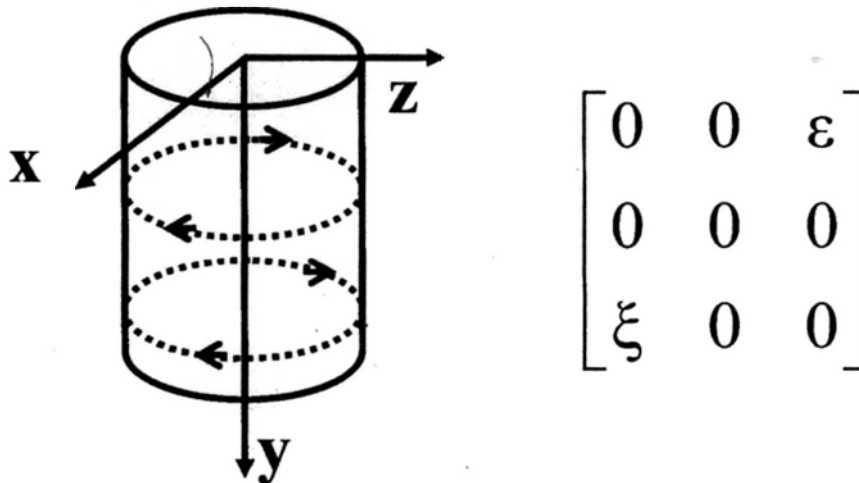
Figure 1.4 Illustration and matrix of vorticose flow field.
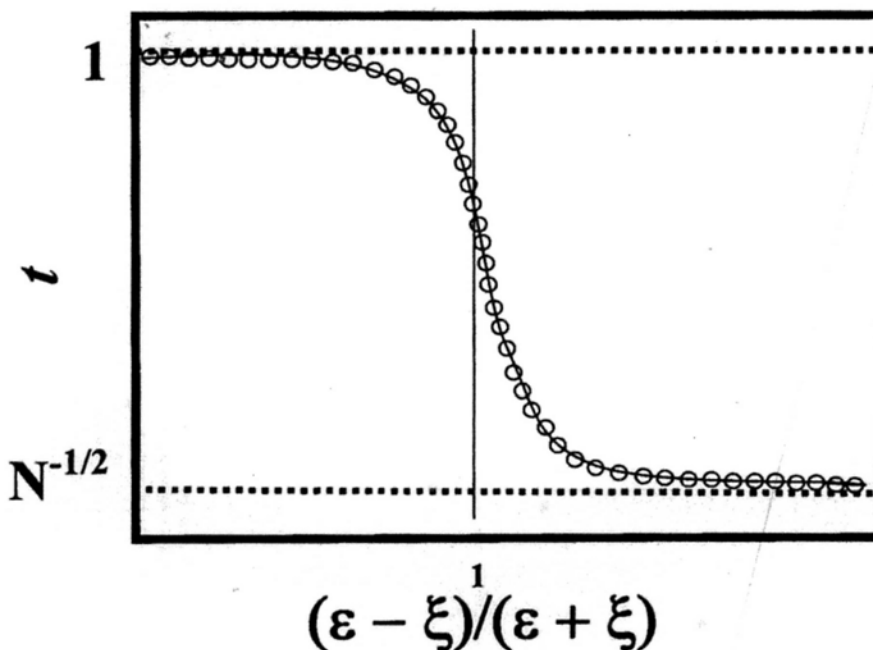
Figure 1.5 The coil to stretched transition of a polymer chain in vorticity[5]

When a polymer chain is under a flow field with particular longitudinal gradients (e.g., $v_x = S_r x$, $v_z = -S_r z$) as shown in figure 1.6. The $t(S_r)$ shows a S shape indicates that there is a bistable equilibrium (figure 1.7). In the range of $1/\tau_R < S_r < \tau_Z$, there are three states of the molecule, that is, coil state (stable state), unstable state, and stretched state. At the particular shear rate value S_r^*, the coil turns to stretch and is reputed as the first order transition.
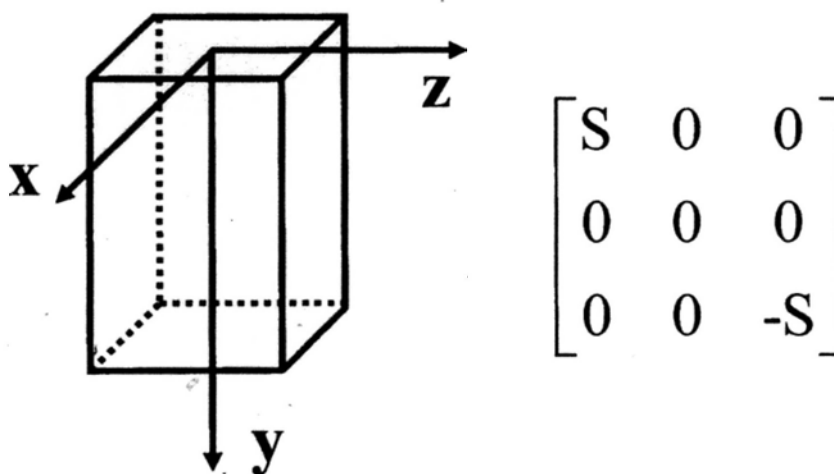
Figure 1.6 Illustration and matrix of shear flow with particular longitudinal gradient.
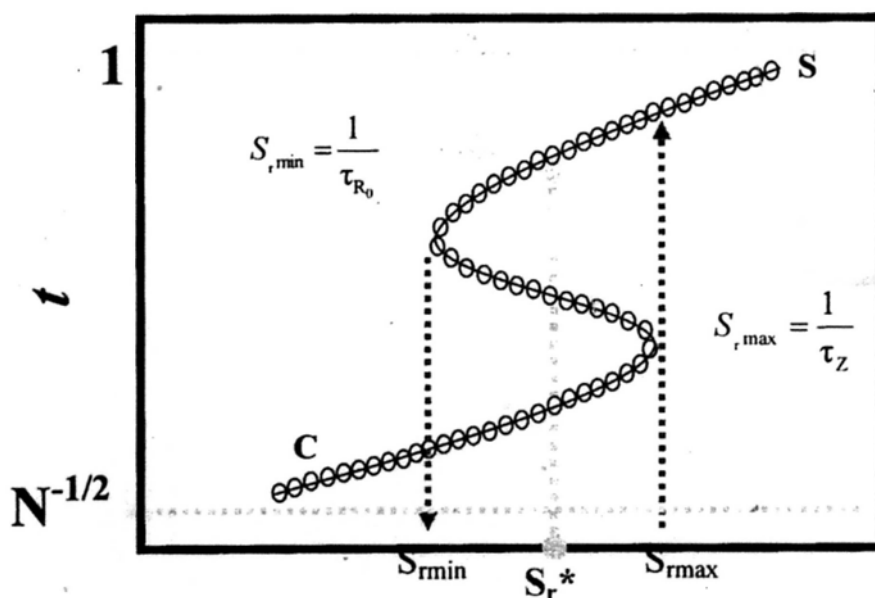
Figure 1.7 The coil to stretched transition of a polymer chain in a "longitudinal gradient", the $S_{rmin} = 1/\tau_R$ and $S_{rmax} = 1/\tau_z$ is order of Rouse and Zimm frequency, respectively.[5]

1.2.3. Pass through nanopores

Generally, the nanopores used in ultrafiltration experiment must satisfy several requirements: i) there are no interactions between nanopores and polymers; ii) the size of nanopores D must be smaller than the polymer size R_g, otherwise, the polymers may pass through the nanopores by diffusion; iii) the cross section of tube must be a constant (no rugosity).[1] Such nanopores can be obtained by particle-track etching[59,60] and has been commercialized.

For a polymer chain confined in a nanotube with length L, it can be viewed as a string of blobs with blob size $\xi = g_\xi{}^\upsilon a$ as shown in Figure 1.8, where g_ξ is the monomer numbers in one blob and is equal to the pore size D here. The confined energy per blob is of the order $k_B T$,[52] the osmotic pressure generated by each blob $p \sim k_B T/D^3$, and the corresponding force to confine a blob in nanotube

$$F_c \sim k_B T/D \tag{1.12}$$

On the other hand, the Stokes force on each blob is related with the flow velocity $V = q/D^2$ and has a relationship of:

$$F_h \sim \eta V D \tag{1.13}$$
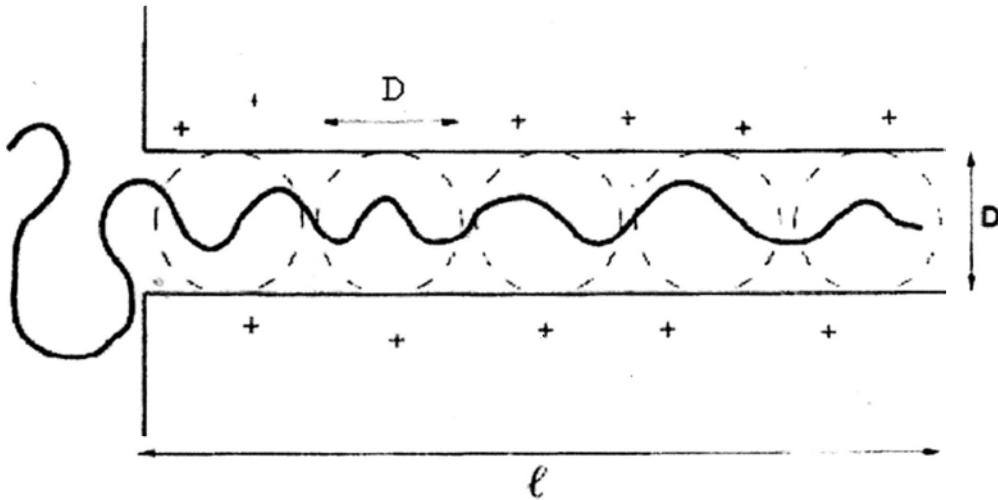
Figure 1.8 Blob picture for partial entry[1]

It is well known that the Stokes force F_h must overcome the confined force so that squeeze one blob into the nanotube.

$$k_B T/D = \eta V D = \eta q_c/D \tag{1.14}$$

Thus the critical current

$$q_c = k_B T/\eta \tag{1.15}$$

7

Once the current is equal or larger than the threshold, the flexible linear chain is able to pass through a much smaller nanopore.[60-62] From the eq (1.15), q_c is irrelative with the molecular weight of polymer chain as well as the pore diameter. It is understandable that once a blob is squeezed into a nanotube, the following parts are easily to be dragged into the tube as threading a needle.

The molecular weight independency has been proved by Anderson in 1984;[63] however, they found the block degree of chains continuously augments when the flow rate decreases as shown in figure 1.9, which is contrary to the predictions. Until recently, Jin[38] et. al firstly experimentally proved such first order transition by ultrafiltration experiments on linear Polystyrene chains passing through nanopores in toluene, the result is shown in figure 1.10.
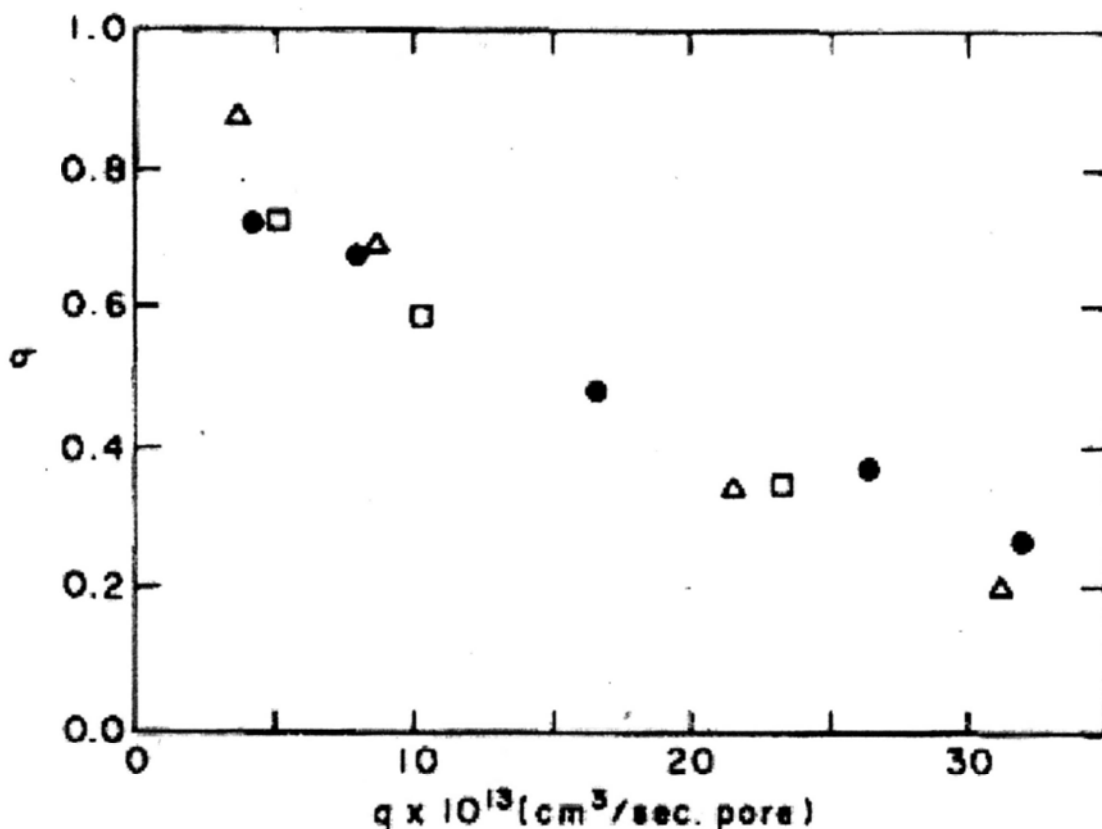
Figure 1.9 Concentration retention vs flow rate through each pore for the molecular weight fractions (1.8 x 10^6, 4.48 x 10^6, 8.42 x 10^6, 2 x 10^7) of polystyrene in 90% CCl$_4$-10% CH$_3$OH at 25 °C; pore radius varied from 400-1000Å.[63]
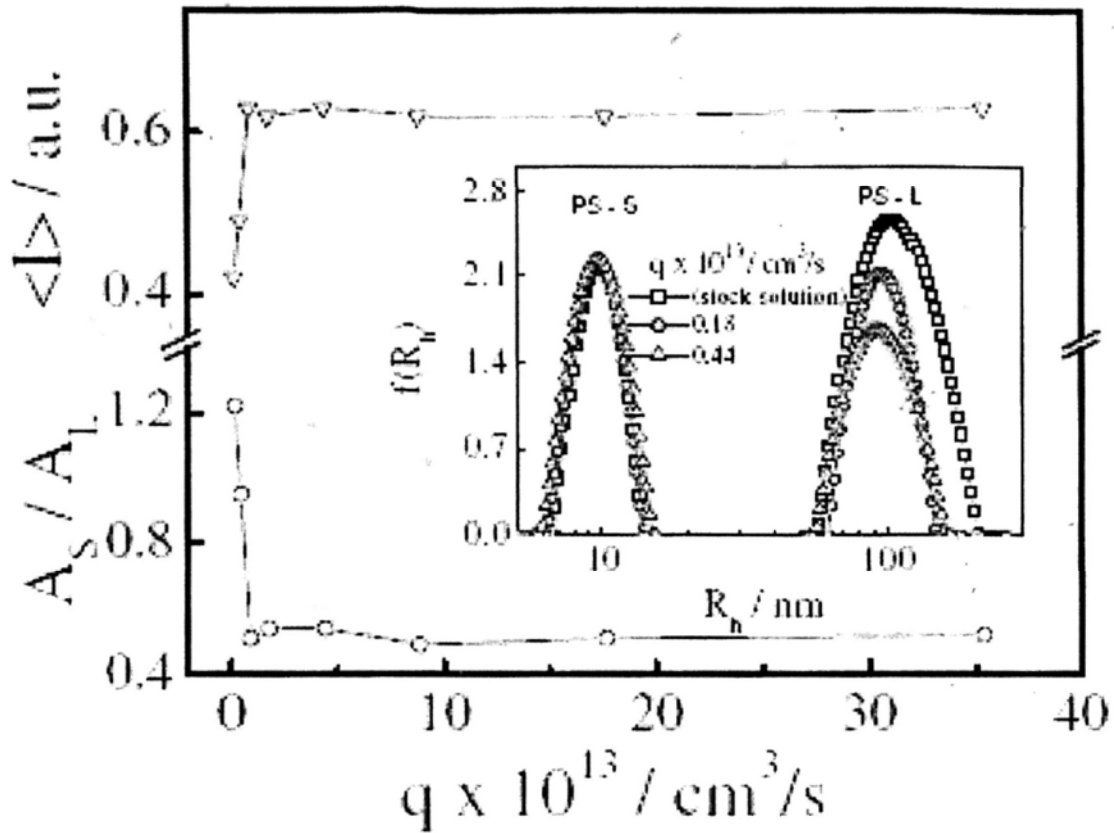
Figure 1.10 Microscopic flow rate (q) dependence of averaged scattered light intensity ($<I>$) and area ratio of the two different Polystyrene linear chains in toluene, with the PS-S chains is much smaller than the pore size, and PS-L chains is much bigger than the pore size.[38]

1.3 Polymer Stars pass through nanopores under flow field

1.3.1 Free energy of Polymer Stars in solution.

The behavior of star shaped polymers in solution is much more complicated compared with linear chains. To reduce the complexity, only uniform stars with f uniform branches joint at one origin are discussed here. Based on the chain grafted on the plane model,[64,65] a single star can be considered as each branch is made of a succession of blobs with a size ξ increasing from the centre of the star to the outside as shown in figure 1.11.[66] When the branch is very long and in a good solvent, we have the radius as follow:

$$R \sim N_{arm}^{3/5} f^{1/5} a \tag{1.16}$$

where N_{arm} is the monomer number in one branch. Based on the free energy of linear chain in solution in eq (1.8), the free energy of stars can be written as

9

$$\frac{A}{k_BT} = \frac{L^2}{R^2} + \frac{R^3}{LD^2}$$

(1.17)
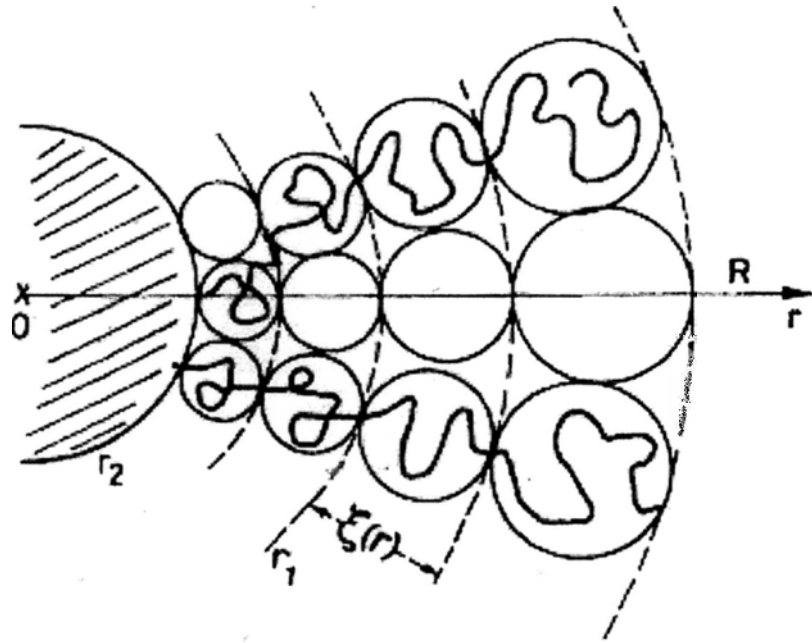
Figure 1.11 A representation of star model: every branch is made of a succession of blobs with a size ξ increasing from the centre of the star to the outside.[66]

1.3.2 Pass through nanopores

Stars trapped in nano tubes have various modes: symmetrical mode and asymmetrical mode as shown in figure 1.12.[44] Figure 1.12b shows an extremely asymmetrical as one arm forward. Therefore, there are various modes of stars are elongated under flow field and enter the nanotube.
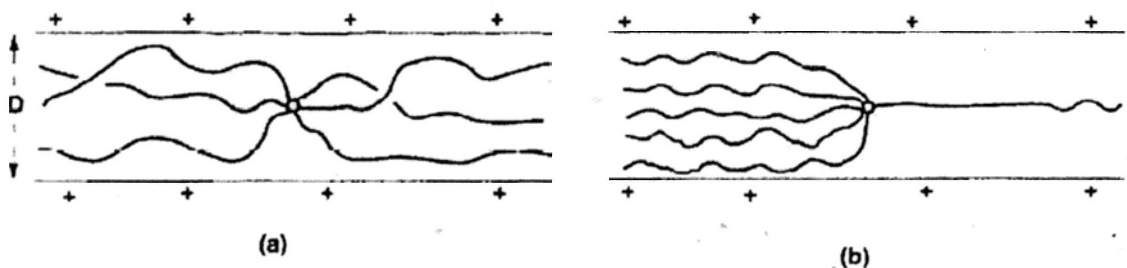
Figure 1.12 Symmetrical mode and Asymmetrical mode (one arm forward) of star (f = 6) trapped in nanotube.[44]

1.3.2.1 Symmetrical mode

When confined in a nanotube, the confined energy of star E_{conf} has a minimum value when the forward arm numbers is equal to backward arm numbers.

$$\frac{\partial\left[E(f_{in})+E(f-f_{in})\right]}{\partial f_{in}}=0 \tag{1.18}$$

For a tube diameter D, the length L of the tube occupied by the star should have a following scaling law by optimizing with eq (1.17) respect to L:

$$L(D) = D \, (R/D)^{5/3} \tag{1.19}$$

In symmetrical mode, with f/2 arms forward, the correlation length is $\xi = D(f/2)^{-1/2}$, and the confined energy is related with the blob numbers confined in the tube:

$$E = k_B T \frac{LD^2}{\xi^3} \cong k_B TN(\frac{a}{D})^{5/3}(f/2)^{11/6} \tag{1.20}$$

and the confined force F_{conf} generated by the osmotic pressure is:

$$F_{conf} \cong E/L = \frac{k_B TD^2}{\xi^3} = \frac{k_B T}{D}(f/2)^{3/2} \tag{1.21}$$

On the other hand, the hydrodynamic force used to squeeze a star into the tube with length l is:[67]

$$F_h(l) = 3\pi \frac{lD^2}{\xi^3}\eta\xi V = 3\pi \frac{lD^2}{\xi^3}\eta\xi V \frac{q}{D^2} = 3\pi \frac{lq\eta(f/2)}{D^2} \tag{1.22}$$

Therefore, the overall energy on the star is:

$$E_{tot} = E_{conf} - E_h = F_{conf}l - \int_0^p dx F_h(x) = F_{conf}l - \frac{1}{2}lF_h(l) \tag{1.23}$$

the energy has a maximum at $l = l^*$

$$l^* = \frac{F_{conf}D^2}{3\pi q\eta(f/2)} = \frac{2F_{conf}D^2}{3\pi q\eta f} \tag{1.24}$$

the corresponding energy barrier should be proportional to $k_B T$, and give a critical current:

$$q_c = \frac{k_B T}{3\pi\eta}(\frac{f}{2})^2 \tag{1.25}$$

1.3.2.2 Asymmetrical mode

1.3.2.2.1 One arm forward

Though the symmetrical mode has the lowest confinement energy, it does not mean the lowest critical current. In one arm forward mode, at $q > q_{c,1}$ (the critical

current of linear chain), the forward one arm will be pulled into the nanotube like stretching of tethered chain,[68] and the drag force is then

$$F_h = 3\pi\eta VL \cong 3\pi\eta Na\frac{q}{D^2} \qquad (1.26)$$

The drag force must overcome confined force to stretch the star pass through nanotube. A combination of eqs (1.21) and (1.26) lead to:

$$q_c = \frac{k_BT}{3\pi\eta}f^{3/2}D/(Na) \qquad (1.27)$$

To make $q > q_{c,1}$, the $N < f^{3/2}D/a$; on the hand, when $N > D/af^{1/2}$, the asymmetric mode wins. Therefore, the eq (1.27) is used in the limitation of $(D/a)f^{-1/2} < N < (D/a)f^{3/2}$. The drag force of the forward one arm must be smaller than the force required for bond rupture; other wise, the forward one arm will be teared out from the star.

1.3.2.2.2 Optimal number of arm forward

The one arm forward model is ultra asymmetric mode, normally, the general asymmetric mode has ϕ ($1 < \phi << f$) arms forward and $f - \phi$ arms backward. When considered ϕ arms entering into the nanotube. The current q must be over the symmetric mode as shown in eq (1.24) and has the relationship of:

$$q/q_{c,1} > \phi^2 \qquad (1.28)$$

The argument of eqs (1.26) and (1.27) are repeated when the criterion is satisfied with the drag force multiplying by ϕ. The eq (1.27) is replaced by:

$$\begin{cases} \phi = f^{1/2}(\dfrac{D}{Na})^{1/3} \\ q_c = \dfrac{k_BT}{3\pi\eta}f(\dfrac{D}{Na})^{2/3} \end{cases} \qquad (1.29)$$

Similar with one arm forward mode, they also have limitations when using eq (1.28) in optimal numbers of arms forward mode. Considering the $\phi > 1$ and $q_c > q_{c,1}$, we have $N < D/af^{2/3}$.

Although the shape dependency of critical current has been used to separation,[69] the experimental proof about star shaped polymer pass through nanopore haven't been given out. Because the stars used in the experiment must satisfy the following requirements: i) uniform arm length in each star; ii) narrowly distributed molecular weight; iii) the size of stars must be bigger than the corresponding pore diameter, otherwise they will pass through nanopores by diffusion.

1.4 Polymer Branches pass through nanopore under flow field

1.4.1 Free Energy of Polymer Branches in solution.

In an ideal branched structure (with no steric interactions),[49] a branch polymer is seen as N single strands connected by cross-link agent.[70,71] In good solvents, based on theory[72,73] and experimental[74] studies, the radius of gyration R_g is shown as follow:

$$R_g \sim aN^{1/2}b^{1/10} \tag{1.30}$$

where b is the monomer numbers between successive branch points. The ideal branched object end-to-end distance R_0[70,71] derived by Zimm and Stockmayer:

$$R_0 = a(bN)^{1/4} \tag{1.31}$$

Like the cases of linear chains and stars, the free energy of branched polymers are also made up of two items, namely, elastic energy and the energy due to intermonomer repulsion

$$E \cong k_B T \left(\frac{R^2}{R_0^2} + \frac{N^2 a^3}{LD^2} \right) \tag{1.32}$$

1.4.2 Confined in a nanotube.

Combination of eqs (1.30) and (1.31), the revised free energy is given as:

$$E \cong k_B T \left(\frac{L^2}{N^{1/2}a^2} + \frac{N^2 a^3}{LD^2} \right) \tag{1.33}$$

Optimizing with respect to L, one can find:

$$\frac{L}{D} = N^{5/6} \left(\frac{a}{D} \right)^{5/3} = \left(\frac{R}{D} \right)^{5/3} \tag{1.34}$$

with the internal concentration as:

$$\sigma = \frac{Na^3}{LD^2} = \left(\frac{D_{min}}{D} \right)^{4/3} \tag{1.35}$$

When $\sigma = 1$,[52] which means the maximum extrusion, leads to a minimum diameter of

$$D_{min} = aN^{1/8}b^{-1/8} \tag{1.36}$$

and a maximum squeezing L is

$$L_{max} = aN^{5/6} \left(\frac{a}{D_{min}} \right)^{5/3} = aN^{3/4}b^{1/4} \tag{1.37}$$

Eqs (1.36) and (1.37) mean that a branch polymer can not be stretched to more than L_{max}, or can not be squeezed into a pore with size smaller than D_{min}.

13

1.4.3 Suction into a nanotube.

The branched polymer confined in a nanotube is also seen as a compact stacking of blobs, with g monomers in each blob and the blob size is ξ as shown in figure 1.13
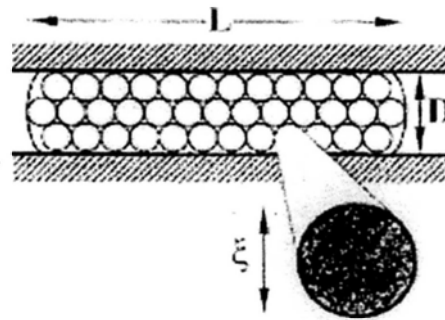
Figure 1.13 An illustration of branched polymer confined in a smaller nano tube. The interior of the polymer is a semidilute solution of correlation length ξ.[44]

Such situation is similar with semidilute solutions with blobs are next to each other. If a branched polymer is squeezed into a certain length y as shown in figure 1.14.
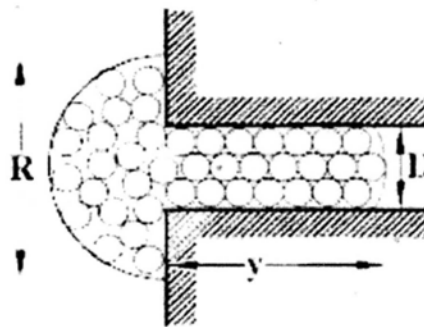
Figure 1.14 A branched polymer is squeezed into a nano tube with length y.[44]

The corresponding free energy related to the hydrodynamic force and confined force is

$$E = F_c y - \int_0^y dy' F_h(y') \tag{1.38}$$

The confined force generated by the osmotic pressure is given as

$$F_c = pD^2 = k_B T D^2 / \xi^3 \tag{1.39}$$

and the hydrodynamic force is related to a stocks force per blob

$$F_h \cong \xi \eta V(D^2 y / \xi^3) = \eta q y / \xi^2 \tag{1.40}$$

As long as the branched polymer is squeezed to a length y*,

$$y^* = F_c \xi^2 / q\eta \tag{1.41}$$

it has a maximum energy barrier of

$$E^* = \frac{1}{2}F_c y^* = \frac{(k_B T)^2}{q\eta}(\frac{D}{\xi})^4 \sim k_B T \tag{1.42}$$

Once the maximum energy barrier is surmounted, the branched polymer can be squeezed into the nanopore, and the critical current is:

$$q_c \cong \frac{k_B T}{\eta}(\frac{D}{\xi})^4 = \frac{k_B T}{\eta}(\frac{R}{D})^{4/3} \tag{1.43}$$

The internal concentration can be rewritten as

$$\sigma = ga^3/\xi^3 \tag{1.44}$$

A combination of eqs (1.35) and (1.44) gives

$$\xi = a(\frac{D}{a})^{4/3} N^{-1/6} \tag{1.45}$$

The single strand between two connected points is seen as a random coil, and it obeys the rule of scaling theory in good solvent:

$$\xi_b = ab^{3/5} \tag{1.46}$$

When $\xi_b = \xi$, the tube diameter has a certain crossover value, D^*

$$D^* = aN^{1/8}b^{19/40} \tag{1.47}$$

1.4.3.1 Weak Confinement

When the tube diameter is larger than D^*, the corresponding $\xi > \xi_b$, such situation is defined as weak confinement. The illustration is shown in figure 1.15.[1,49]
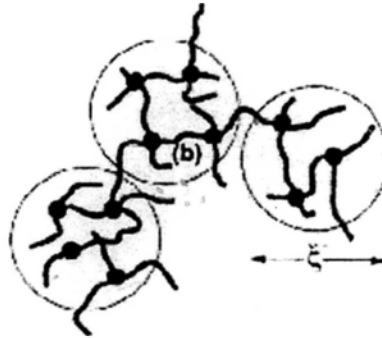
Figure 1.15 Weak confinement of branched polymer in nanotube.[1]

In the regime, the relationship between ξ and b obeys the scaling role of branched polymer in good solvent:

$$\xi = ab^{1/10}g^{1/2} \tag{1.48}$$

A combination of eqs (1.43), (1.45) and (1.48) gives a rewritten q_c as

$$q_C = \frac{k_B T}{\eta} N^{\frac{2}{3}} \left(\frac{a}{D}\right)^{4/3} b^{\frac{2}{15}} \qquad (1.49)$$

1.4.3.1 Strong Confinement

On the contrary hand, when the tube diameter is smaller than D^*, the corresponding $\xi < \xi_b$, it is defined as strong confinement as shown in figure 1.16.
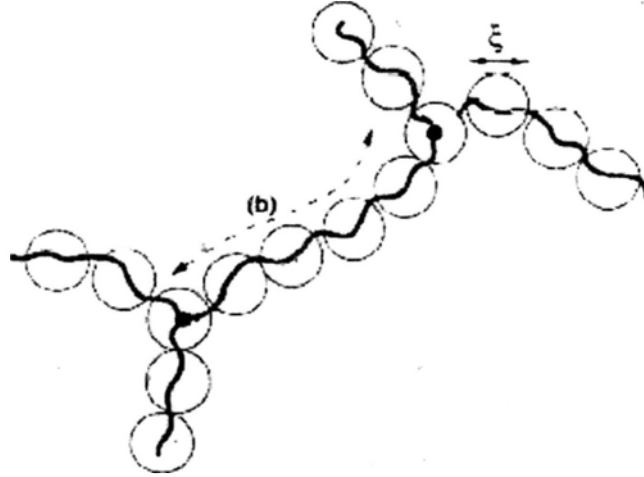
Figure 1.16 Weak confinement of branched polymer in nanotube.[1]

In the regime of $D^* > D > D_{min}$, the blob is smaller than the strand between two cross-linking points and obeys scaling role of random coil in good solvent:

$$\xi = ag^{3/5} \qquad (1.50)$$

A combination of eqs (1.43), (1.45) and (1.50) gives a rewritten q_c as

$$q_C = \frac{k_B T}{\eta} \left(\frac{N}{b}\right)^{1/2} \qquad (1.51)$$

As shown in eq (1.51), the q_c in strong confinement is irrelative with the tube diameter.

In a word, either D satisfies $D_{min} < D < D^*$ or $D > D^*$, the critical current q_c is related with the molecular weight (proportional to N) and the distance between branch points,[1] such dependency can be used in separations. In 1998, Duke et. al.[75] designed a "microdevice", which is made of three rectangular obstacles and can be used to separate biomolecules with different sizes, however, only globular, colloidal particles bigger than 10 μm are suitable; and then Meunier et. al.[53,69] used monolithic columns to separate polymers with different molecular topology.

1.5 Polymer micelles pass through nanopore under flow field

1.5.1 Polymer micelles in solution.

It is well known that micellization of block copolymers can spontaneous happen in selective solvent at a concentration above critical micelle concentration (CMC). Below CMC, only the molecularly dissolved block copolymers are present in solution, known as unimers; while above CMC, unimers are accumulated and formed micelles, and in the case the multi-molecular micelles and unimers coexist in solutions; Furthermore at higher concentration, micelles place in an orderly arrangement and formed gel, the concentration at which gelling occurs is called critical gel concentration (CGC). The three regimes of block copolymers in solution are illustrated in figure 1.17.[76] Usually, the micellization of block copolymers takes place via a closed association process, leading to a narrowly distribution of molar mass and size.[77]

$$C < CMC \qquad C \geq CMC \qquad C \geq CGC$$
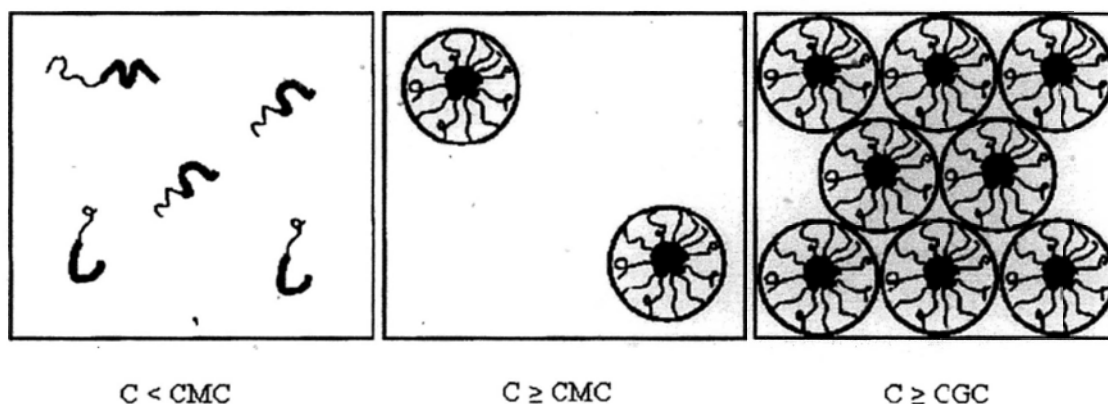
Figure 1.17 Three concentration regimes of block polymers in selected solutions.[76]

1.5.2 Pass through nanopores

One of keys of stretching micelle and passing through a smaller nanotube is the interaction strength among the insoluble blocks in the core.[78] Because there are various kinds of insoluble blocks packing mode in the core (shown in figure 1.18), the corresponding hydrodynamic drag forces have a wide distribution as shown in figure 1.19. If the insoluble blocks are too long or the soluble parts are too short, polymeric micelles cannot be disintegrated even under an extremely high flow rate.Further more, the ultrafiltration method gives a good way to establish the interaction strength and the chain packing of the insoluble core.
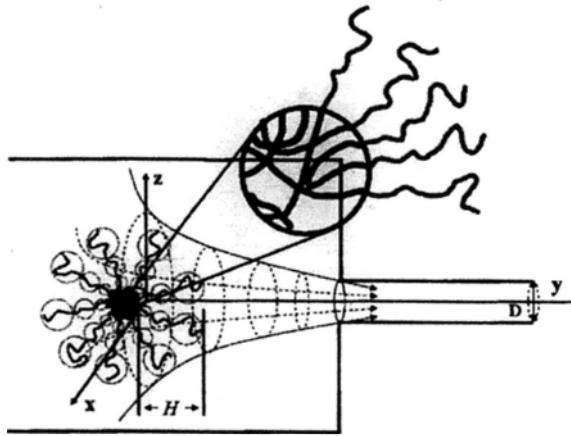
Figure 1.18 Schematic of ultrafiltration of a polymeric core-shell micelle made of a block copolymer chains through a smaller pore under an elongational flow. The enlarged picture shows different kinds of chain packing of insoluble blocks in the core.[78]
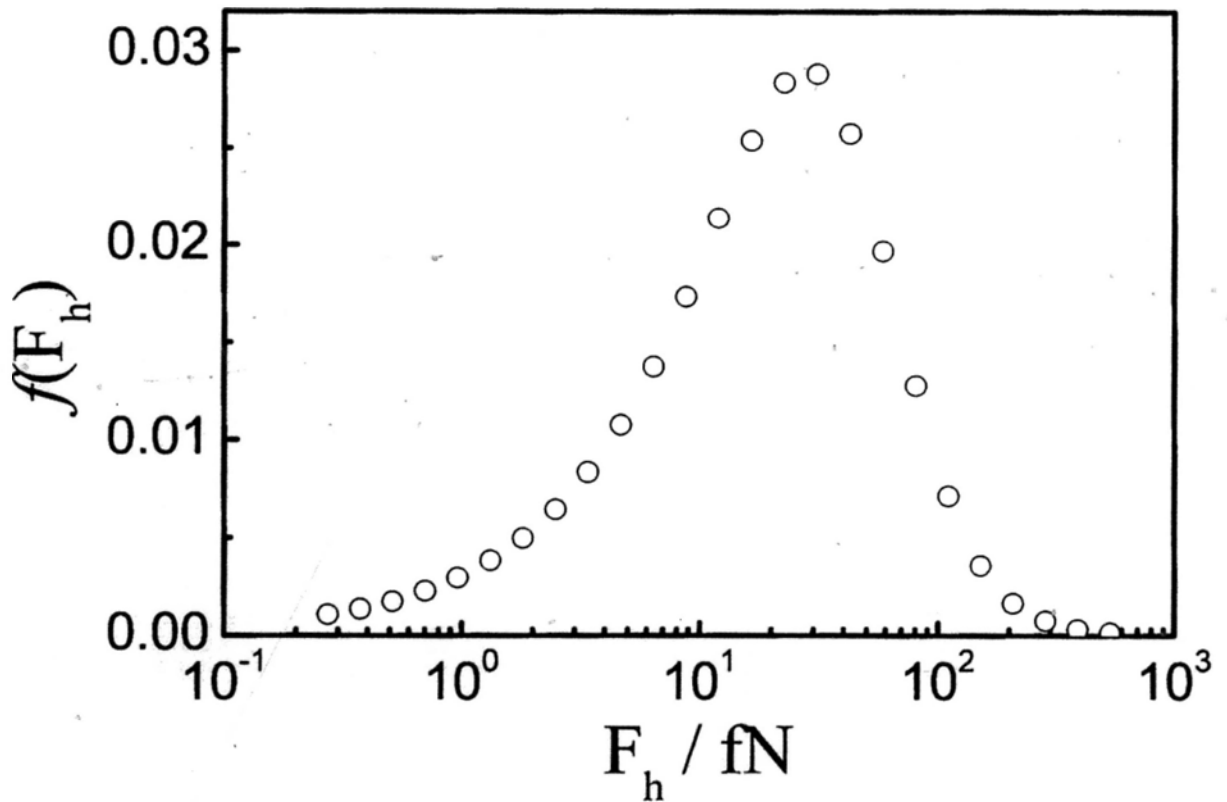
Figure 1.19 Distribution of hydrodynamic force ($f(F_h)$) required to rupture polymeric micelles made of $(St)_{180}$-b-$(Iso)_{500}$ in n-hexane at 25.0 °C.[78]

1.6. Our main goal

The previous theories have been put forward for years, but there are seldom experimental evidences to support. In this thesis, we focus our study on the polymer

linear chains and star shaped polymers pass through nanopores under flow field in dilute regimes. We first synthesized serious linear chains and star polymers by anionic polymerization with the help of self-designed homemade vaccum system. Then we ultrafiltrated these polymers in dilute solution with small nanopores, combined with Laser Light Scattering testing, the behavior of these polymers when they pass through nanopores were established. Based on the experimental results, we have firstly proved the critical flow rate of linear chains passing through nanopores is independent on the chain length as prediceted.[1] However, the experimental q_c is around ~10-100 time smaller than the predicted one and was related with the pore diameter. And for star polymer passing through nanopores, we found the q_c with the same arm number are independent on the arm length and the optimal forward arm numbers do not exist., which are contrary to the previous theories also. With the help of the experimental data, we modified the previous theories and established a new one.

1.7 References

[1] de Gennes, P. G. Adv. Polym. Sci. **1999**, 138, 91

[2] Fox, M. E.; Szoka, F. C.; Fréchet J. M. J. Acc. Chem. Res. **2009**, 42, 1141.

[3] Peterlin, A. J. Polym. Sci., Polym. Lett. **1966**, 4, 287.

[4] Peterlin, A. Pure Appl. Chem. **1966**, 12, 563.

[5] de Gennes, P. G. J. Chem. Phys. 1974 , 60, 5030.

[6] Nguyen, T. Q.; Kausch, H.-H. Editors Flexible polymer chain dynamics in elongational flow: theory and experiment Springer-Verlag: Berlin Heidelberg 1999.

[7] Pincus, P. Macromolecules **1976**, 9, 386.

[8] Nowicki, W.; Nowicka, G.; Narkiewics-Michalek, J. Euro. Polym. J. **2010**, 46, 112.

[9] Slonkina, E.; Kolomeisky, A. B. J. Chem. Phys. **2003**, 118, 7112.

[10] Wyart, F. B. Europhys Lett. **1995**, 30, 387.

[11] Huopaniemi, I.; Luo, K. J. Chem. Phys. **2006**, 125, 124901.

[12] Klushin, L. I.; Skvortsov, A. M.; Hsu, H. P.; Binder, K. Macromolecules **2008**, 41, 5890.

[13] Sung, W.; Park, P. J. Phys. Rev. Lett. **1996**, 77, 783.

[14] Deen, W. M. AIChe J. **1987**, 33, 1409.

[15] Lai, P. Y. Macromol. Theory Simul. **1999**, 8, 382.

[16] Buguin, A.; Wyart-Brochard, F. Macromolecules 1996, 29, 4937.

[17] Morrison, G.; Hyeon, C.; Toan, N. M.; Ha, B.-Y.; Thirumalai, D. Macromolecules **2007**, 40, 7343.

[18] Grosberg, A. Y.; Nechaev, S.; Tamm, M.; Vasilyev, O. Phys. Rev. Lett. **2006**, 96, 228105.

[19] Geissler, P. L.; Shakhnovich, E. I. Phys. Rev. E. **2002**, 65, 056110.

[20] Daoudi, S.; Brochard, F. Macromolecules **1978**, 11, 751.

[21] Lemak, A. S.; Lepock, J. R.; Chen, J. Z. Proteins: Struct., Funct., Genet. **2003**, 51, 224.

[22] Szymczak, P. J. Chem. Phys. **2006**, 125, 164903.

[23] Tian, P.; Smith, G. D. J. Chem. Phys. **2003**, 119, 11475.

[24] Jaspe, J.; Hagen, S. J. Biophys. J. **2006**, 91, 3415.

[25] Larson, R. G.; Perkins, T. T.; Smith, D. E.; Chu, S. Phys. Rev. E **1997**, 55, 1794.

[26] Cathey, C. A.; Fuller, G. G. J. Non-Newtonian Fluid Mech. **1990**, 34, 63.

[27] Janeshitz-Kriegl, H. J. Adv. Polym. Sci. **1969**, 6, 170.

[28] Link, A.; Springer, J. Macromolecules **1993**, 26, 464.

[29] Zizenis, M.; Springer, J. Polymer **1994**, 35, 3156.

[30] Nguyen, T. Q.; Yu, G.; Kausch, H.-H. Macromolecules **1995**, 28, 851.

[31] Carrington, S. P.; Odell, J. A. J. Non-Newtonian Fluid Mech. **1996**, 67, 269.

[32] Pope, D. P.; Keller, A. Coll. Polym. Sci. **1978**, 255, 633.

[33] Odell, J. A.; Keller, A.; Miles, M. J. Polymer **1985**, 26, 1219.

[34] Farrell, C. J.; Keller, A. Coll. Polym. Sci. **1978**, 256, 966.

[35] Smith, K. A.; Merrill, E. W.; Peebles, L. H.; Banijamali, S. H. Colloq. Int. CNRS **1975**, 233, 341.

[36] Menasveta, M. J.; Hoagland, D. A. Macromolecules **1991**, 24, 3427.

[37] Muller, A. J.; Odell, J. A.; Keller, A. J. Non-Newtonian Fluid Mech **1988**, 30, 99.

[38] Jin, F.; Wu, C, Phys. Rev. Letts. **2006**, 96, 237801.

[39] Ge, H.; Jin, F.; Li, J. F.; Wu, C. Macromolecules **2009**, 42, 4400.

[40] Nguyen, T. Q.; Kausch, H. H. Adv. Polym. Sci. **1992**, 100, 73.

[41] Delong, C. D.; Hoagland, D. A. Macromolecules **2008**, 41, 4887.

[42] Helfand, E.; Fredrickson, G. H. Phys. Rev. Lett. **1989**, 62, 2468.

[43] van Egmont, J. W.; Fuller, G. G. Macromolecules **1993**, 26, 7182.

[44] Brochard-Wyart, F.; De Gennes, P. G. C. R. Acad. Sci. Paris **1996**, 323II, 473.

[45] Dondos, A.; Papanagopoulos, D.; de Gennes, P. G.; Brochard-Wyart, F. Macromol. Theory Simul. **1999**, 8, 147.

[46] Ripoll, M.; Winkler, R. G.; Gompper, G. Phys. Rev. Lett. **2006**, 96, 188302.

[47] Meunier, D. M.; Stokich, T. M.; Gillespie, D.; Smith, P. B. Macromol. Symp. **2007**, 257, 56.

[48] Gay, C.; Raphaël, E. Adv. Colloid. Interface. Sci. **2001**, 94, 229.

[50] Sakaue, T.; Raphaël, E.; de Gennes, P. G.; Wyart-Brochard, F. Europhys. Lett. **2005**, 72, 83.

[51] Vilgis, T. A.; Haronska, P.; Benhamou, M. J. Phys. II France **1994**, 4, 2187.

[52] Vilgis, T. A. J. Phys. II France **1992**, 2, 2097.

[53] Edam, R.; Meunier, D. M.; Mes, E. P. C.; Van Damme, F. A.; Schoenmakers, P. J. J. Chromatogr. A **2008**, 1201, 208.

[54] Hong, L. Z.; Jin, F.; Li, J. F.; Lu, Y. J.; Wu, C. Macromolecules **2008**, 41, 8220.

[55] Hendrickson, G. R.; Lyon, L. A. Angew. Chem. Int. Ed. **2010**, 49, 2193.

[56] Teraoka, I. Eds. Polymer Solutions An Introduction to Physical Properties. John Wiley & Sons, INC.; New York; 2002.

[57] Zimm, B. H. J. Chem. Phys. **1956**, 24, 269.

[58] Debye, P.; Bueche, A. M. J. Chem. Phys. **1948**, 16, 573.

[59] Fleischer, R.; Price, P.; Walker, R M. Nuclear track in solids University of California Press, **1975**.

[60] Quinn, J. A.; Anderson, J. L.; Ho, W. S.; Petzny, W. J. Biophys. J. **1972**, 12, 990.

[61] Nguyen, Q. T.; Neel, J. J. Membr. Sci. **1983**, 14, 111.

[62] Beerlage, M. A. M.; Heijnen, M. L.; Mulder, M. H. V.; Smolders, C. A.; Strathmann, H. J. Membr. Sci. **1996**, 113, 259.

[63] Long, T. D.; Anderson, J. L. J. Polym. Sci.: Polym. Phys. Ed. **1984**, 22, 1261.

[64] Alexander, S. J. Physique **1977**, 38, 983. See also De Gennes, P. G. in Solid State Physics, Seitz and Turnbull eds., Supp. (Academic Press) **1978**, 14, p1.

[65] De Gennes, P. G. Macromolecules **1980**, 13, 1069.

[66] Maoud, M.; Cotton, J. P. J. Physique **1982**, 43, 531.

[67] De Gennes, P. G. Transport, Disorder and Mixing, Guyon, E. Ed., Kluwer (Dordrecht, Netherlands), **1988**, pp. 203.

[68] Brochard-Wyart, F. Europhys. Lett. **1995**, 30, 387.

[69] Meunier, D. M.; Simith, P. B. Macromolecules **2005**, 38, 5313.

[70] De Gennes, P. G. Biopolymers **1968**, 6, 715.

[71] Zimm, B.; Stockmayer, W. J. Chem. Phys. **1949**, 17, 1301.

[72] Isaacson, J.; Lubensky, T. J. Physique Paris **1980**, 41, L469.

[73] Daoud, M.; Joanny, J. F. J. Physique Paris **1981**, 42, 1359.

[74] Adam, M.; Delsanti, M.; Munch, J. P.; Durand, D. J. Physique Paris **1987**, 48, 1809.

[75] Duke, T. A. J.; Austin, R. H. Phys. Rev. Lett. **1998**, 80, 1552.

[76] Hamley, I. W. Block Copolymers in Solution: Fundamentals and Applications John Wiley & Sons: Chichester, **2005**.

[77] Hadjichristidis, N.; Pipas, S.; Floudas, G. A., Block Copolymers: Synthetic Strategies, Physical Properties, and Applications. John Wiley & Sons, Inc.: Hoboken, N. J., 2003.

[78] Hong, L. Z.; Jin, F.; Li, J. F.; Lu, Y. J.; Wu, C. Macromolecules **2008**, 41, 8220.

Chapter 2

Principle of Laser Light Scattering and Instrumentation

2.1 Introduction of LLS

When a beam of monochromatic, coherent light is incident on a dilute macromolecule solution or suspension of colloidal particles and the solvent refractive index is different from that of the solute (macromolecules or colloidal particles), the incident light is scattered by each illuminated macromolecule or colloidal particle in all directions.[1,2] The scattered light waves from different macromolecules or particles mutually interfere, or combine, at a distant, fast photomultiplier tube (PMT) or avalanche-photodiode (APD) detector and produce a net scattered intensity I(t) or photon counts n(t) which is not uniform on the detection plane. If all the macromolecules or particles are stationary, the scattered light intensity at each direction would be a constant i.e., independent of time. However, in reality, all the scatters in solution are undergoing constant Brownian motions, and this fact leads to both fluctuations of the scattered intensity pattern on the detection plane and the fluctuations of I(t) with time if the detection area is sufficiency small. The fluctuation rates can be related to different relaxation processes such as translational and rotational diffusions as well as internal motions of the macromolecules. The faster the relaxation process, the faster the intensity fluctuations will be.

In a broad definition, laser light scattering (LLS) could be classified as inelastic (e.g., Raman, fluorescence, and phosphorescence) and elastic (no absorption) light scattering. However, in polymer and colloid science, light scattering is normally referred to in terms of static (elastic) or dynamic (quasi-elastic) measurements, or both of the scattered light.[1] Static LLS as a classical and absolute analytical method measures the angular distribution of time-average scattered intensity. On the other hand, dynamic LLS measures the intensity fluctuations instead of the average light intensity (this is the reason the word dynamic comes from), and its essence may be explained as follows. When the incident light is scattered by a moving macromolecule or particle, the detect frequency of the scattered light will be slightly

higher or lower than that of the original incident light owing to the Doppler effect, depending on whether the particle moves towards or away from the detector. Thus, the frequency distribution of the scattered light is slightly broader than that of the incident light. This is why dynamic LLS is also called quasi-elastic light scattering (QELS). The frequency broadening ($\approx 10^5$-10^7 Hz) is so small in comparison with the incident light frequency ($\approx 10^{15}$ Hz) so that it is very difficult to detect the broadening directly in the frequency domain. However, it can be effectively recorded in the time domain through a time correlation function. For this reason, dynamic light scattering is sometimes known as intensity fluctuation spectroscopy. If we use digital photons to measure the intensity fluctuations, the term photon correlation spectroscopy (PCS) is then used to refer to the technique described here.

The recorded observation of the light scattering can be traced back to 1802 when Richard, J. B noticed the light path of the gold colloid. However, the first man who made experimental investigation on light scattering was Tyndall. He observed the scattering of the natural light when it passed through a colloid dispersion. In 1881, based on Maxwell theory of electromagnetic field, Rayleigh derived that the intensity of the scattered light by the non-absorption, non-interaction and optically isotropic small particles is reversely proportional to the fourth power of the incident wavelength. In 1944, Debye measured the molecular weight of macromolecules in dilute solution by using light scattering method. Later, Zimm[12] proposed the famous Zimm plot by extrapolating both concentration and angular angle to zero value at a single coordinate. Since then, light scattering, strictly, static light scattering as a classical and absolute analytical method has been widely used to characterize both synthetic and natural macromolecules. However, light scattering at that time was limited in measuring scattered intensity at different angles and concentrations, from which three parameters of macromolecules, namely the weight-average molecular weight (M_w), z-average root-mean-square radius of gyration ($<R_g^2>^{1/2}$, simply R_g) and the second-order virial coefficient (A_2) can be obtained. This situation was changed in the 1960s with the invention of laser. In 1964, Cummins[13] first reported using lasers as source of incident radiation for the study of macromolecular solutions, poly(styrene), and during the last two decades, thanks to the advance of stable laser, ultrafast electronics and personal computers, LLS, especially dynamic LLS has evolved from a very special instrument for physicists and physical chemists to a routine analytical tool in polymer laboratories or even to a daily quality-control device in production lines.[6,7]

Commercially available research-grade LLS instruments are normally capable of making static and dynamic measurements simultaneously for studies of colloidal particles in suspension or macromolecules in solution as well as in gels and viscous media.

2.2 Static Laser Light Scattering

2.2.1 Scattering by a small particle

The electric field of a light wave acting on a particle induces it in a dipole which oscillates with the same frequency as the incident light (Figure 2.1). An oscillating dipole produces a secondary oscillating field and it radiates electromagnetic energy. In other words, the particle scatters the incident light. Consider a single, optical isotropic particle (a macromolecule or a colloid particle) with a polarizability α at origin o (Figure 2.1) in vacuum. When the particle is much smaller than the wavelength of the incident light λ_0 (in practice, smaller than $\lambda_0/20$), the electric field of the incident light

$$\vec{E} = \vec{E_0} \exp[i(2\pi\nu t - \phi)] \tag{2.1}$$

is homogeneous within the particle; it induces in it a dipole $\vec{\mu} = \alpha\vec{E}$. The electric field oscillates with frequency ν and so does the induced dipole. When the electric field is not too strong, the induced dipole is proportional to the field:

$$\vec{\mu} = \alpha\vec{E} = 4\pi\varepsilon_0\alpha'\vec{E} \tag{2.2}$$

here α' is the polarizability volume[11] of the particle and ε is dielectric coefficient at vacuum.
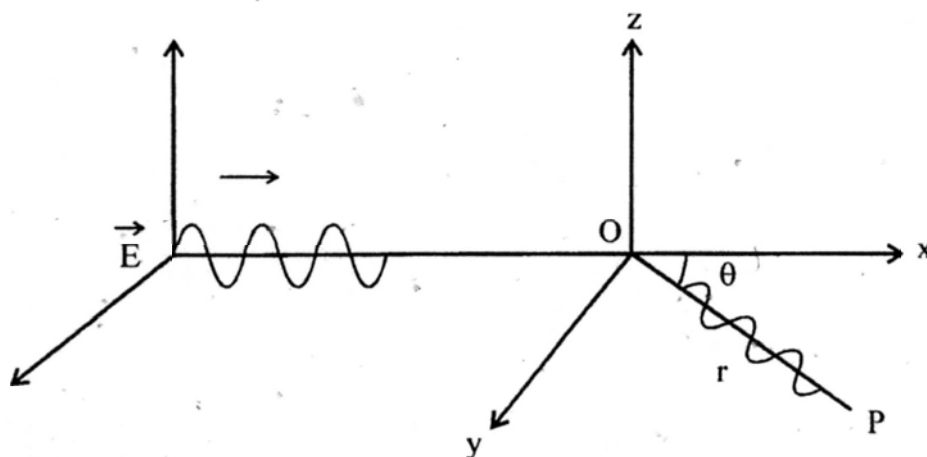
Figure 2.1 Three dimensional coordinates where origin o represents a scatter and P is observation point at xoy plane. The vertically polarized incident beam causes polarization in the scatter, which radiates into different direction.

According to Maxwell electromagnetic equations, the electric field generated by the oscillating dipole at point p with distance r from origin o and angle θ from the incident light is

$$\vec{E}_s = \frac{d^2\vec{p}/dt^2}{4\pi\varepsilon_0 rc^2} = \frac{d^2(\vec{\mu_0}+\vec{\mu})/dt^2}{4\pi\varepsilon_0 rc^2} = -\frac{4\pi^2\alpha'}{r\lambda_0^2}\vec{E} \qquad (2.3)$$

where c is the velocity of light in vacuum and α' is the polarizability volume. $\vec{p}$ is the total dipole of the particle, i.e., the summation of the permanent $\vec{\mu_0}$ and the induced dipole $\vec{\mu}$. Since $\vec{\mu_0} \ll \vec{\mu}$ at room temperature and $\vec{\mu_0}$ is independent of high frequency electromagnetic field, we have adopted $d^2\vec{p}/dt^2 = d^2\vec{\mu}/dt^2$ in equation (2.3). Thus, the time-average scattered intensity i ($kJ \cdot m^{-2} \cdot s^{-1}$) of the particle at point p is

$$i = \varepsilon_0 c \langle E_s^2 \rangle = \frac{16\pi^4\alpha'^2}{\lambda_0^4 r^2}(\varepsilon_0 c < E^2 >) = \frac{16\pi^4\alpha'^2}{\lambda_0^4 r^2}I_0 \qquad (2.4)$$

where I_0 is the intensity of primary light. Equation (2.4) shows that the scattered intensity is proportional to the square of molecular weight since for particles made from a given isotropic material, α' is proportional to their molecular weight. On the other hand, $i/I_0 \propto \lambda_0^{-4}$, means that the scattering is much stronger for light of a shorter wavelength. This explains why the sky is blue because the scattering is stronger toward the short-wavelength end of the visible spectrum.

2.2.2 Scattering by many small-particle system

When there are N independent same small particles in volume V, the total scattered intensity per unit scattering volume I is the simple summation of the scattered intensity of N/V particles:

$$I = i(N/V) = \frac{16\pi^4 N\alpha'^2}{V\lambda_0^4 r^2}I_q \qquad (2.5)$$

Define $R = Ir^2/I_0$ (known as Rayleigh ratio named after the "father" of the theory of light scattering), we have

$$R = \frac{16\pi^4 N\alpha'^2}{V\lambda_0^4} \qquad (2.6)$$

where R (dimension of L) is dependent on the concentration, the size and the nature of the particles.

2.2.3 Scattering by real systems

For a real system, two kinds of interference must be considered. One is the intraparticle interference (i.e, the particle is not so small, dimension $> \lambda/20$, that light scattered from two scattering elements within the volume of the same particle has a significant phase difference), and the other is from the interference between different particles. In the first case, a larger particle with volume V' is convenient to assume that it is composed of N' scattering units each with equivalent volume and polarizability volume α_o'. For each scattering unit, the scattered intensity of it at observation point p can still be expressed by equation (2.3). Thus, the scattered field of the whole particle at point p is the superposition of the electric field of all N' units:

$$\overrightarrow{E_s} = \sum_{l=1}^{N'} \overrightarrow{E_{s,l}} = -\frac{4\pi^2}{\lambda_0^2 r} \alpha'_o \overrightarrow{E_0} \sum_{l=1}^{N'} \exp[i(2\pi v t - \phi_l)] \qquad (2.7)$$

Further, the time-average scattered intensity at point p becomes

$$i = \varepsilon_o c \left\langle E_s^2 \right\rangle = \frac{16\pi^4 \alpha'^2_o}{\lambda_0^4 r^2} I_o \left\langle \sum_{l=1}^{N'} \sum_{m=1}^{N'} \exp[i(\overline{h} \cdot \overrightarrow{r_{lm}})] \right\rangle \qquad (2.8)$$

where $\Delta\phi_{lm} = \phi_l - \phi_m$ is phase difference between scattering unit l and m at point p. As can be seen from Figure 2.2,
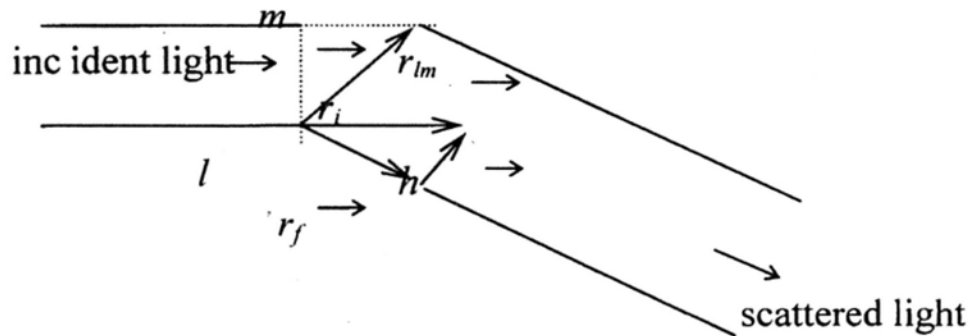

Figure 2.2 A schematically show of the scattering vector and the interference of scattered light inside a larger particle.

$$\Delta\phi_{lm} = \overline{h} \cdot \overrightarrow{r_{lm}} \qquad (2.9)$$

28

where $\vec{r}_{lm} = \vec{r}_m - \vec{r}_l$ and $\vec{h} = \vec{r}_i - \vec{r}_f$ is called scattering vector which is the difference of the unit vector in the direction of the incident beam ($\vec{r}_i$) and the one along the scattered beam ($\vec{r}_f$), and the vector module

$$h = |\vec{h}| = \frac{4\pi n}{\lambda_o} \sin\left(\frac{\theta}{2}\right) \tag{2.10}$$

where n is the refractive index of the medium. With increasing θ, h increases and h^{-1} has been used as a spatial resolution ruler with which static LLS is able to probe the size of colloidal particles and macromolecules at a finite angle. By averaging over all possible orientations ($\vec{r}_{lm}$) of the particle, we finally have

$$i(\theta) = \frac{16\pi^4}{r^2 \lambda_0^4} I_o {\alpha'_o}^2 \sum_{l=1}^{N'} \sum_{m=1}^{N'} \frac{\sin(h\, r_{lm})}{h\, r_{lm}} \tag{2.11}$$

where θ is the inclined angle from direction of primary beam to that of line op, as is shown in Figure 2.1. When $\theta \to 0$,

$$i(\theta \to 0) = \frac{16\pi^4}{r^2 \lambda_0^4} I_o {\alpha'_o}^2 N'^2 \tag{2.12}$$

Note $N' \alpha_o' = \alpha'$ so that equation (2.12) is the same as equation (2.4). We then define an angular scattering function $P(\theta)$ as

$$P(\theta) = \frac{R(\theta)}{R(0)} = \frac{1}{N'^2} \sum_{l=1}^{N'} \sum_{m=1}^{N'} \frac{\sin(h\, r_{lm})}{h\, r_{lm}} \tag{2.13}$$

After developing $\sin(h\, r_{lm})$ into a Taylor series ($\sin x = x - x^3/6 + ...$) and retain the two leading terms, the result reads

$$P(\theta) = 1 - \frac{h^2}{6N'^2} \sum_{l=1}^{N'} \sum_{m=1}^{N'} r_{lm}^2 + \cdots \tag{2.14}$$

where $\dfrac{1}{2N'^2} \sum_{l=1}^{N'} \sum_{m=1}^{N'} r_{lm}^2$ is defined as the mean square of radius of gyration R_g^2. Thus

$$P(\theta) = 1 - (1/3)h^2 R_g^2 + \cdots \tag{2.15}$$

which is related to the conformation of the larger particles and that is why it is also called the structure factor (or form factor). For N independent larger particles in volume V, equation (2.11) can be re-written as

$$R(\theta) = \frac{16\pi^4 N}{V\lambda_0^4} \alpha' P(\theta) \tag{2.16}$$

It is interesting to note that when the above discussion is applied to a homogeneous

pure gas or liquid, we will find that the scattered intensity is zero in all directions except in the direction of incident beam. It is because for any selected small scattering element in the scattered volume we can always find another one whose electric field at point p is counterweight of the former by interference. Then the scattered waves will exactly cancel each other. All the volume elements can be paired up in this way. However, light scattering does exist, even for pure gas and liquid of small molecules. It is because the molecules are undergoing random movement all the time and the properties of individual volume elements will fluctuate from the average properties. The light waves scattered by individual elements will not have identical amplitudes and thus they will not canceled totally by interference. As one of the many properties, polarization volume α_l' of a scattering unit l will also more or less deviate its most probable value α_o' as: $\alpha_l' = \alpha_o' + \delta\alpha_o'$, and it is the existence of $\delta\alpha_o'$ that leads to the light scattering of pure gas and liquid. Followed the above treatment, we divide scattering volume V into N scattering units and substitute α_o' in equation (2.7) with $\alpha_o' + \delta\alpha_o'$. We know the term α_o' will contribute nothing to scattered intensity because of the interference of all units so that only the term $\delta\alpha_o'$ needs to be considered. Equation (2.7) then reads

$$\overrightarrow{E_s} = \sum_{l=1}^{N} \overrightarrow{E_{s,l}} = -\frac{4\pi^2}{\lambda_0^2 r}\overrightarrow{E_0}\sum_{l=1}^{N}\delta\alpha'_l \exp[i(2\pi\nu t - \phi_l)] \tag{2.17}$$

Similar to deriving equation (2.8), taking time-averaged scattered intensity and following the definition of Rayleigh ratio, we can rewrite the equation (2.17) as

$$R(\theta) = \frac{16\pi^4}{V\lambda_0^4}\sum_{l=1}^{N}\sum_{m=1}^{N}\delta\alpha'_l\,\delta\alpha'_m \exp[i\vec{h}(\overrightarrow{r_m}-\overrightarrow{r_l})] \tag{2.18}$$

where $\delta\alpha_l'$ and $\delta\alpha_m'$ are still random functions of time and space. We need to further average equation (2.18) over time. For this purpose, it is convenient to separate the terms in the double sum into terms for which $l = j$ and $l \neq j$.

$$R(\theta) = \frac{16\pi^4}{V\lambda_0^4}\left[\sum_{l=1}^{N}\sum_{m=1}^{N}<(\delta\alpha'_l)^2> + \sum_{l\neq m}^{N}\sum_{m=1}^{N}<\delta\alpha'_l\,\delta\alpha'_m> \exp[i\vec{h}(\overrightarrow{r_m}-\overrightarrow{r_l})]\right] \tag{2.19}$$

The fluctuation of $\delta\alpha_l'$ and $\delta\alpha_m'$ are independent of each other and $<\delta\alpha> = 0$. Therefore, $<\delta\alpha_l'\delta\alpha_m'> = <\delta\alpha_l'><\delta\alpha_m'> = 0$ and equation (2.19) turns to be

$$R(\theta) = \frac{16\pi^4}{V\lambda_0^4}\left[\sum_{l=1}^{N}\sum_{m=1}^{N}<(\delta\alpha'_l)^2>\right] \tag{2.20}$$

The time-average fluctuation of polarization volume of the small scattering unit,

$<(\delta\alpha_l)^2>$ should be a constant and is written as $<(\delta\alpha_o)^2>$. Thus, $\sum_{l=1}^{N}\sum_{m=1}^{N}<(\delta\alpha'_l)^2>=$ $N^2<(\delta\alpha_l)^2>$ and equation (2.20) turns to be

$$R = \frac{16\pi^4}{V\lambda_o^4}N^2\cdot<(\delta\alpha'_o)^2> = \frac{16\pi^4}{V\lambda_o^4}\cdot<(\delta\alpha')^2> \tag{2.21}$$

where we have used the relation $\delta\alpha' = N\delta\alpha'_o$. Now the remained question is to find the expression of $<(\delta\alpha)^2>$. Consider a macromolecule solution or a colloid dispersion, α' is a function of concentration C and density ρ. $\delta\alpha' = (\partial\alpha'/\partial C)\,\partial C + (\partial\alpha'/\partial\rho)\partial\rho$. Since C and ρ are independent of each other, we have

$$<(\delta\alpha')^2> = (\frac{\partial\alpha'}{\partial C})^2<(\delta C)^2> +(\frac{\partial\alpha'}{\partial\rho})^2<(\delta\rho)^2> \tag{2.22}$$

Thus, for a dilute solution, equation (2.21) becomes

$$R_{solution} = \frac{16\pi^4}{V\lambda_o^4}(\frac{\partial\alpha'}{\partial C})^2<(\delta C)^2> +\frac{16\pi^4}{V\lambda_o^4}(\frac{\partial\alpha'}{\partial\rho})^2<(\delta\rho)^2> \tag{2.23}$$

where $\frac{16\pi^4}{\lambda_0^4}(\frac{\partial\alpha'}{\partial C})^2<(\partial C)^2>$ and $\frac{16\pi^4}{\lambda_0^4}(\frac{\partial\alpha'}{\partial\rho})^2<(\partial\rho)^2>$ are the excess Rayleigh ratio of the solution (R_{excess}) and that of the solvent ($R_{solvent}$) respectively. R_{excess} is the net scattering intensity of the solute by substracting the intensity of solvent from that of the solution. According to Clausius-Mossotti equation,[11] $\varepsilon_r - 1 = 4\pi\alpha'/V$ and $\varepsilon_r = n^2$, we have

$$(\frac{\partial\alpha'}{\partial C}) = (\frac{\partial\alpha'}{\partial\varepsilon_r})(\frac{\partial\varepsilon_r}{\partial n})(\frac{\partial n}{\partial C}) = \frac{n}{2\pi}(\frac{dn}{dc}) \tag{2.24}$$

On the other hand, we know from thermodynamics that the concentration fluctuation can be expressed as $<(\delta C)^2> = \frac{k_B T}{(\partial^2 A/\partial C^2)_{TV}}$ and $(\frac{\partial^2 A}{\partial C^2})_{TV} = -\frac{1}{CV_m}(\frac{\partial\mu}{\partial C})_{TV}$,

where V_m and μ are respectively the partial volume and chemical potential of the solvent. And the change in concentration can cause the change in osmotic pressure, namely $(\frac{\partial\mu}{\partial C})_{T,V} = (\frac{\partial\mu}{\partial\pi})_{T,V}(\frac{\partial\pi}{\partial C})_{T,V} = -(\frac{\partial\mu}{\partial P})_{T,V}(\frac{\partial\pi}{\partial C})_{T,V} = -V_m(\frac{\partial\pi}{\partial C})_{T,V}$

In dilute macromolecular solution, $\frac{\pi}{C} = \frac{RT}{M}(1+A_2 CM+\cdots)$ where A_2 is the second-order virial coefficient. Thus

$$\left(\frac{\partial \pi}{\partial C}\right)_{T, V} = \frac{RT}{M}(1 + 2A_2CM + \cdots) \quad \text{and} \quad <(\delta C)^2> = \frac{CM}{N_A V(1 + 2A_2CM + \cdots)}$$

Now substitute $<(\delta C)^2>$ and equation (2.24) into the expression of R_{excess}, we have

$$R_{excess} = \frac{4\pi^2 n^2}{\lambda_o^4 N_A}\left(\frac{dn}{dC}\right)^2 \frac{CM}{1 + 2A_2CM + \cdots} \qquad (2.25)$$

Rearrange equation (2.25) by defining $K = 4\pi^2 n^2 (dn/dC)^2 / (N_A \lambda_0^4)$, we get

$$\frac{KC}{R} = \frac{1}{M} + 2A_2C + \cdots \qquad (2.26)$$

where we have omitted the footnote "excess" in R_{excess}. For larger macromolecules, construction factor must be introduced; thus

$$\frac{KC}{R(\theta)} = \frac{1}{MP(\theta)} + 2A_2C \qquad (2.27)$$

The last question in deriving basic equation of static LLS is the polydispersity in real cases. From equation (2.15) we know $P(\theta) = 1 - (1/3)h^2 R_g^2 + \cdots$. Thus, in the limit of vanishing concentration $C \to 0$,

$$R(\theta) = KCMP(\theta) = KCM[1 - (1/3) h^2 R_g^2 + \cdots] \qquad (2.28)$$

Considering the additive nature of the excess Rayleigh ratio, for a polydispersed polymer solution at $C \to 0$

$$R(\theta) = \sum_i R(\theta)_i = \sum_i KC_i M_i[1 - (1/3)h^2 R_{g,i}^2 + \cdots] \qquad (2.29)$$

If we divide equation (2.29) by the total polymer concentration $C = \sum_i C_i$, we get, after slightly re-arrangement,

$$\frac{R(\theta)}{KC} = \frac{\sum_i C_i M_i}{\sum_i C_i}\left(1 - \frac{h^2 \sum_i C_i M_i R_{g,i}^2}{3\sum_i C_i M_i} + \cdots\right) \qquad (2.30)$$

or

$$\frac{R(\theta)}{KC} = M_w[1 - (1/3)h^2 <R_g^2>_z + \cdots] \qquad (2.31)$$

Now, come back to equation (2.27). When $h^2 R_g^2 \ll 1$, omitting the higher order terms in series, we get

$$\frac{KC}{R(\theta)} = \frac{1}{M_w}[1 + \frac{1}{3}h^2 <R_g^2>_z] + 2A_2C \qquad (2.32)$$

This is the basic equation of static LLS which is frequently shown in scientific

papers. Naturally, the molar mass in the equation, $M_w = \sum_i C_i M_i / \sum_i C_i$, is weight-average; and the mean square radius of gyration, $<R_g^2>_z = \sum_i C_i M_i R_{g,i}^2 / \sum_i C_i M_i$, is z-average. It shows that with $R(\theta)$ measured at a series of C and h, we are able to determine $<R_g^2>_z$ from the slope of $[KC/R(\theta)]_{C\to0}$ versus h^2; A_2 from the slope of $[KC/R(\theta)]_{\theta\to0}$ versus C; and M_w from $[KC/R(\theta)]_{C\to0,K\to0}$. The Zimm plot, i.e., $KC/R(\theta)$ versus $(h^2 + kC)$ with k being an adjustable constant, allows both h and C extrapolations to be made on a single coordinate plane.[12,14] It should be mentioned that Equation (2.32) is valid under the restriction that the polymer solution exhibits no adsorption, no fluorescence, and no depolarized scattering. For branched structures, the Berry[15] plot ($[KC/R(\theta)]^{1/2}$ vs $h^2 + kC$) is more adequately used because it often removes much of the curvature observed in the angular dependence of the Zimm plot. If the structure is expected to be large and globular, the Berry plot is not linearized but still shows upturn. In these cases, it is often appropriate to apply a modified Guinier[16,17] plot, i.e., $\ln[KC/R(\theta)]$ vs $h^2 + kC$ that removes the upturn even more efficiently.

In practice, the Rayleigh ratio is determined by a relative method; namely, by measuring the scattering intensity of a standard such as benzene or toluene, we can calculate the Rayleigh ratio of a give solution by

$$R_{vv}(\theta) = R_{vv}^o(\theta) \frac{I(\theta)_{solution} - I(\theta)_{solvent}}{I(\theta)_{standard}} (\frac{n_{solvent}}{n_{standard}})^\gamma \qquad (2.33)$$

where the subscript "vv" means both the incident and the scattered light are vertically (z-axis direction in Figure 2.1) polarized; I and n are, respectively, the time-averaged scattered light intensity and the refractive index. The term $(n_{solvent}/n_{standard})^\gamma$ is a refraction correction for the scattering volume and γ is a constant between 1 and 2, depending on the detection geometry of the light scattering instrument, because we should compare the same scattering volume from the solution and the reference standard. If we take the incident light as the x-direction and the scattered light as the y-direction (i.e., $\theta = 90°$), we only need to have a linear correction of the refraction in the x-direction if a slit is used to determine the scattering volume, i.e., $\gamma = 1$ because we have already seen all the scattered lights in the z-direction (vertical). On the other hand, if a pinhole with a size much smaller than the diameter of the incident beam at the center of the scattering cell, we have to correct the refraction in both the x- and

z-directions, i.e., $\gamma = 2$. However, if the pinhole size is comparable to the beam diameter, $1 < \gamma < 2$. In practice, we should avoid this situation by choosing either a slit or a smaller pinhole.[2,5]

2.3 Dynamic Laser Light Scattering

Motions (translational, rotational or internal motion) of macromolecules or colloidal particles in solution can be conveniently studied by using dynamic laser light scattering (dynamic LLS). Measurement at a single scattering angle (or at a finite h) gives information on the dimension of macromolecules or colloidal particle in the solution with reasonable accuracy. Unlike the static LLS version, dynamic LLS does not rely on the excess scattering intensity between the pure solvent and a dilute solution. The signal from the slowly moving polymer is unambiguously separated from the signal that originates from the rest of the solution. The principle of dynamic LLS has been untilized in some commercial particle-sizing systems for many years. The measurement and data analysis are automated. Users only need to prepare clean solutions by filtration. In recently years, dynamic LLS has been also used as an on-line detector in size exclusion chromatography (SEC).[5] Nowadays, the most commonly used method in quasi-elastic light scattering (QELS) is the digital technique of photon correlation spectroscopy (or optical mixing) which measures the intensity fluctuation of scattered light in time domain. Practically there are two basic forms of optical mixing: heterodyne and homodyne (self-beating). By heterodyne mixing we refer to the mix of the scattered light with a reference beam (local oscillator) unshifted or shifted in frequency from the incident light beam. In self-beating optical mixing the scattered wave is not mixed with a reference signal but directly detected. Here we only consider the self-beating intensity-intensity time correlation spectroscopy.

2.3.1. Power spectrum of scattered light

Now we consider again an N particle (macromolecule or colloidal particles) scattering system with scattering volume V. We view N particles as N scatters. Thus, the scattered field as well as the scattered intensity at point p in Figure 2.1 can still be expressed using equation (2.7) and (2.8) and they are,

$$\vec{E}(t) = \sum_{i=1}^{N} \vec{E_i}(t) = -\frac{4\pi^2}{\lambda_0^2 r} \alpha'_o \, \vec{E_0} \sum_{i=1}^{N} \exp i[2\pi vt - \phi_i(t)] \tag{2.34}$$

and

$$I(t) \propto \sum_{i=1}^{N} \sum_{j=1}^{N} \exp i\, \vec{h}[\vec{r_i}(t) - \vec{r_j}(t)] \tag{2.35}$$

Note $\phi_i(t)$ represents the phase term of ith particle and is now a function of time due to the motion of the particles. Same situation should be applied to $I(t)$ and $\Delta\phi_{ij}(t)$ because $\Delta\phi_{ij}(t) = \vec{h} \cdot \vec{r_{ij}}(t)$ and $\vec{r_{ij}}(t)$ will have different orientation at different time t. When the scatters are undergoing Brownian motion, $\vec{E}(t)$ has a randomly modulated phase. The scattered light is broadened in frequency with an optical frequency distribution, or, power spectrum $S(\omega)$ as illustrated in Figure 2.3.
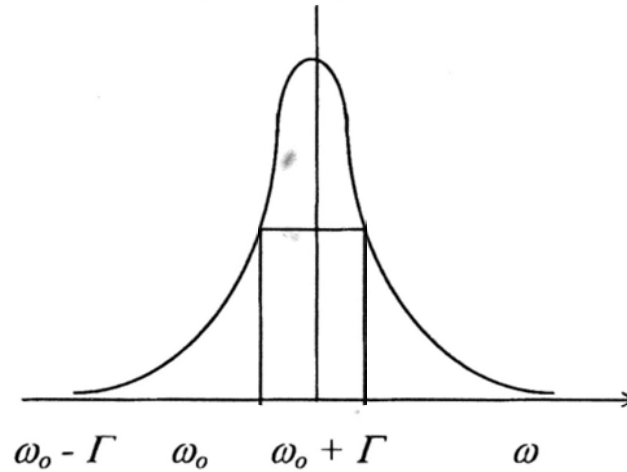
Figure 2.3 The power spectrum $S(\omega)$ of scattered light: a Lorentzian optical frequency distribution centered by the angular frequency of the incident light ω_0 with line width of Γ.

Since the motion of the particles has no preferred direction, the optical spectrum of scattered light contains a continuous distribution of frequencies, i.e., Lorentzian distribution centered by ω_0, the angular frequency of the incident light:

$$S(\omega) = \frac{2\Gamma}{\Gamma^2 + (\omega - \omega_o)^2} \tag{2.36}$$

It can be seen from Figure 2.3 and equation (2.36) that when $\omega = \omega_o$, $S(\omega) = 2/\Gamma$; and when $\omega = \omega_o \pm \Gamma$, $S(\omega) = 1/\Gamma$. That means when the scattered frequency shifts a distance of Γ from ω_o, the density function of power spectrum $S(\omega)$ is half the value that of its peak value. For this reason, Γ is called half-width at half-height, or simply, line-width. As stated before, it is difficult to measure Γ (or $S(\omega)$) directly

in frequency domain because $\Gamma << \omega_o$. It is known from mathematics that $S(\omega)$ and the field-field autocorrelation function $<E(0)E^*(t)>$ are a pair of Fourier transform and inverse Fourier transform:

$$< E(0)E^*(t) > = \int_{-\infty}^{\infty} S_x(\omega)\exp(-i\omega\ t)d\omega \qquad (2.37)$$

$$S(\omega) = \frac{1}{2\pi}\int_{-\infty}^{\infty} < E(0)E^*(t) > \exp(i\omega\ t)dt \qquad (2.38)$$

These two equations are known as Wiener-Khintchine theory. Thus, $S(\omega)$ and $<E(0)E^*(t)>$, two functions originally located in frequency domain and time domain respectively, are now connected with each other.

2.3.2 Siegert relation[2]

Another important equation in dynamic LLS is Siegert relation. Without a local oscillator (i.e., a constant fraction of the incident light reaching the detector from various intentional sources, such as surface scratching or reflection), the self-beating of the scattered electric field leads to normalized intensity-intensity autocorrelation function, $g^{(2)}(h,t)$ based in essence on the Sieget relation:

$$g^{(2)}(h,t) = 1 + \left|g^{(1)}(h,t)\right|^2 \qquad (2.39)$$

where $g^{(2)}(h,t) \equiv [<I(h,0)I(h,t)> / <I(h,0)>^2]$ and $g^{(1)}(h,t) \equiv [<E(h,0)E^*(h,t)> / <E(h,0)E^*(h,0)>]$ is the normalized field-field time correlation functions. Thus, the intensity-intensity time correlation function

$$G^{(2)}(h,t) = <I(h,0)I(h,t)> = <I(h,0)>^2\ g^{(2)}(h,\ t)$$
$$= <I(h,0)>^2[1 + |\ g^{(1)}(h,\ t)|^2] \qquad (2.40)$$

The significance of introducing $g^{(2)}(h,t)$ and $G^{(2)}(h,t)$ lies in the fact that $G^{(2)}(h,t)$ and $<I(h,0)>$ can be measured experimentally. In practice, the detection area can not be zero no matter how small it is. Therefore, the scattered light detected can not be purely coherent and an instrument parameter, β (<1), is introduced in equation (2.40):

$$G^{(2)}(h,t) = A(1 + \beta\left|g^{(1)}(h,t)\right|^2) \qquad (2.41)$$

where $A(\equiv< I(h,0) >^2)$ is the baseline, t is the delay time, β is a parameter depending on the coherence of the detection optics, and $I(t)$ is the detected scattered intensity or photon counts at time t, including contributions from the solvent and the solute. Therefore, $G^{(2)}(h,t) = <[I_{solvent}(h,0) + I_{solute}(h,0)][I_{solvent}(h,t) + I_{solute}(h,t)] >$ and

36

equation (2.41) becomes

$$G^{(2)}(h,t) = A\left\{1 + \beta\left[\frac{I_{solvent}}{I_{solution}} \mid g^{(1)}_{solvent}(h,t)\mid + \frac{I_{solute}}{I_{solution}} \mid g^{(1)}_{solute}(h,t)\mid\right]^2\right\} \quad (2.42)$$

where all the cross terms have been dropped by assuming that the light scattered by solvent molecules and particles is not correlated. It should be noted that $\mid g^{(1)}_{solvent}(h,t)\mid$ decays much faster than $\mid g^{(1)}_{solute}(h,t)\mid$ because small solvent molecules diffuse much faster than larger particles. Thus, after a very short delay time, equation (2.42) becomes

$$G^{(2)}(h,t) \cong A[1 + \beta\left(\frac{I_{solute}}{I_{solution}}\right)^2 \mid g^{(1)}_{solute}(h,t)\mid^2]$$

$$= A[1 + \beta_{app}\left|g^{(1)}_{solute}(h,t)\right|^2] \quad (2.43)$$

where $\beta_{app} = \beta(I_{solute}/I_{solution})^2$. For a dilute solution, the scattered intensity from solvent molecules could become appreciable (i.e., $I_{solute} \leq I_{solution}$) and thus the apparent coherence β_{app} would be lower, i.e., $G^{(2)}(h,0)$ appears to have a very low value than expected. We should be aware of this situation, especially for weakly scattered dilute and low-molar-mass polymer solution. For example, if $I_{solute} = I_{solvent}$, $\beta_{app} = \beta/4$. It should be noted that β is constant for each particular optical geometry of the scattering instrument. In fact, I_{solute} can be estimated from β_{app} if the values of β at different scattering angles have been pre-calibrated with a narrowly distributed latex standard whose scattering intensity is much stronger than water (solvent), as first demonstrated by Sun et al[18].

2.3.3 Translational diffusions

Now we will see how to get the information about the motion of the particles from the measured intensity-intensity time correlation function $G^{(2)}(h,t)$. Generally, the relaxation of $\mid g^{(1)}(h,t)\mid$ includes both diffusion (translation and rotation) and internal motions. Let us first consider the translational diffusion relaxation of the particles. For monodispersed spherical scatters, $\mid g^{(1)}(h,t)\mid$ is theoretically represented as an exponential decay function:

$$\mid g^{(1)}(h,t)\mid = G\exp(-\Gamma t) \quad (2.44)$$

where G and Γ are the factor of proportionality and the line-width, respectively and $\Gamma = \tau_c^{-1}$, the characteristic decay time representing the rate of dynamic relaxation in

self-beating. For a polydispersed polymer sample with a continuous distribution of molar mass M, equation (2.44) may be generalized as

$$|g^{(1)}(h,t)| = \int_0^\infty G(\Gamma)\exp(-\Gamma t)d\Gamma \qquad (2.45)$$

where $G(\Gamma)$ is called the line width distribution and $G(\Gamma)d\Gamma$ is the statistic weight of the particles or macromolecules which possess line width Γ. For a dilute solution, Γ measured at a finite scattering angle is related to C and h by[19]

$$\Gamma = h^2 D_0 (1+k_d C)(1+ f h^2 <R_g^2>_z) \qquad (2.46)$$

where D_0 is the translational diffusion coefficient of the solute molecule at $C \to 0$, k_d is the diffusion second virial coefficient, and f is a dimensionless parameter depending on polymer chain structure and solvent (For polymers with flexible chains in a good solvent, f is between 0.1 and 0.2). Hence, for small C and h, $D_0 \approx \Gamma h^2$ and it is apparent that $|g^{(1)}(h,t)|$ decays faster at a higher scattering angle. Figure 2.4 demonstrates the linear dependence of the line with Γ on the scattering vector h and shows that this relaxation mode has diffusive character.
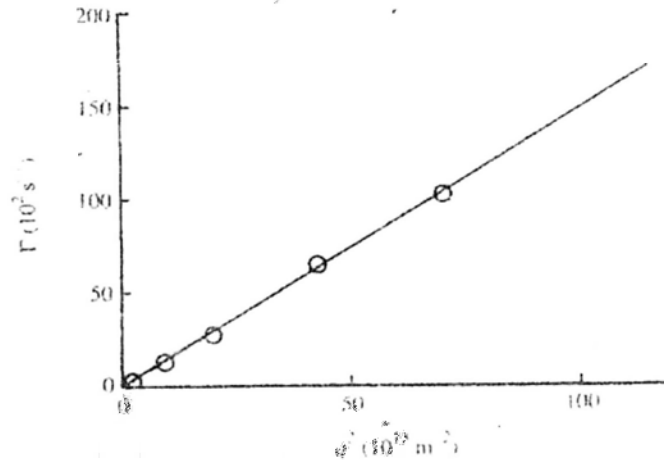
Figure 2.4 Linear dependence of the characteristic line width Γ on scattering vector h.

It should be noted that by the definition of $|g^{(1)}(h,t)|$, $G(D_0) = h^2 G(\Gamma)$, the translational diffusion coefficient distribution, is an intensity distribution. And, since $|g^{(1)}(h,t)|$ approaches unity as $t \to 0$, we have

$$|g^{(1)}(h \to 0, t \to 0)| = \frac{\langle E(h,0)E^*(h,t \to 0)\rangle}{\langle E(h,0)E^*(h,0)\rangle} = \int_0^\infty G(\Gamma)d\Gamma = \int_0^\infty G(D_0)dD_0 = 1 \quad (2.47)$$

The average diffusion coefficient $<D_0>$ is defined as

$$< D_0 > = \int_0^\infty G(D_0)D_0 dD_0 \qquad (2.48)$$

Further, the translational diffusion coefficient D_0 may be related to the molecular friction factor f through the Stokes-Einstein relation

$$D_0 = k_B T / f \qquad (2.49)$$

where k_B and T are the Boltzmann constant and the absolute temperature respectively. For a hard sphere with a radius of R, $f = 6\pi\eta R$, where η is the viscosity of the solvent. For a polymer coil, R is replaced by its hydrodynamic radius R_h, so that

$$R_h = \frac{k_B T}{6\pi\eta D_0} \qquad (2.50)$$

2.3.4   Analysis of the correlation function profile

Equation (2.45) indicates that once $|g^{(1)}(h,t)|$ is determined from $G^{(2)}(h,t)$ through equation (2.41), $G(\Gamma)$ and then $G(D_0)$ can be computed from the Laplace inversion of $|g^{(1)}(h,t)|$.[7,25,26] In the last three decades, many computation programs were developed. At the earlier stage, the computation speed was a very important factor in the development of the programs. This constraint has gradually been removed because the personal computer has become faster and faster in the last 10 years. Among many programs, the CONTIN program developed by Provencher[27] is still one of the most widely used and accepted programs for this computation. However, it should be noted that equation (2.41) is one of the first kind Fredholm integral equations. Its inversion is an ill-conditioned problem because of the bandwidth limitation of photon correlation instruments, some unavoidable noises in the measured time correlation function, and a limited number of data points. In other words, the data of $g^{(1)}(h,t)$ do not always provide information necessary and sufficient to determine $G(\Gamma)$ uniquely. Thus, in practice, reducing the noise in the measured intensity-intensity time correlation function becomes more important than choosing a program for data analysis. For this reason, it is crucial that the sample solution is cleaned (i.e., made "dust-free") very thoroughly before it is subjected to laser light scattering measurements. A common guideline is to keep the relative difference between the measured and calculated baselines not exceeding 0.1%. The error analysis related to the above problem can be found elsewhere.[28,29]

It is worth to note that there is a temptation among the users of dynamic LLS to

extract too much information from the measured intensity-intensity time correlation function. In the literature, three or even four peaks in $G(D_0)$ were often reported. It is meaningless because they were actually extracting "data" from experimental noises. It has to be warned that even a bimodal distribution of $G(D_0)$ has to be well justified by other physical evidence or pre-experimental knowledge. This does not mean that many of the Laplace inversion programs developed in the past are useless. On the contrary, they have been quite successful in retrieving the desired information, especially in terms of the average line width $<\Gamma>$ ($\equiv \int_0^\infty \Gamma G(\Gamma)d\Gamma$) and the relative width ($\mu_2/<\Gamma>^2$) of the line-width distribution ($G(\Gamma)$) with $\mu_2 = \int_0^\infty (\Gamma - <\Gamma>)^2 G(\Gamma)d\Gamma$. Therefore, the Laplace inversion as a very helpful method in the analysis of the line width distribution $G(\Gamma)$, should be used with a clear understanding of its ill-conditioned nature and its limitations.

In practice, if one is only interested in the determination of $<\Gamma>$ and $\mu_2/<\Gamma>^2$, a fast but more limited cumulants analysis adopted by Koppel[30] can be used, wherein $[G^{(2)}(h,t) -A]/A$ is expanded as

$$\ln \frac{G^{(2)}(h,t) - A}{A} = (1 + \ln \beta) - <\Gamma> t + \frac{\mu_2 t^2}{2!} - \frac{\mu_3 t^3}{3!} + \cdots \qquad (2.53)$$

where

$$\mu_m = \int_0^\infty (\Gamma - <\Gamma>)^m G(\Gamma)d\Gamma \qquad (2.54)$$

is the mth moment of the line-width distribution $G(\Gamma)$. A mth order cumulants fit means that all the terms higher than t^m in equation (2.53) are terminated in the data analysis. The first cumulant Γ, sometimes also called the initial slope, is an important quantity, since it can be calculated for many physical systems and situations.[31,32] The second cumulant μ_2 is a measure of the width of the distribution. For unimodal distributions of slightly polydispersity polymers in solution, the following relation has been derived:[32]

$$\mu_2 / \Gamma^2 \approx (M_z / M_w - 1) / 4 \qquad (2.55)$$

It is worth noting that, in practice, the cumulants fit can be used for a relatively narrow characteristic line-width distributions. For $\mu_2/<\Gamma>^2 < \sim 0.2$, the second order cumulants fit is normally sufficient, while when $\mu_2/<\Gamma>^2$ is in the range ~ 0.2-0.3, the third order cumulants fit is required. For even higher values of $\mu_2/<\Gamma>^2$, higher order expansions should be used. However, it is often difficult to find how many terms are sufficient to

obtain a meaningful results because using too many terms in the cumulants fit might lead to an over-fitting of experimental noises. Therefore, for a broadly distributed sample, the use of cumulants fit is very tedious. On the other hand, the use of CONTIN could yield reliable $<\Gamma>$ and $\mu_2/<\Gamma>^2$ values under all conditions as long as the measured time correlation function was obtained within a proper bandwidth range and the photon counts have sufficient statistics, e.g., the baseline (A) has a total counts over 10^6. However, it warns that the line-width distribution obtained from the Laplace inversion is only an estimate. One should be aware of the limitations, yet must realize that the Laplace inversion methods can provide useful information and distinguish between unimodal and multimodal line-width distributions, especially, when the peak positions are separated by a factor of more than 2.

2.4 Practice of Laser Light Scattering

A laser light scattering spectrometer contains a limited number of components; namely the light source, the optics, the cell holder and the detector. Nowadays, an LLS instrument should have a digital output (single photon counting) from a fast photomultiplier, i.e., the output current pulse have already been treated by pre-amplifier/amplifier/discriminator before it is connected to a time correlator which is often a single plug-in board to a PC computer.

2.4.1   Light source.

Traditionally, the light source is a helium-neon (He-Ne) laser with a wavelength of 632.8 nm and an output power of 5-50 mW or an argon-ion (Ar^+) laser with a wavelength of 488 or 514.5 nm and an output power of 50-400 mW. Krypton lasers have also been used because of their wavelength can be longer than 632.8 nm of the He-Ne laser. The additional cost and somewhat short plasma tube life are drawbacks.

The laser used in dynamic light scattering should have a TEM_{00} mode with a Gaussian intensity profile so that it can be focused to produce a higher power density for the incident beam, which leads to a smaller scattering volume and a higher coherent factor in the optical mixing experiment. Many commercial laser companies can produce stable laser light sources suitable for LLS experiments. A laser with a beam amplitude RMS noise less than 0.5% should be chosen so that the noise level of the intensity-intensity time correlation function in dynamic LLS will not be affected and a

long-term amplitude stability less than ±1% for the convenience of time-averaged scattered light intensity measurements. It should be noted that in dynamic LLS measurements, long-term stability is usually not very important since the maximum delay time is normally no more than a few minutes, typically less than 1 second.

2.4.2 Optics and cell design.

The mechanical parts of Laser Light Scattering instrument is called goniometer including a cell holder and an co-axial and accurately angular-controlled rotatable arm on which the fast and sensitive avalanche photo diode (APD) detector is located. The conventional sample cell holder in LLS normally consists of a hollow cylindrical brass block with an outside diameter of 50-80 mm and an inside diameter of 10-20 mm which matching the outside diameter of the scattering cell. The brass block is normally placed inside a cylindrical optical glass cup filled with a refractive index matching fluid (e.g, xylene, toluene, and silican oil) whose refractive index is very close to that of optical glass (~1.5) to reduce surface scattering and the curvature of the scattering cell. A water circulation from a thermostat precisely controls the temperature of index matching vat. A proper alignment of the optical path is normally judged by the constant scattered intensity for benzene or toluene after scattering volume correction by $\sin\theta$ to within 1% (if the scattering volume is chosen by a slit) or 2% (if a small pinhole is used) over an angular range ~15-150°. In principle, the scattering cell with an optical quality should be used. However, in practice, a selected normal cylindrical sample vial can also be used as the scattering cell, which greatly reduces the experimental cost and make the scattering cell disposable.

2.4.3 Detector

A high quantum efficiency avalanche photo diode (APD) detector in Geiger mode is used. APD detector has a higher photon count rate than a conventional photo multiplier tube (PMT), leading to a faster and more sensitive response to photon irritations. Overall quantum efficiencies of 70 percent at 633 nm are reachable for modern APDs, which is very suitable for the light source (λ = 632.8 nm) we are using as the range of wavelength for the maximum performance of the detector lies between 600 nm to 750 nm. The output signal is then treated by amplifier before it is connected

to the multiple tau digital time correlator situated in a PC computer. The APDs show a very low dark count (< 30 Hz) contribution and response to signal pulse quickly enough for dynamic light scattering sampling. The rotatable arm makes it possible for the APD detector to get both dynamic and static data at different angles.

2.4.4 Sample Preparation

If a macromolecule can be dissolved in more than one solvent, the choice of solvent for LLS should be made generally according to the following guidelines: 1) colorless to avoid the adsorption correction, 2) a higher contrast, i.e., a higher dn/dC, and 3) less polar and less viscous to make the dust-free easier.

2.4.5 Differential refractometer

To have a good accuracy in the estimates of M_w, $<R_g^2>_z$ and A_2, the specific refractive index increment (dn/dC) must be evaluated with a high accuracy because the relative error in dn/dc is doubled in the errors in M_w, $<R_g^2>_z$ and A_2. The dn/dc is usually measured by using a differential refractometer for solutions of the polymer at different concentrations in the dilute regime. Fitting the plot of Δn as a function of c by a straight line through the origin gives the value of dn/dC. The measurement of dn/dC must be done at the same temperature and wavelength as those in the light-scattering measurement.

In our refractometer,[33] a small pinhole with a diameter 400μm is illuminated with laser light. The illuminated pinhole is imaged to a position sensitive detector by a lens located at an equal distance ($2f$-$2f$) form the pinhole and the detector. A temperature-controlled refractometer cuvette is located in front of the lens. When sample was injected into the cuvette, the displaced light beam refracted at the boundary between the sample and reference liquid from the center of the detector was transferred into output voltage and measured by a digital voltmeter. Since the laser source of the set up can be changed, by choosing a laser source with the same wavelength of the source used in Laser Light Scattering experiment, correction is no needed for the refractive index increment measured. This novel design has made the measurement of Δn much easier and provides reliable and accurate values of (dn/dC) from the instrument's stability.

2.5 Ultrafiltration experimental setup and data analysis

The ultrafiltration experimental setups are illustrated in figure 2.5. A double layer membrane (Whatman, Anotop 10) with two different pore sizes (20 and 100 nm) were used and the detail structure is shown in figure 2.6. Each smaller pore with diameter 20 nm or 100 nm is covered by a larger pore with diameter 200 nm. The average pore density is 5×10^8 per membrane, and the length of the smaller pore is 1μm. Such double-layer structure can prevent some possible interference among flow fields generated by different pores, leading to a pure elongation flow without any rotational ones as required by the theory.
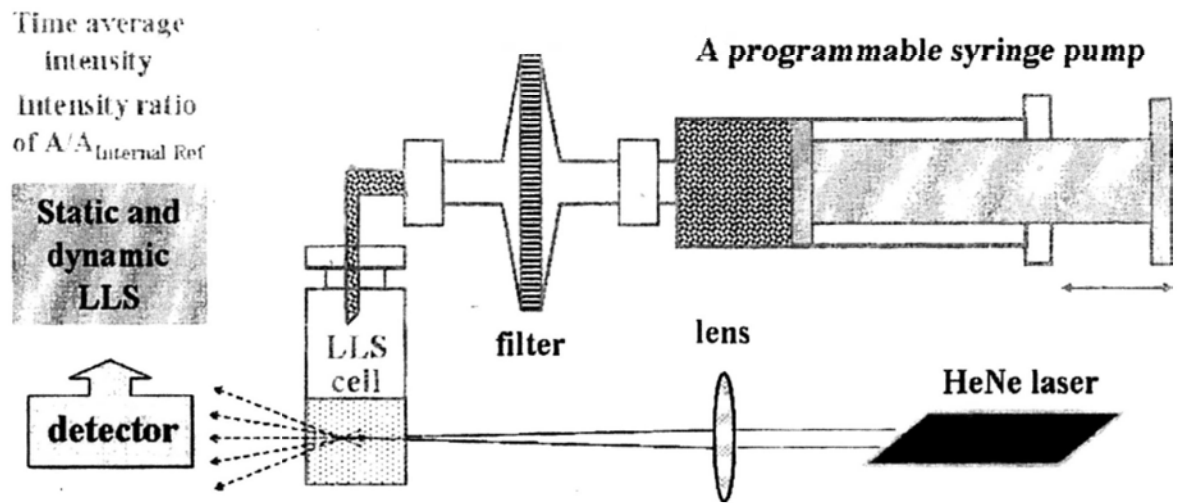

Figure 2.5 The illustration of ultrafiltration experimental setup.
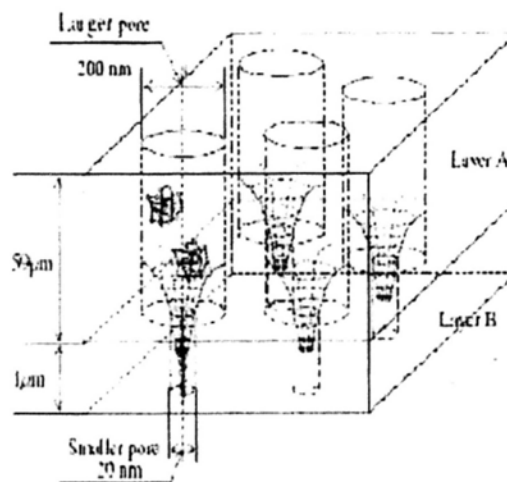

Figure 2.6 Illustration of Structure of membrane filter

A gas tight syringe (SGE, 5 mL) is used to contain polymer solution, and a syringe pump (Harvard Apparatus, PHD 2000) and an incubator (Stuart Scientific, S160D)arat (± 0.1 °C) were used to control the flow rate and temperature respectively. The polymer solution were ultrafitrated and collected by a LLS cell as shown in figure 2.5 and further characterized by a combination of static and dynamic laser light scattering.

Two polymers were used in each ultrafiltration, namely, with one is bigger than the pore size and the other one is much smaller than the pore size. Note that the smaller one has no retention concentration at any flow rate and works as internal reference; the bigger ones could be deformed and pass through the nanopores as long as the flow rate is overcome critical flow rate q_c.

In each ultrafiltration, the concentrations of the large and short polymer chains (C_L and C_S) are properly chosen so that $C_L M_L / C_S M_S \sim 1$, where M_L and M_S are the molar mass of the large and short chains, respectively. Therefore, the corresponding time-average scattered light intensities from short and large chains are similar, i.e., $<I_L>/<I_S> \sim 1$. $<I_L>/<I_S>$ equals the area ratio of their corresponding peaks in $G(\Gamma)$. The area under each peak (A) is proportional to the time-averaged intensity of the light scattered from one PS standard. Therefore, the area ratio of the two peaks (A_l/A_S) equals the ratio of the scattered light intensities (I_L/I_S) of small and larger polymers in the solution mixture.

$$A_S/A_L = I_S=I_L = C_S M_S / C_L M_L \qquad (2.56)$$

and the total time-averaged scattered light intensity ($<I>$) of the solution mixture at infinite dilution solution and the zero scattering angle equals the sum of I_S and I_L, i.e.,

$$<I> = (I_S + I_L) = P(C_S M_S + C_L M_L) \qquad (2.57)$$

where P is a constant for a given type of polymer and solvent. The left sides of Eqs. (2.56) and (2.57) can be measured from dynamic and static LLS, respectively. For a given solution mixture, P, M_S, and M_L are three known constants .C_S and C_L can be calculated from Eqs. (2.56) and (2.57). Then the block degree of the bigger polymer can be calculated based on the C_S and C_L as shown in figure 2.7.
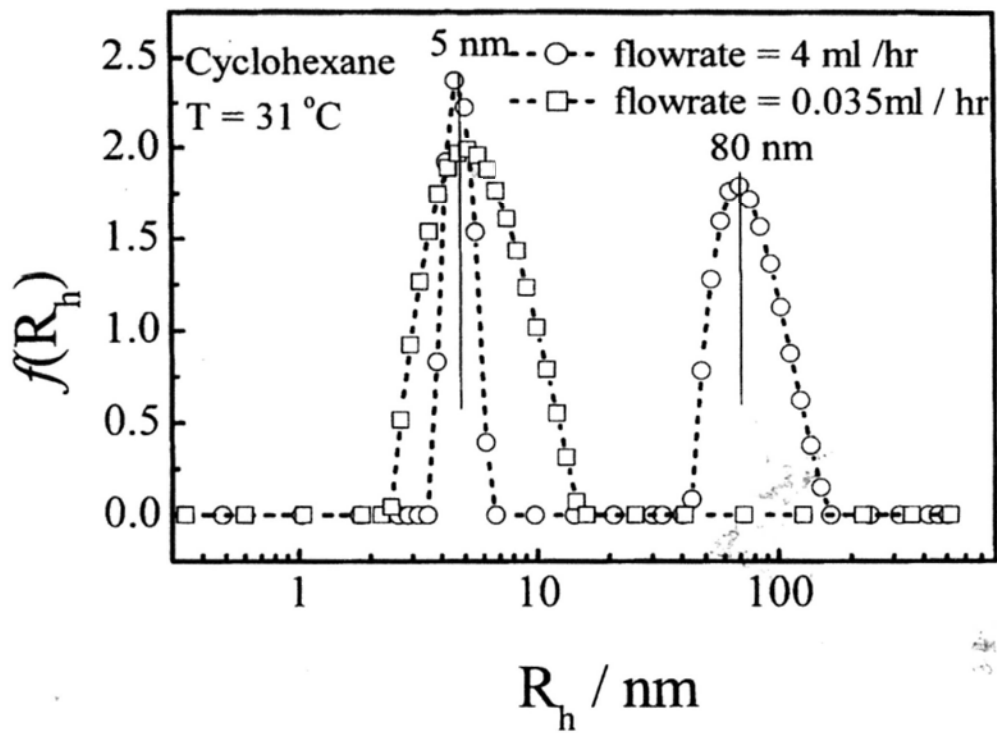
Figure 2.7 The hydrodynamic radius distribution of two kinds of Polystyrene chains in cyclohexane after ultrafiltrating with two different flow rates.

2.6 References

[1]   Chu, B. *Laser Light Scattering: Basic Principles and Practice*, 2nd ed.; Academic Press: New York, 1991.

[2]   Berne, B. J.; Pecora, R. *Dynamic Light Scattering*, John Wiley & Sons Press: New York, 1972.

[3]   Huglin, M. B. Ed., *Light Scattering from polymer solution*, Academic Press: New York, 1972.

[4]   Schmitz, K. S. Ed., *An introduction to Dynamic Light Scattering by Macromolecules*, Academic Press: Boston, 1990.

[5]   Wu, C.; Chu, B. *Light Scattering* In Tanaka, T. Ed., *Experimental Methods in Polymer Science*, Academic Press: San Diego, 2000. pp 1-56.

[6]   Brown, W. Ed., *Light Scattering: Principles and Development*, Clarendon Press: Oxford, 1996.

[7]   Brown, W. Ed., *Dynamic Light Scattering: The method and some applications*, Clarendon Press: Oxford, 1993.

[8]   Wu, C.; Gao, J. *Modern Laser Light Scattering: a powerful tool for the study of macromolecules and colloids*, In He, T. B.; Hu, H. J. Eds., *New Developments in Polymer Science Abroad*; Chemical Industry Press: Beijing, 1997.

[9]   Teraoka, T. *Polymer Solutions: An Introduction to Physical Properties*, John Wiely & Sons Press: New York, 2002.

[10]   Munk, P. *Introduction to Macromolecular Science*; John Wiley & Sons Press: New York, 1989.

[11]   Atkins, P. W. *Physical Chemistry*; 6th ed., Oxford University Press: Oxford, 1998.

[12]   Zimm, B. H. *J. Chem. Phys.* **1948**, *16*, 1099.

[13]   Cummins, H. Z.; Knable, N.; Yeh, Y. *Phys. Rev. Lett.* **1964**, *12*, 150.

[14]   Burchard, W. *Light Scattering Techniques* In *Physical Techniques for Study of Food Biopolymers;* Ross-Murphy, S. B., Ed., Blackie Academic & Professional: London, 1995, Chapter 4.

[15]   Berry, G. C. *J. Chem. Phys.* **1966**, *44*, 4550.

[16] Guinier, A. *Ann. Phys.* **1939**, *12*, 161.

[17] Guinier, A.; Fournet, G. *Small Angle Scattering of X-rays*; Wiely: New York, 1955.

[18] Sun, S. T.; Nishio, I.; Swislow, G.; Tanaka, T. *J. Chem. Phys.* **1980**, *73*, 5971.

[19] Stockmayer, W. H.; Schmidt, M. *Macromolecules* **1984**, *17*, 509.

[20] Russo, P.S., In *Dynamic Light Scattering: The method and some applications*, Brown, W, Ed., Clarendon Press: Oxford, 1993. Chapter. 12.

[21] de Gennes, P. G. *Scaling Concepts in Polymer Physics;* Cornell University Press: Ithaca, NY, 1979.

[22] Shibayama, M.; Norisuye, T. *Bull. Chem. Soc. Jpn.* **2002**, *75*, 641 and the references therein.

[23] Adam, M.; Delsanti, M.; Munch, J. P.; Durand, D. *Phys. Rev. Lett.* **1988**, *61*, 706.

[24] Martin, J. E.; Wilcoxon, J. *Phys. Rev. Lett.* **1988**, *61*.373.

[25] Chu, B.; Ford, J. R.; Dhadwal, H. S. *Methods Enzymol.* **1983**, *117*, 256.

[26] Chu, B.; Wu, C.; Ford, J. R. *J. Colloid Interface Sci.* **1985**, *105*, 473.

[27] Provencher, S. W. *J. Chem. Phys.* **1976**, *64*, 2772.

[28] Raczek, J. *Eur. Polym. J.* **1983**, *19*, 607.

[29] Nordmeier, E.; Lechner, M. D. *Polym. J.* **1989**, *21*, 623.

[30] Koppel, D. E. *J. Chem. Phys.* **1972**, *57*, 4814.

[31] Akcasu, Z. *Polymer*, **1980**, *21*, 866.

[32] Akcasu, Z.; Han, C. C. *Polymer*, **1981**, *22*, 1019.

[33] Wu, C., Xia, K.Q. *Review of Scientific Instruments*, **1994**, *65*, 587.

Chapter 3
Star Polymers synthesized by Living Anionic Polymerization

3.1 Introduction

3.1.1 History of anionic polymerization

Anionic addition polymerization is a chain growth polymerization, whose propagation is through monomers reacting with strong electronegative group.[1] Anionic polymerization dates back to the early part of the 20th century, when Matthews, Strange in England and Harries in Germany used sodium and potassium to initiate the polymerization of isoprene.[2,3] Then in 1934, Ziegler and his coworkers reported using sodium, lithium or alkyllithium species to polymerize butadiene, isoprene, and 2,3-dimethylbutadiene.[4-6] It was the first unambiguous report of using lithium or its derivatives in the polymerization of dienes.[7]

It was not until the post of the Second World War, the formal recognition of an anionic mechanism was set up. Firstly, Beaman[8] polymerized methacrylonitrile, a polor monomer, with initiating by strong bases as Grignard reagents and triphenylmethylsodium. He also suggested such polymerization was proceeded by the nucleophilic attacking the growing carbanion on the electrophilic double bond of the monomer; Then Sanderson and Hauser[9] further showed nonpolar monomer, namely styrene could also be polymerized by sodamide, in the case of liquid ammonia as the solvent. Though the molecular weights was low due to proton transfer from the ammonia solvent, they proposed it was initiated by the amide anion and propagated in carbanionic mechanism. It was also at that time, Walling et al. published another significant paper describing the copolymerization of styrene and methyl methacrylate induced by various initiators, based on which they tested the character of the propagation step,[10] the profound differences in copolymer compositions led them to conclude the polymerization initiated by sodium or potassium must be carbanion in náture, such observation has been one of the strongest evidence for certification of anionic nature of sodium initiated polymerization.

With the help of Moshe Levy and Ralph Milkovich, Szwarc developed an all-glass, high-vacuum technique apparatus, which could effectively prevent the

interference by impurity like atmosphere. They proved that the styrene anions are undying and could propagate as long as new monomers are added.[11,12] Since then, with the development of high vacuum technique, the anionic polymerization method is widely used in synthesizing macromolecules with more complicated architectures.[6,13-22]

3.1.2 Mechanism of anionic polymerization.

Normally, there are three addition polymerization mechanisms of unsaturated (or cyclic) monomers, i.e., free radical, cationic, and anionic polymerization respectively.[7] The addition polymerizations are usually divided into three steps, namely, chain initiation, chain propagation, and chain termination or chain transformation. However, for living polymerizations, the formal termination pathway is lacked.[1,7] In present paper, the anionic polymerization of styrene and dienes are mainly discussed.

3.1.2.1 Initiation Reaction.

Usually, alkyllithium compounds and other organometallic compounds are used to initiate vinyl monomers in hydrocarbon solvents or in polar media with presence of a variety of ionic species.[1] However, the initiation rate in polar solvent is too rapid to be measured, and the metal alkyls in non polar solvents are limited in lithium alkyls because of solubility.[23] The initiation rate of hydrocarbon monomers in hydrocarbon solvents by alkyllithium initiators not only depends on the monomer, the initiator, the solvent, and the temperature, but also depends on the associated degree of the alkyllithium compound in the solvent.[24,25] Generally, the addition of Lewis bases is able to dissociate the aggregation of alkyllithium and accelerate the initiation rate.

There are three types of initiators in anionic polymerization: (i) alkali metals, (ii) radiacal anions, and (iii) organoalkali compounds.

(i)   Alkali metals

The initiation by alkali metals is a heterogeneous process by transferring electrons to monomers on the surface of the metal.[26] The initially formed radical anions rapidly dimerize to form dianions and continue growing in solution sequentially. Because of the heterogeneous initiation, new active chain ends are

generated continually during the subsequent propagation reactions. As a result, the distribution of molecular weights are broad ($M_w/M_n = 3-10$).[1]

However, when alkali metals are used to initiate α-methylstyrene in polar solvents such as tetrahydrofuran, homogeneous difunctional initiators are formed. It is because the α-methylstyrene has low ceiling temperature, and the formations of dimmers or tetramers not only depend on the alkali metal system, but also temperature and concentration.[27]

(ii) Radical anions

Radical anions are formed by reacting alkali metals with aromatic hydrocarbons in polar aprotic solvents.[26] Naphthalene is the mostly used to react with Na metal in THF:

The radical anions can only be efficiently formed in polar aprotic solvents such as THF and glymes,[26] and the stability of these complexes depends on the electron affinity of the hydrocarbons, the order is shown as follows:[7]

anthracene > phenanthrene > naphthalene > biphenyl
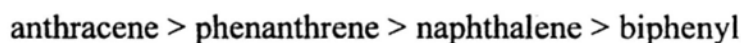
Namely, only in the dipolar aprotic solvents these aromatic radical anions can be used. The electrons transfer reversely between radical anions and monomers, resulting in difunctional endings of anions, styrene is taken as an example:
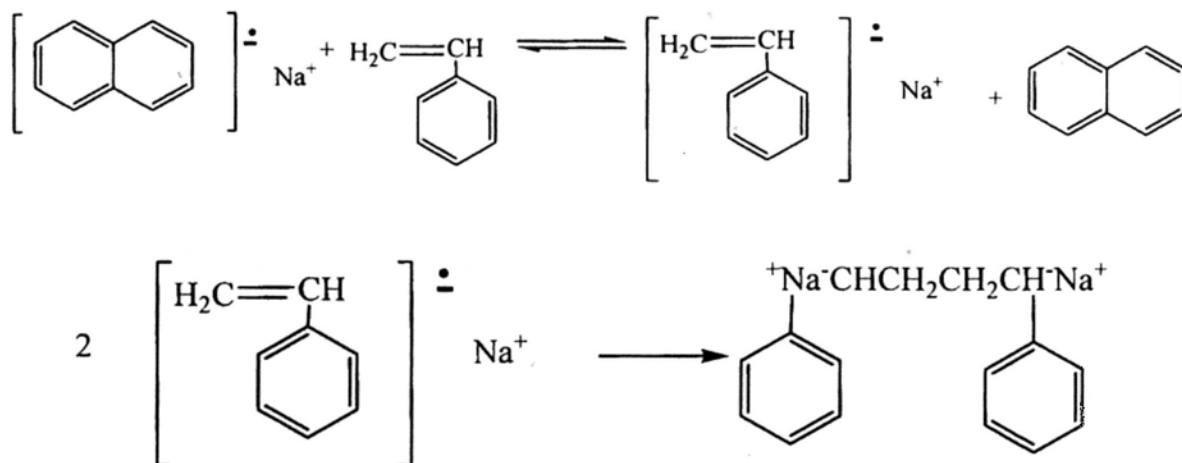
The difunctional growing ending is very useful when synthesizing triblock copolymers, cyclic polymers, telechelics, or more complicated structures as the H-, super H- and Π-shaped polymers.[27]

(iii) Alkyllithium compounds

Because of the commercially availability, alkyllithium compounds are the most versatile and useful anionic initiators.[27] The reactivity of the alkyllithium initiators is directly related with their associated degree, namely, a lower associated degree lead to a higher initiator reactivity.[28,29] The associated degree and the reactivity of various alkyllithium initiators for dienes polymerization is shown as follows:[30]

methyllithium (2) > sec-BuLi (4) > i-PrLi (4-6) > t-BuLi (4) > n-BuLi (6)

and for styrene

methyllithium (2) > sec-BuLi (4) > i-PrLi (4-6) > i-BuLi > n-BuLi (6) > t-BuLi (4)

Though it is effective to use alkyllithium initiators to polymerize styrene and dienes, they are too reactive to be used in polymerizing methacrylates. It is because the alkyllithium initiators will attack the carbonyl group. To avoid the side-reactions, less reactive initiators[31-35] are introduced like using n-BuLi to react with 1,1-diphenylethylene, DPE.

There are other initiators like fluorenyl carbanions, cumyl potassium, 1,1-diphenylmethylcarbanions which are used to initiate the polymerization of styrenes, alkyl methacrylates, and dienes.[1] An appropriate initiator not only has relatively high reactivity, but also avoids side reactions. In a word, the reactivity of appropriate initiator is comparable with the propagating carbanionic species.

3.1.2.2 Propagation Reaction

The propagation step is a bimolecular reaction between the growing chain and the monomer. However, for anionic polymerization the propagation is influenced by the nature of the medium (solvent) and counterion, with the latter one is introduced by the initiator. The general agreement is that the propagation rate is always the first order in monomer concentration, but various of fractional orders related to the concentration of growing chains (i.e., initiator concentration).[36-40] Such situations are due to the dissociation model, as mentioned previously.

3.1.2.3. Termination reaction

Since the carbanions are so strong bases, nearly all the Bronsted-Lowry defined acid, even water, must be avoided in case of terminating growing end.[41] Substances like carbon dioxide and oxygen should also be kept away from the system for their presence will turn the reactive anion to a stable one, which will also terminate the reaction,[42] they should also be avoided. It is well known that ether could react with alkyllithium compounds and form alkenes and lithium alkoxide by cleavage reaction, as shown below[43]

$$RCH_2CH_2OR' + R''Li \rightarrow R''H + RCH=CH_2 + LiOR'$$

The decomposition rates of alkyllithium compounds in ethers depend on the structure of alkyllithium and ether structure as well as the reaction temperature. The reactivity order of alkyllithiums with ethers is 3' > 2' > 1', and the stability of alkyllithium compounds in ethers is: diethyl ether > THF > ethylene glycol dimethyl ether.[1] The reaction rate of alkylmetals with ether is: Li > Na > K.[44] In a word, polar solvents and additives reduce stability of chain end, all of these should be strictly avoided.

3.2 Experimental section

3.2.1. Experimental setups

Because of the extremely high reactivity of carbanions, the anionic polymerizations need to be carried out under the following conditions to obtain polymers with predictable molecular weights and narrow molecular weight distributions: (i) substances that might terminate or transfer growing carbanions should be rigorously excluded; (ii) the reaction conditions like temperature and concentration should be uniform; (iii) the ratio of initiation to propagation rates should be high. To satisfy the above requirement, various laboratory-scale setups including inert atmosphere and high vacuum techniques[45-47] are developed and used.[27,48-51] The inert atmosphere methods are based on using a glove box with the application of a slight overpressure of inert gases (typically N_2 or Ar), the details can be found elsewhere[45-47,52] and will not be discussed in the thesis.

The high-vacuum techniques have been quickly developed since scientists found one of the key points of anionic polymerizations is rigorously experimental techniques.[48] Now, the high vacuum technique is still considered to be the best way to maintain the purity of the system. It includes high vacuum line and specially blown glasswares. Generally, the high vacuum techniques have the follow characteristics:

(i)   All the purification, transfer of reagents as well as polymerization are carried out under high vacuum, the working pressure is at least below ~ 10^{-5} Torr.

(ii)   Before polymerizing, the polymerization reactor is purified by rinsing with n-butyllithium solutions or corresponding initiator solutions used in the experiment. Such process can remove impurities that may react with the initiator or kill the growing carbanions ending.

(iii)   The solvent ampoules, monomer ampoules and coupling agent ampoules are directly connect with polymerization reactors, the connection between ampoules and reactors must be gas tired but easy to be broken. All the apparatuses should be connected with vacuum line directly or indirectly.

3.2.2 Home made high vacuum system

In the present thesis, a home made high vacuum system is used to do the anionic polymerization. Different from previous methods, a new improved design of Rotaflo® high vacuum stopcock is used to take the place of the traditional break-seals connections. Such stopcock can be operated over a pressure range of +1 bar to 10^{-9} Torr and temperature range of $-20°C$ to $200°C$. Further more, the novel connector is easier to handle than break-seal connections and can be used repeatedly. As shown in figure 3.1 by linking a male conically tapered joint with a female one, break and seal the two glasswares connection is easily carried out without glass blowing techniques.
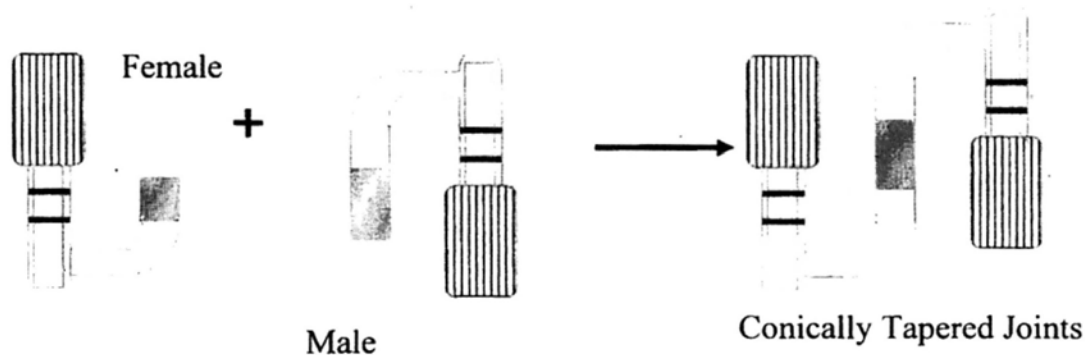
Figure 3.1 Novel connector in home made high vacuum system. Two Rotaflo® high performance stopcocks are connected by a male and a female ground joint.

3.2.2.1 High vacuum line

In the anionic polymerization, the carbanions are easy to be killed by impurities, in this case high vacuum line is widely used in purifying reagent as well as removing impurities in polymerization reactor. The illustration of the home made high vacuum line is shown in Figure 3.2. The main parts of the high vacuum line are rotary pump, diffusion pump, two liquid nitrogen cold traps and stopcocks. First, the rotary pump is applied to reduce the pressure of the system to 10^{-3} Torr; then the diffusion pump is run to further decrease the pressure of the system to 10^{-6} Torr. The two liquid

nitrogen traps are employed to condense any volatile substances for preventing impurities entering the systems as well as protecting oil of the two pumps from contamination. The stopcocks are used to link bubble flowmeter and glassware with the main vacuum line. They also play an important role of controlling the conversion of vacuum and argon atmosphere. All the glass apparatuses including the reactors are linked to the high vacuum line through PORTEX PCV high vacuum tubing.
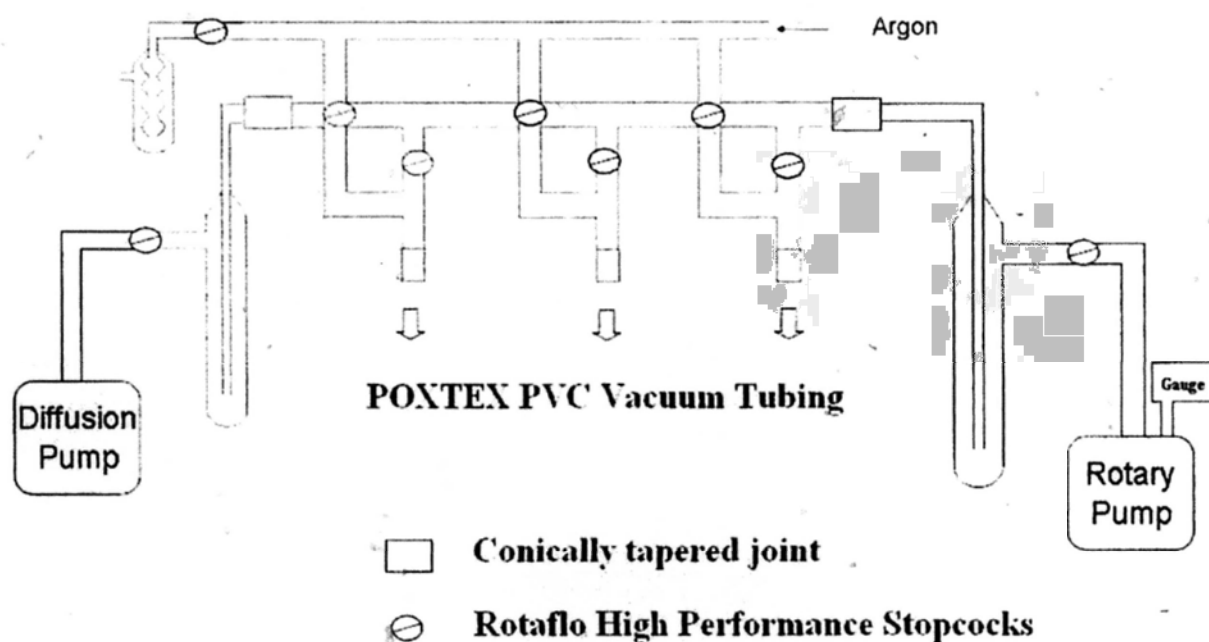
Figure 3.2 Home made high vacuum line with argon system.

3.2.2.2 Interchangeable glasswares

The interchangeable glassware apparatus used for monomer and solvent purification and for polymerization are shown in Figure 3.3.

Reactor: Reactor is used to do the anionic polymerization. Normally, the main part of reactor is a round bottom flask with several necks upward and one neck downward. One of the upward necks is connected with the vacuum line by POXTEX PVC vacuum tubing, and the other upward necks are connected with the various ampoules by conically tapered joints as shown in figure 3.1. The downward neck is made to pick up sample during the polymerization as shown in figure 3.4. The most important thing is each neck contains a Rotaflo® high performance stopcock, which is used to switch the channel between two connected glasswares or the glasswares to high

vacuum line.
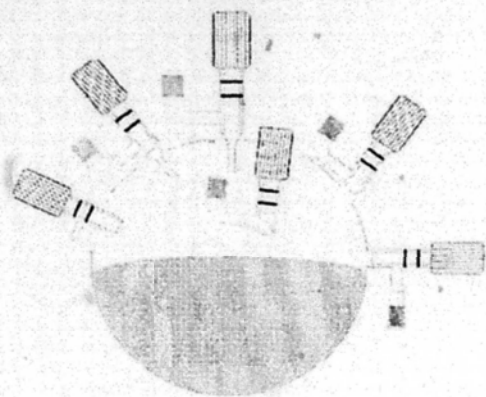
Reactor

Initiator Burette

Solvent Ampoule

Monomer Ampoule

Coupling agent
Ampoule

Fractional Distillation Set 1
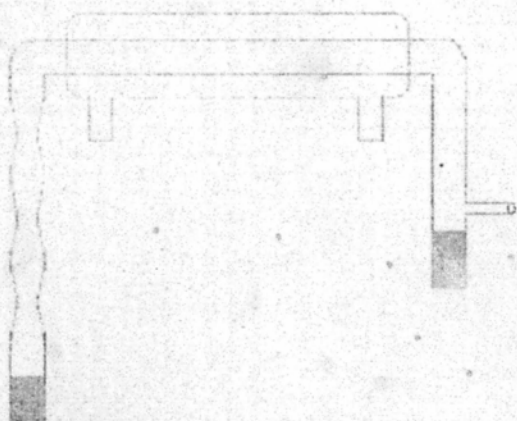
Fractional Distillation Set 2
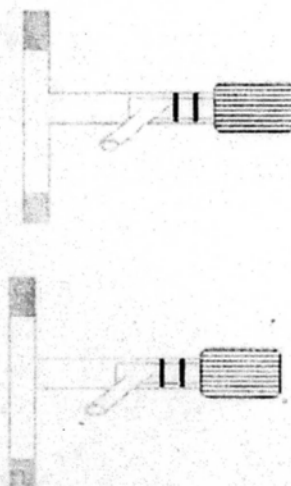
T shape connector 1

T shape connector 2

Figure 3.3 Interchangeable glassware apparatus

Initiator Burette: The initiator burette is made of pipette with two Rotaflo® high performance stopcocks at each end. The upward stopcock is connected to vacuum line. Also, under argon atmosphere initiator solution is injected into initiator burette through the upward stopcock. The downward stopcock contains a male conically tapered joint. Such male conically tapered joint can link with female joint on the reactor as shown in figure 3.1.

Solvent ampoule: The solvent ampoule is made of a cylindrical flask with a Rotaflo® high performance stopcocks and a male conically tapered joint.

Monomer ampoule: The monomer ampoule is similar with the solvent ampoule, except that the volume of monomer ampoule is smaller than which of solvent ampoule.

Coupling ampoule: The coupling ampoule is similar with the monomer ampoule.

Fractional distillation set 1, 2: The fractional distillation sets are made of vigreux column, condenser and two conically tapered joints at each end. They are used in distillation of monomers and solvents.

T shaped connector 1, 2: T shaped connectors are made of a Rotaflo® high performance stopcock with two conically tapered joints at each end. Normally, they are used in sampling during polymerization as shown in figure 3.4. Besides, they are also used in reagent transfer.

Figure 3.4 Illustration of sampling during anionic polymerization

3.2.2.3 Purification of reagents

Because of the high reactivity of anionic centers towards atmosphere (moisture, oxygen, carbon dioxide) and other contaminants, all the reagents should be purified before doing anionic polymerization. The purification methods of chemicals can be found any where.[27,53] In present thesis, a combination of the traditional methods and home made high vacuum line is used to purify reagents.
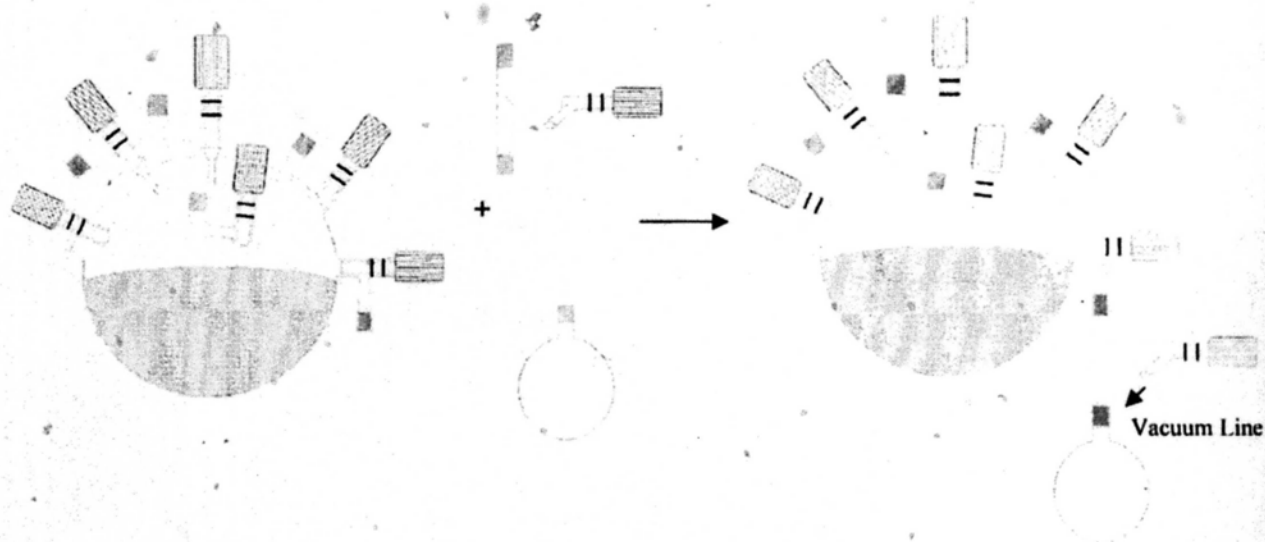
(i) Solvent:

Cyclohexane (≥99%, bp: 80.7 °C, Lab-Scan) is used as solvent in anionic polymerization. Cyclohexane is refluxed with sodium stick over 24 hours, and then fractional distillation set 2 is used to distill cyclohexane into a round bottom flask which containing a small amount of n-BuLi and styrene. The product of n-BuLi and styrene is PSLi, which shows orange color in solvent and used as moisture indicator. The second distillation is carried out by using fractional distillation set 1, the solvent is distilled into a solvent ampoule.

(ii) Monomer:

Styrene (St, ≥ 99%, 10-15 ppm *4-tert*-butylcatechol inhibitor, bp: 145~146 °C, Sigma-Aldrich). Styrene is dried over finely grounded CaH_2 over 24 hours, and then fractional distillation set 2 is used to distill styrene into a round bottom flask under reduced pressure. The round bottom flask is containing an appropriate amount of dibutylmagnesium (DBMg, 1 M in heptane). Subsequently, the second distillation is carried out by using fractional distillation set 1 and the styrene is distilled into a monomer ampoule under reduced pressure. The monomer ampoule is weighted before and after distillation to obtain the amount of styrene. To avoid autopolymerization, the purified styrene needs to be diluted as quickly as possible, so a proper quantity of cyclohexane is distilled into the monomer ampoule under argon atmosphere. The concentration of monomer in solution is around 10%-20%.

(iii) Coupling agent

1,4-Divinylbenzene (DVB, ~ 80%, 1000 ppm *p-tert*-butylcatechol inhibitor, bp: 195 °C, Sigma-Aldrich): The purification of DVB is similar with styrene, except the concentration of DVB in solution is 0.1%~0.5%.

3.2.3 Polymerization of Star Polymer

3.2.3.1 Methods of synthesize star polymers

Star polymers are branched polymers containing several linear chains linked to a central core. Generally speaking, there are two synthetic methods to get star shaped polymers, namely, core first method and arm first method.[16] The core first method uses multifunctional initiators to initiate polymerization, while the arm first method uses multifunctional coupling agents to link living macroanionic chains. For core first method, in order to obtain star polymers with uniform arms, narrow molecular weight distribution and controllable molecular weights, the multifunctional initiators have to fulfill the following requirements: i) all the functional group must be equally reactive; ii) all the functional group must have the same initiation rate; iii) the initiation rate must be much higher than the propagation rate. Even if all the above requirements are satisfied, the multifunctional initiators tend to aggregate which make the polymerization complicate. For arm first method, mono-disperse molecular weight of polymer chains are synthesized first, then coupling agents are added to link the macroanionic chains. Also because such method can control all the synthetic steps absolutely, it is considered to be the most efficient way to synthesize well-defined star polymers.[16] Among various coupling agents in anionic polymerization, DVB is a powerful linking agent, considering it can efficiently get stars with growing arm numbers by slowly and gradually adding of DVB in macroanionic chains.[54-58]

3.2.3.2 Polymerization Procedure

The synthesis of star polymers is performed by the novel home made high vacuum system as shown in Figure 3.5, Rotaflo® high performance stopcocks are connected by a male and a female ground joint, such design can be used to replace the conventional break-seal connector in high vacuum systems and easy to operate.

Before attached the reagents ampoules to the main reactor, the reactor containing a stirring bar is flame dried and pumped by rotary pump at least for one hour to remove volatile species. After then, all the ampoules containing purified reagents are attached to the main reactor by conically tapered joints as shown in figure 3.5.

Figure 3.5 Assembled apparatus of home made high vacuum system.

The diffusion pump is used to pump the system to the vacuum level of 10^{-6} Torr. The stopcock of connection between the main reactor and vacuum line is switched off, while the stopcocks of connection between the main reactor and the monomer ampoule, the main reactor and solvent ampoule are turned on. Solvent and monomer flow into the main reactor spontaneously because of vacuum. Then the stopcock of initiator ampoule is turned on, and a small amount of initiator solution is dropwise added into the reactor with stirring. As soon as light yellow existence in the colorless solution, the stopcock is turned off. Shake the main reactor and make the solution rinse the whole reactor thoroughly. Because solution is containing initiator at the moment, which is able to kill the remaining impurities left in the reactor. After exhausting all the initiator and impurity, demanded amount of initiator is quickly added. The solution suddenly turns to orange and the polymerization start. Normally, the reaction lasts for about 2 hour until all the monomers is consumed. Samples are taken from the downward neck on the main reactor as shown in the figure 3.4, then are diluted by cyclohexane and tested by LLS at their theta temperature (~ 34.5 °C) to measure their radius of gyration ($<R_g>$). Based on the Flory scaling of Polystyrene linear chain in cyclohexane at theta temperature, i.e., $R_g \cong 1.107 \times 10^{-2} M^{0.6}$,[65] the molecular weight of linear chain can be calculated. The combination of molecular weight of the PS linear samples and the quantity of the monomer used in the polymerization gives the quantity of carbanions left in solution:

$$[Carbanion] = \frac{weight\ of\ monomer}{molecular\ weight\ of\ \text{PS linear chain}} \qquad (3.1)$$

And the coupling agent, a required amount of DVB solution is added into the reaction solution with the ratio of [DVB]:[Carbanion] = 0.7:1 can also be estimated based on the eq (3.1). Normally, the coupling reactions last for 1 hour $\sim$ 3 days, depending on the molecular weight of the living PSLi linear chain, namely, the longer PSLi linear chain is, the longer time coupling reaction needed. Before the next addition of DVB, a small amount of reaction solution is taken from the downward neck and tested by the LLS. Afterwards, DVB solution is added repeatedly with 0.7 equiv of carbanion each time. Finally, series of stars with different arm numbers but same arm length are obtained.

3.2.3.3 Fragmentation of PS stars

The linked star polymers with DVB show broad distributions. To get narrow molecular weight distribution samples, fragmentation is carried out to separate stars with different arm numbers but identical arm length as shown in follow steps, 1). 1,4-dioxane is used to dissolve the polymer at 80 °C with concentration around 0.03 g/mL, 2) drops of ethanol is added until the solution became slightly milky, 3) put the solution into water bath at room temperature for few weeks. The stars with more arm numbers, namely, more weighted stars deposit in advance. 4) repeat step 2 to 3.

3.2.4 Characterization by Laser Light Scattering (LLS)

A modified commercial LLS spectrometer (ALV/DLS/SLS-5022F) equipped with a multi-τ digital time correlator (ALV5000) and a cylindrical 22 mW UNIPHASE He-Ne laser (λ_0 = 632 nm) was used. The details of the LLS instrumentation and theory can be found elsewhere.[59,60]

In dynamic LLS, the intensity-intensity time correlation function ($G^{(2)}(\tau)$) [= $<I(0)I(\tau)>$] of each polymer solution at different photo-reaction stages was measured in the scattering angle (θ) range 20°-90°. $G^{(2)}(\tau)$ can be related to the normalized field-field autocorrelation function $|g^{(1)}(\tau)|$ ($\equiv$ [$<E(0)E^*(\tau)>/<E(0)E^*(0)>$]) via the Siegert relation as[61]

$$G^{(2)}(\tau) = A[1 + \beta |g^{(1)}(\tau)|^2] \qquad (3.2)$$

where A ($\equiv <I(0)>^2$) is the measured baseline and β ($\approx$ 0.95) is a constant related to the coherence of the detection optics. For a polydisperse system, $g^{(1)}(\tau)$ is related to the distribution of the characteristic linewidth $G(\Gamma)$ by[59,60]

$$|g^{(1)}(t)| = \int_0^\infty G(\Gamma)e^{-\Gamma t} d\Gamma \qquad (3.3)$$

For a diffusive relaxation, Γ is related to the translational diffusion coefficient D by $\Gamma = Dq^2$. In principle, $G(\Gamma)$ can be calculated from the Laplace inversion according to equation (3.3).[61,62] D is further related to the hydrodynamic radius R_h by Stokes-Einstein equation: $R_h = k_B T/(6\pi\eta_0 D)$.

In static LLS, the excess absolute time-averaged scattered light intensity, known as the excess Rayleigh ratio $R_{vv}(q)$, of a dilute polymer solution at concentration C (g/mL) is related to the weight average molar mass M_w, the root-mean square z-average radius of gyration $<R_g^2>_z^{1/2}$ (or written as $<R_g>$), and the scattering vector q as

$$\frac{KC}{R_{vv}(h)} \approx \frac{1}{M_w}(1 + \frac{1}{3} < R_g^2 > h^2) + 2A_2C \qquad (3.4)$$

where $K = 4\pi^2 n^2 (dn/dC)^2/(N_A \lambda_0^4)$ and $h = (4\pi n/\lambda_0)\sin(\theta/2)$ with N_A, dn/dC (=0.171 mL/g, 34.5 °C, cyclohexane; =0.109 mL/g, 25 °C, toluene), n and λ_0 being the Avogadro number, the specific refractive index increment, the solvent refractive index and the wavelength of the light in vacuum, respectively; and A_2 is the second virial coefficient.

3.3 Result and discussion

PSLi linear chains were initiated by a controlled amount of n-Butyllithium through home made vacuum system, and then linked by DVB to form stars. The PS one arm and formed stars were analyzed by the gel permeation chromatography (GPC) and as shown in figure 3.6.
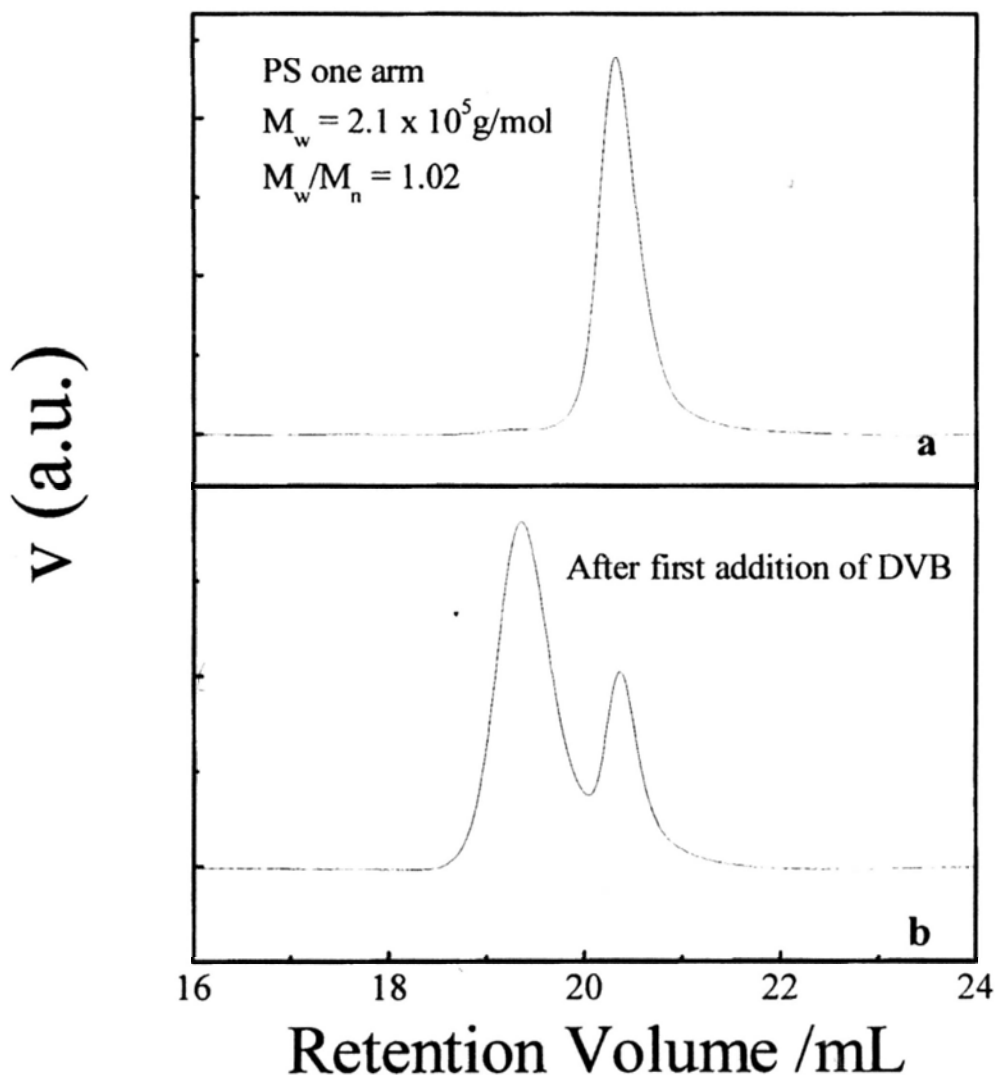
Figure 3.6. Comparison of PS before and after DVB addition.

As shown in figure 3.6a, based on the home made vacuum system, a mono-disperse PS linear chain was obtained with molecular weight = 2.1 x 10^5 g/mol and M_w/M_n = 1.02. With the addition of DVB and coupling for 3 days, a mixture of star and linear chains were received as shown in figure 3.6b. Here, the arm first method shows another merit, the arm length could be tested accurately without cutting off from the formed stars.
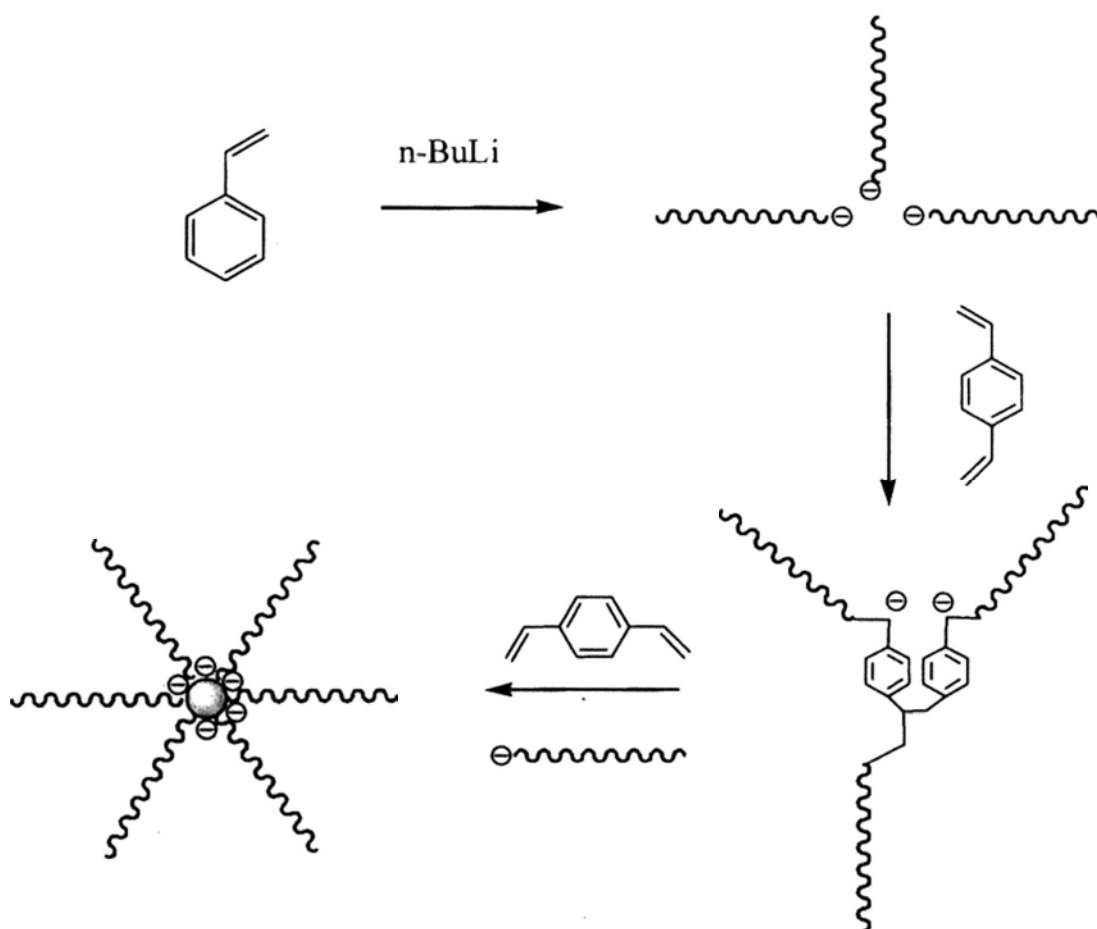
Scheme 3.1 Reaction mechanism for linking living PSLi with DVB

It has been reported,[63] the traditional coupling method which uses chlorosilane as linking agents takes a long time and low efficiency. Normally, 4-arm stars with arm molecular weight of 10^5 g/mol and larger require up to 4 weeks to complete. More than that, stars with more arm numbers are also difficulty to obtain. It is because the small core of the traditional coupling agent makes the functional groups to get close to each other, if one of the functional group reacts with a living chain, the steric hindrance makes it very difficult for the remaining chains to approach to the rest

functional groups. However, the DVB coupling method can solve the problem. DVB can react with living anionic linear chain and form a core with multi-functional groups as shown in scheme 3.1. Stars are obtained by living reaction between anionic chains and some of the functional groups which are far away from each others. Beside, two formed stars also can be linked through the DVB.[54,58] Normally, the DVB coupling method took 3 days to form star with 6 arms and molecular weight of each arm $M_{w\_arm} = 2.1 \times 10^5$ g/mol, and further took one week to form more arms stars.

Though the DVB coupling method obtains broad molecular weight distribution stars, the stepwise addition of DVB solution can obtain a series of stars with different arm numbers but identical arm length. Further more, stars with different molecular weights, namely, identical arm length but different arm numbers are efficiently separated by the fragmentation method. The fragmentation method has been proved to obtain narrow molecular weight distributed polymer linear chains in our lab.[64] As shown in figure 3.7, a series of stars with different arm numbers but identical arm length, the narrowly distributed samples prove the method is valid.
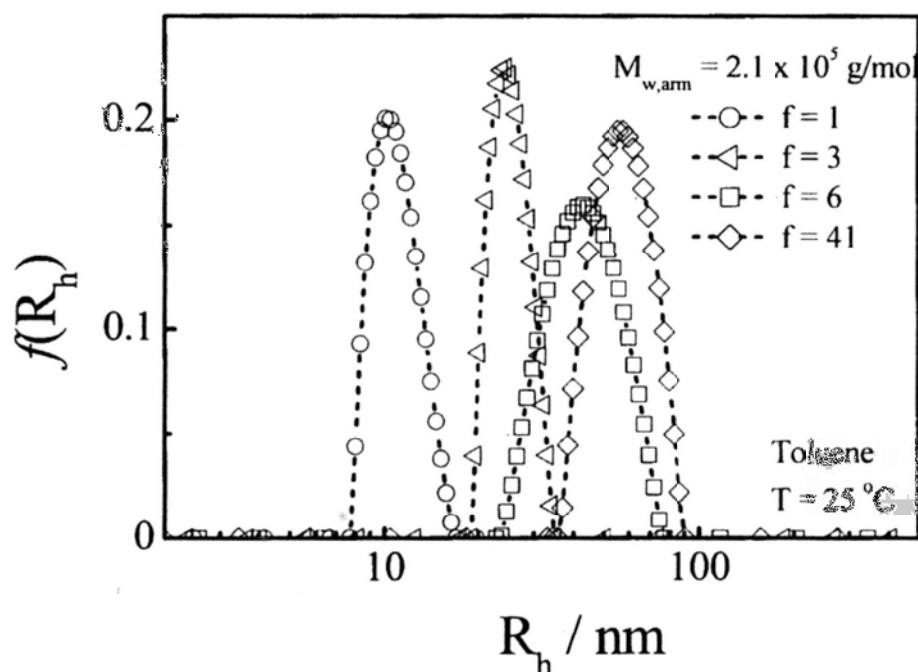
Figure 3.7 Hydrodynamic radius distribution ($f(R_h)$) of PS one arm and stars with 3, 6, 41 arms in toluene at the room temperature, where $M_{w\_arm} = 2.1 \times 10^5$ g/mol.

Based on the figure 3.8, a typical Zimm-plot of Star-6A in toluene, we can obtain the weight-average molar mass of the final stars ($M_{w,star}$) from intercept of

$[KC/R_{vv}(\theta)]_{c\to 0, \theta \to 0}$, and then the arm number (f) from $M_{w,star}/M_{w,arm}$.
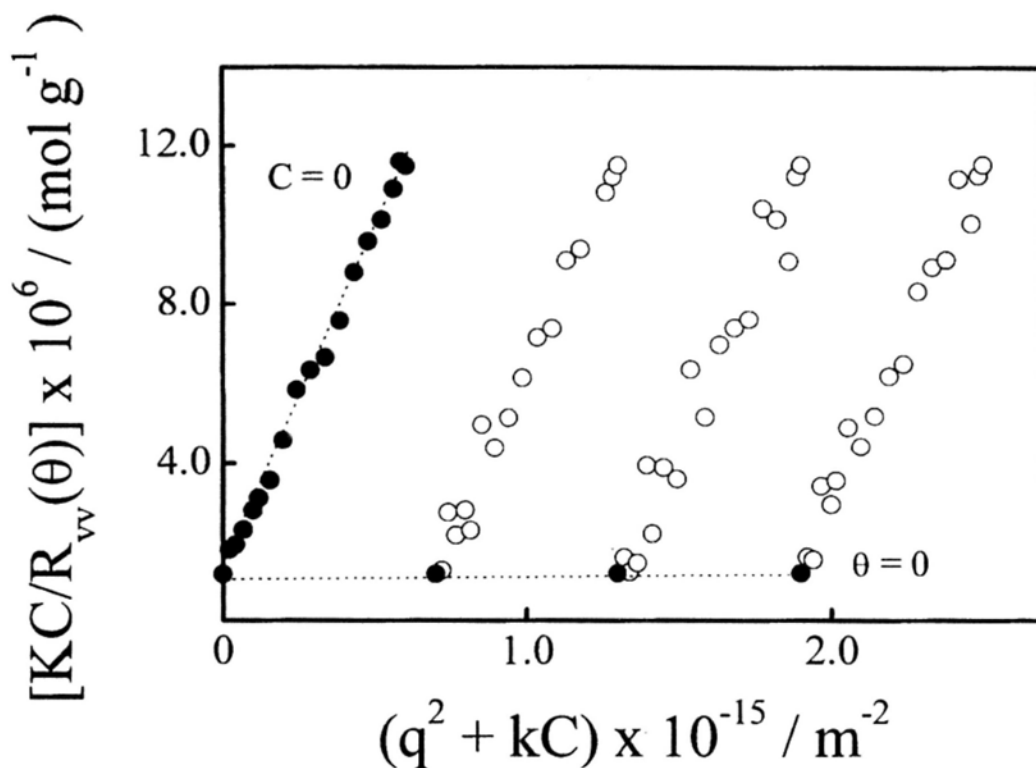
Figure 3.8 Typical Zimm-plot of star-6A in Toluene at T = 25 °C, where the star concentration ranged from 2.10×10^{-5} to 1.05×10^{-4} g/mL.

Table 3.1 PS star polymers obtained by DVB coupling and fragmentation method.

Code	Arm number	$M_{w,arm}$ / g mol^{-1}	$M_{w,star}$ / g mol^{-1}	M_w/M_n
Star-41	41.1	2.1×10^5	8.6×10^6	1.15
Star-6A	5.9	8.2×10^4	4.9×10^5	1.08
Star-6B	6.1	1.3×10^5	7.8×10^5	1.12
Star-6C	6.1	2.1×10^5	1.3×10^6	1.10
Star-6D	6.0	3.5×10^5	2.1×10^6	1.12
Chain1	1.0	5.9×10^5	5.9×10^5	1.01
Chain2	1.0	4.3×10^4	4.3×10^4	1.05

Following the method, stars with various arm lengths and numbers and narrowly

molecular weight distribution were obtained by the combination of DVB coupling living anionic chains and fragmentation method and the sample details are shown in Table 3.1.

3.4 Conclusion.

A novel home made vacuum system is established and used in the anionic polymerization. Such vacuum system uses Rotaflo® high performance stopcocks to take place of the traditional break-seals connection. The design does not need glass blower technique, and can be used repeatedly and easy to be operated. The incremental addition of DVB into living PSLi linear chains method provide a series of stars with different arm numbers but sharing identical arm lengths. The DVB coupling method is also proved to be more efficient in linking living anionic linear chains, especially when chains have relatively high molecular masses. The fragmentation method is used to obtain stars with narrow molecular weight distributions. The combination of anionic polymerization based on DVB coupling method and fragmentation method offers well-defined stars. All these star and linear chain samples are used in the further ultrafiltration experiment.

3.5 References

[1] Hsieh, H.; Quirk, R. *Anionic Polymerization: Principles and practical applications*; Marcel Dekker, Inc: New York, **1996**.

[2] Matthews, F. E.; Strange, E. H. British Patent **1910**, 24, 790.

[3] Harries, C. H. *Justus Liebigs Ann. Chem.* **1911**, 383, 157; U. S. Patent 1913, 1058056.

[4] Ziegler, K.; Dersch, F.; Willthan, H. *Justus Liebigs Ann. Chem.* **1934**, 511, 13.

[5] Ziegler, K.; Jacob, L. *Justus Liebigs Ann. Chem.* **1934**, 511, 45.

[6] Ziegler, K.; Jakob, L.; Willthan, H.; Wen, A. *Justus Liebigs Ann. Chem.* **1934**, 511, 64.

[7] Morton, M. *Anionic Polymerization: Principles and Practice.* Academic Press: New York, **1983**.

[8] Beaman, R. G. *J. Am. Chem. Soc.* **1948**, 71, 1595.

[9] Sanderson, J. J.; Hauser, C. R. *J. Am. Chem. Soc.* **1949**, 71, 1595.

[10] Walling, C.; Briggs, E. R.; Cummings, M.; Mayo, F. R. *J. Am. Chem. Soc.* **1950**, 72, 48.

[11] Szwarc, M. *Nature* **1956**, 178, 1168.

[12] Szwarc, M.; Levy, M.; Milkovich, R. *J. Am. Chem. Soc.* **1956**, 78, 2656.

[13] Bywater, S. *Prog, Polym. Sci.* **1975**, 4, 27.

[14] Se, K. *Prog. Polym. Sci.* **2003**, 28, 583.

[15] Wack, R.; Rembaum, A.; Coombes, J. D.; Szwarc, M. J. *Am. Chem. Soc.* **1957**, 79, 2026.

[16] Hadjichristidis, N.; Pitsikalis, M.; Pispas, S.; Iatrou, H. *Chem. Rev.* **2001**, 101, 3747.

[17] Hirao, A.; Loykulnant, S.; Ishizone, T. *Prog. Polym. Sci.* **2002**, 27, 1399.

[18] Jagur-Grodzinski, J. *J. Polym. Sci. Polym. Chem.* **2002**, 40, 2116.

[19] Hong, K. L.; Uhrig, D.; Mays, J. W. *Curr, Opin. Solid State Mat. Sci.* **1999**, 4, 531.

[20] Hirao, A.; Hayashi, M. *Acta Polym.* **1999**, 50, 219.

[21] Hirao, A.; Nakahama, S. *Acta Polym.* **1998**, 49, 133.

[22] Hadjichristidis, N.; Iatrou, H.; Pitsikalis, M.; Pispas, S.; Avgerpoulos, A. *Prog. Polym. Sci.* **2005**, 30, 725.

[23] Bywater, S. *Prog. Polym. Sci.* **1994**, 19, 287.

[24] Worsfold, D. J.; Bywater, S. *Can. J. Chem.* **1960**, 38, 1891.

[25] Graham, G.; Richtsmeier, S.; Dixon, D. A. *J. Am. Chem. Soc.* **1980**, 102, 5759.

[26] Szwarc, M. *Adv. Polym. Sci.* **1983,** 49, 1.

[27] Hadjichristidis, N.; Iatrou, H.; Pispas, S.; Pitsikalis, M. *J. Polym. Sci. Polym. Chem.* **2000**, 38, 3211.

[28] Hsieh, H. L. *J. Polym. Sci. A-3* **1965**, 153, 163.

[29] Selman, C. M.; Hsieh, H. L. *Polym. Lett.* **1971**, 9, 219.

[30] Hsieh, H. L.; Glaze, W. H. *Rubber Chem Techbnol* **1970**, 43, 22.

[31] Hatada, K.; Kitayama, T.; Ute, K. *Prog. Polym. Sci.* **1988**, 13, 189.

[32] Yuki, H.; Hatada, K. *Adv. Polym. Sci.* **1979**, 31, 1.

[33] Allen, R. D.; Long, T. E.; McGrath, J. E. *Polym. Bull.* **1986**, 15, 127.

[34] Varshney, S. K.; Jacobs, C.; Hautekeer, J. P.; Bayard, P.; Jerome, R.; Fayt, R.; Teyssie, P. *Macromolecules* **1991**, 24, 4997.

[35] Ozaki, H.; Hirao, A.; Nakahama, S. *Macromolecules* **1992**, 25, 1391.

[36] Morton, M.; Bostick, E. E.; Livigni, R. A.; Fetters, L. J. *J. Polym. Sci. Part A.* **1963**, 1, 1735

[37] Francois, B.; Sinn, V.; Parrod, J. *J. Polym. Sci. Part C.* **1963**, 4, 375.

[38] Guyot, A.; Vialle, J. *J. Macromol. Sci. Chem.* **1970**, A4, 107.

[39] Worsfold, D. J.; Bywater, S. *Can. J. Chem.* **1964**, 42, 2884.

[40] Alvarino, J. M.; Bello, A.; Guzman, G. M. *Eur. Polym. J.* **1972**, 8, 53.

[41] Glasse, M. D. *Prog. Polym. Sci.* **1983**, 9, 133.

[42] Fetters, L. J. Firer, E. M. *Polymer* **1977**, 18, 306.

[43] Wakefield, B. J.; Lovell, P. A. *Introduction to Polymers.* Chapman & Hall: London, **1991**.

[44] Young, R. N.; Quirk, R. P.; Fetters, L. J. *Adv. Polym. Sci.* **1984**, 56, 1.

[45] Glusker, D. L. S., Yoncoskie, B. *J. Polym. Sci.* **1961**, 49, 297.

[46] Kwon, K.; Lee, W.; Cho, D.; Chang, T. *Korea Polym. J.* **1999**, 7, 321.

[47] Ndoni, S.; Papadakis, C. M.; Bates, F. S.; Almdal, K. *Rev. Sci. Instrum.* **1995**, 66, 1090.

[48] Worsfold, D. J.; Bywater, S. *Can. J. Chem.* **1960**, 38, 1891.

[49] Storey, R. F.; Nelson, M. E. *J. Appl. Polym. Sci.* **1997**, 66, 151.

[50] Uhrig, D.; Mays, J. W. *J. Polym. Sci. Polym. Chem.* **2005**, 43, 6179.

[51] Morton, M.; Fetters, L. *J. Rubber Chem. Technol.* **1975**, 48, 359.

[52] Shefelbine, T. A.; Vigild, M. E.; Masten, M. W.; Hajduk, D. A.; Hillmyer, M. A.; Cussler, E. L.; Bates, F. S. *J. Am. Chem. Soc.* **1999**, 121, 8457.

[53] Armarego, W. L. F.; Chai, C. L. L. *Purification of Laboratory Chemicals.* 5th ed.; Butterworth-Heinemann: Oxford, **2003**.

[54] Lee, H.-J.; Lee, K.; Lee, S. N. *J. Polym. Sci.: Part A: Polym. Chem.* **2006**, 2579.

[55] Worsfold, D. J. *Macromolecules* **1970**, 30, 90.

[56] Frater, D. J. ; Mays, J. W.; Jackson, C. *J. Polym. Sci. Part B: Polym. Phys.* **1997**, 35, 141.

[57] Bi, L.-K.; Fetters, L. J. *Macromolecules* **1976**, 9, 732.

[58] Lee, H.-J.; Lee, K.; Choi, N. *J. Polym. Sci. Part A: Polym. Chem.* **2005**, 43, 870.

[59] Berne, B.; Pecora, R. *Dynamic Light Scattering.* Plenum Press: New York, **1976.**

[60] Chu, B. *Laser Light Scattering,* 2nd ed.; Academic Press: New York, **1991**.

[61] Berne, B. J.; Pecora, R. *Dynamic Light Scattering* Plenum Press: New York, 1976.

[62] Brown, W.; Nicolai, T. In *Dynamic Light Scattering, the Methods and Application,* Brown, W. Ed.;Clarendon, Oxford, 1993. pp273.

[63] Clarke, N.; Colley, F. R.; Collins, S. A.; Hutchings, L. R.; Thompson, R. L. *Macromolecules* **2006**, 39, 1290.

[64] Wu, C.; Zhou, S. Q. *Macromolecules* **1995**, 28, 8381.

[65] Appelt, B.; Meyerhoff, G. *Macromolecules* **1980**, *13*, 657.

Chapter 4
How much force is needed to stretch a coiled chain in solution?

4.1 Introduction

In 1970s, de Gennes and Pincus[1,2] used the Rouse model[3] to show that linear polymer chains in a good solvent could undergo a first-order coil-to-stretch transition to pass through a pore much smaller than its coiled size under an elongation flow field with a sufficient hydrodynamic force, independent of both the chain length and the pore size. Namely, a coiled polymer chain can pass through a small pore as long as the flow rate (q) is higher than a threshold [$q_c \simeq k_B T/(3\pi\eta)$], where $k_B T$ and η is the Boltzmann constant, the absolutely temperature, and the solvent viscosity, respectively.

On the other hand, it has been suggested that the electrostatic blob model for a polyelectrolytes chain would also be applicable for the coil-to-stretch transition of a neutral chain in an ultrafiltration experiment.[4,5] In principle, the stretching of a neutral chain under an elongational flow and the extension of a polyelectrolyte chain under the electrostatic repulsion have a similar physical nature, but not identical. Namely, a neutral chain can be stretched as a string of blobs under an elongational flow. The blob size decreases as the shear rate increases. Finally, each blob can be fully stretched with a sufficiently strong shear force.

It is not difficult to realize that the passing through a small pore occurs only when the blob size (ξ_b) of a stretched chain in a flow filed is smaller than the pore size (D). Therefore, the critical flow rate is associated with the relative size of the blob to the pore. Whether a coiled chain can pass through a small pore is related to its local deformability, i.e., the entering of the first blob into the pore, at which the entropic confinement force ($k_B T/D$) is overcame by the hydrodynamic force ($3\pi\eta q_c/D$), where it has assumed that each blob is a nondraining ball with a diameter identical to the pore size (D).[1,2] Note that here only the short-range interaction is relevant. In principle, one can reversibly use q_c to characterize the local deformability. To our knowledge, the predicted chain-length and pore-size independence of q_c has not been confirmed in experiments because such a first-order coil-to-stretch transition has not been observed for a long time. Recently, we have observed such a discontinuous

first-order transition by ultrafiltrating linear polystyrene chains through specially constructed small pores (20 nm).[6]

Note that the rigidity of polymer chain has been traditionally characterized in terms of the persistence length (l_p), an important parameter not only in polymer research but also in the study of protein unfolding under an exerted force.[7-9] Normally, l_p is deduced from the measured average radius of gyration ($<R_g^2>^{1/2}$).[10] For a more rigid chain,[11] l_p can be indirectly estimated from the intrinsic viscosity ($[\eta]_\theta$).[12] Also note that the developments of electron microscopy[13,14] and AFM[15-17] lead to some direct measurements of l_p in terms of the conformation change and the force required to extend a polymer chain. It should be emphasized that a combination of magnetic tweezer and hydrodynamic force can also be used to measure the weaker *enthalpy* elasticity of a long and more rigid DNA chain.[18]

4.2 Experimental section

4.2.1 Sample preparations

In the current ultrafiltration experiments, we find q_c from the abrupt change of the relative retention [(C_0 - C)/C_0] of linear chains, where C_0 and C are polymer concentrations respectively before and after the solution passes through smaller pores. At this critical flow rate, the hydrodynamic force starts to overcome the entropic confinement force. Therefore, we can estimate how much force is needed to stretch a coiled chain into a string of blobs with a size of D. In this study, the solution temperature dependent ultrafiltration of linear polystyrene (PS) chains in cyclohexane was measured by using the Whatman membranes with two different pore sizes (20 and 100 nm). The average pore density is 5×10^8 per membrane, and the length of each pore is 1μm. The membranes have a double-layer structure that prevents some possible interference among flow fields generated by different pores, leading to an elongation one as required by the theory.

In order to increase the accuracy, we used a solution mixture of two PS samples with different chains lengths; namely, long chains (PS-L, $M_w > 2.2 \times 10^6$ g/mol, $M_w/M_n < 1.10$ and $<R_h> 25$ nm) and short chains (PS-S, $M_w = 4.4 \times 10^4$ g/mol, $M_w/M_n = 1.13$ and $<R_h> = 5$ nm). Note that there is no retention for short PS chains at any flow rate. The solution mixture of PS-S ($C_S = 1.00 \times 10^{-2}$ g/mL) and PS-L ($C_S = (2.4-20.0) \times 10^{-5}$ g/mL) with a volume ratio of ~1:1 was used as the stock solution. In

each ultrafiltration experiment, the macroscopic flow rate (Q) and temperature were controlled by a syringe pump (Harvard Apparatus, PHD 2000) and an incubator (Stuart Scientific, S160D) ($\pm$ 0.1 °C), respectively. In our setup, at the lowest used flow rate of 0.005 mL/h, the linear moving rate is 3.56 x 10^{-6} cm/s. The minimum linear moving rate of the pump (motor) is 3 x 10^{-7} cm/s, 10 times smaller than the rate used. Therefore, the flow used can be treated as a continuous one. A combination of static and dynamic laser light-scattering (LLS) measurements enables us to accurately determine the relative retention concentration [(C_0 - C)/C_0] of longer chains under different macroscopic flow rates by using short chains as an internal reference.[6]

4.2.2 Laser Light Scattering (LLS)

A modified commercial LLS spectrometer (ALV/DLS/SLS-5022F) equipped with a multi-τ digital time correlator (ALV5000) and a cylindrical 22 mW UNIPHASE He-Ne laser (λ_0 = 632 nm) was used. The incident beam was vertically polarized with respect to the scattering plane. The details of the LLS instrumentation and theory can be found elsewhere.[19]

In dynamic LLS, the intensity-intensity time correlation function ($G^{(2)}(\tau)$) of each polymer solution was measured before and after each ultrafiltration. $G^{(2)}(\tau)$ is related to the normalized field-field autocorrelation function $|g^{(1)}(\tau)|$. The Laplace inversion of each $g^{(1)}(\tau)$ leads to a line-width distribution $G(\Gamma)$[20,21] that can be further converted to a hydrodynamic radius distribution $f(R_h)$ by using the Stocks-Einstein equation.

In static LLS, the excess absolute time-averaged scattered light intensity, known as the excess Rayleigh ratio $R_{vv}(h)$, of a dilute polymer solution at concentration C (g/mL) is related to the weight-average molar mass M_w, the root-mean square z-average radius of gyration $<R_g^2>_z^{1/2}$ (or written as $<R_g>$), and the scattering vector h as

$$\frac{KC}{R_{vv}(h)} \approx \frac{1}{M_w}(1 + \frac{1}{3}<R_g^2>h^2) + 2A_2C \quad (4.1)$$

where $K = 4\pi^2n^2(dn/dC)^2/(N_A\lambda_0^4)$ and $h = (4\pi n/\lambda_0)\sin(\theta/2)$ with N_A, dn/dC, n and λ_0 being the Avogadro number, the specific refractive index increment, the solvent refractive index and the wavelength of the light in vacuum, respectively; and A_2 is the second virial coefficient. For PS in cyclohexane at 34.5 °C and in toluene at 25

°C dn/dC = 0.171 mL/g and 0.109 mL/g, respectively.

4.3 Result and discussion

Figure 4.1 shows how the measured $(C_0 - C)/C_0$ depends on the flow rate (Q) for polystyrene chains with different lengths in cyclohexane, where the pore diameter (D) is 20 nm. It clearly shows that there is no retention for the shortest chain because its size is smaller than the pore size; while for the longer chains, the retention nearly starts at an identical flow rate ($\sim 2.0 \times 10^{-2}$ mL/h) in spite of their different lengths, which confirms with the de Genne's prediction, namly, the q_c of linear chains is irrelative with the chain length. Besides, such a critical flow rate or threshold for long PS chains to pass through smaller pores is well-defined because the coil-to-stretching is a first-order transition.[2] In this way, we were able to accurately measure the critical flow rate (Q_c) of longer PS chains through small pores.

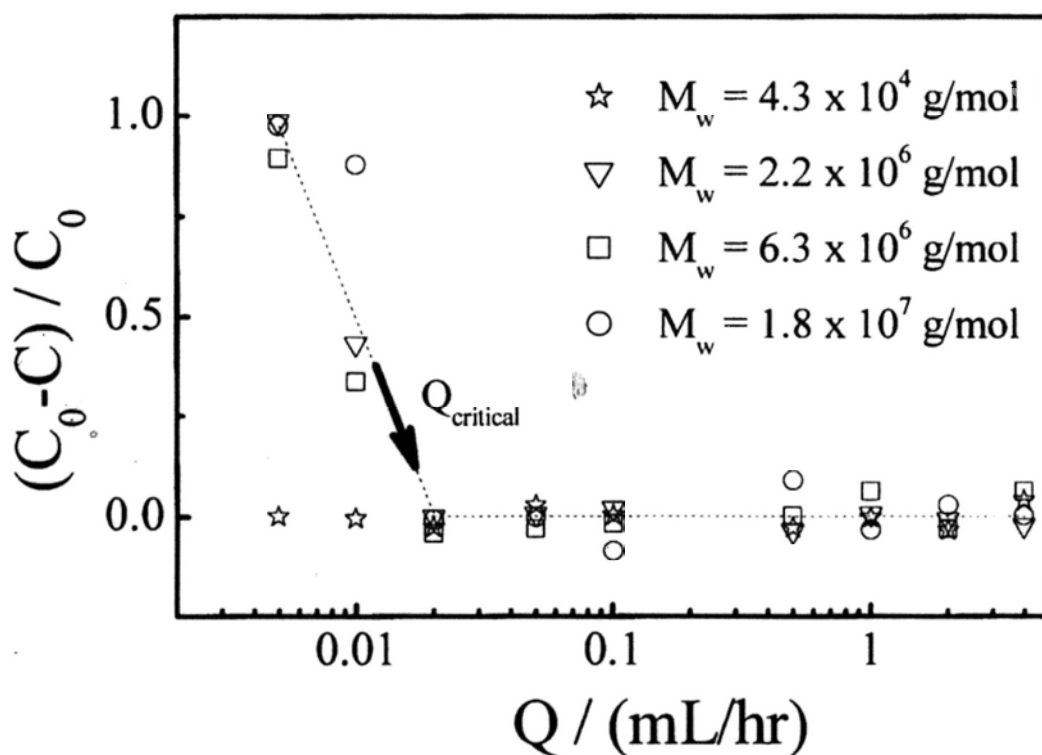**Figure 4.1** Macroscopic flow rate (Q) dependence of retention concentration of different molecular weights PS linear chains in cyclohexane at T = 34.5°C .

On the other hand, it has been known that for long PS chains in cyclohexane the theta temperature (Θ) is $\sim$34.5 °C,[22] at which the chains behave like a Gaussian coil.[23] Figure 4.2 shows that the light-scattering measured average radius of gyration

($<R_g>$) of long PS chains ($M_w = 1.8 \times 10^7$ g/mol, $M_w/M_n = 1.06$ and $<R_h> = 100$ nm), specially synthesized by high-vacuum anionic polymerization, monotonely decreases with the solution temperature, corresponding to a volume decrease of three times. As expected, the chain deformation at different temperatures should be different because of their different swelling degrees. At higher temperatures, it would require a stronger force to overcome the entropic force to deform a given chain. On the other hand, when the chain is collapsed in a poor solvent with stronger segment-segment interaction, the force required to deform it would also be higher.
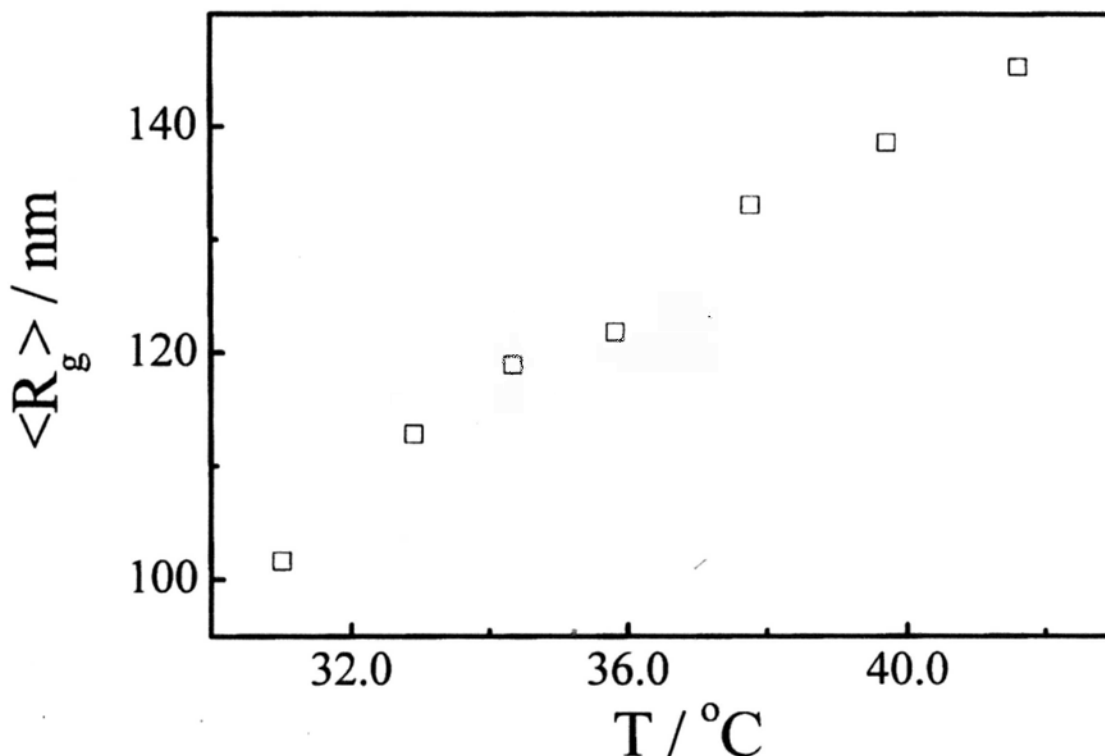
Figure 4.2 Solution temperature dependence of average radius of gyration $<R_g>$ of long polystyrene chains (PS-L) in cyclohexane.

Figure 4.3 shows passing or nonpassing of long PS chains through small pores (20 nm) at different temperatures. For a given number of small pores on each membrane (N), we can convert the macroscopic flow rate (Q) into the average microscopic flow rate (q = Q/N) and the average flow velocity ($v = q/D^2$) inside each pore. As discussed before, q_c is directly related to the hydrodynamic force (F_h) required to stretch a coiled polymer chain in solution by $F_h = 3\pi\eta(q/D^2)L_c$, where L_c is the effective length along the flow direction. For a nondraining hard ball with a diameter of D, $L_c = D$. For a given pore size, Our experimental results show that q_c remains a constant, 5.56×10^{-15} mL/s at T = Θ, for the three PS samples measured, independent

of the chain length as predicted by de Gennes.[24]

Figure 4.3 Phase diagram of passing or blocking of long PS-L chains in cyclohexane through small pores (20 nm) at different solution temperatures, where hollow and filled symbols respectively represent passing and blocking.
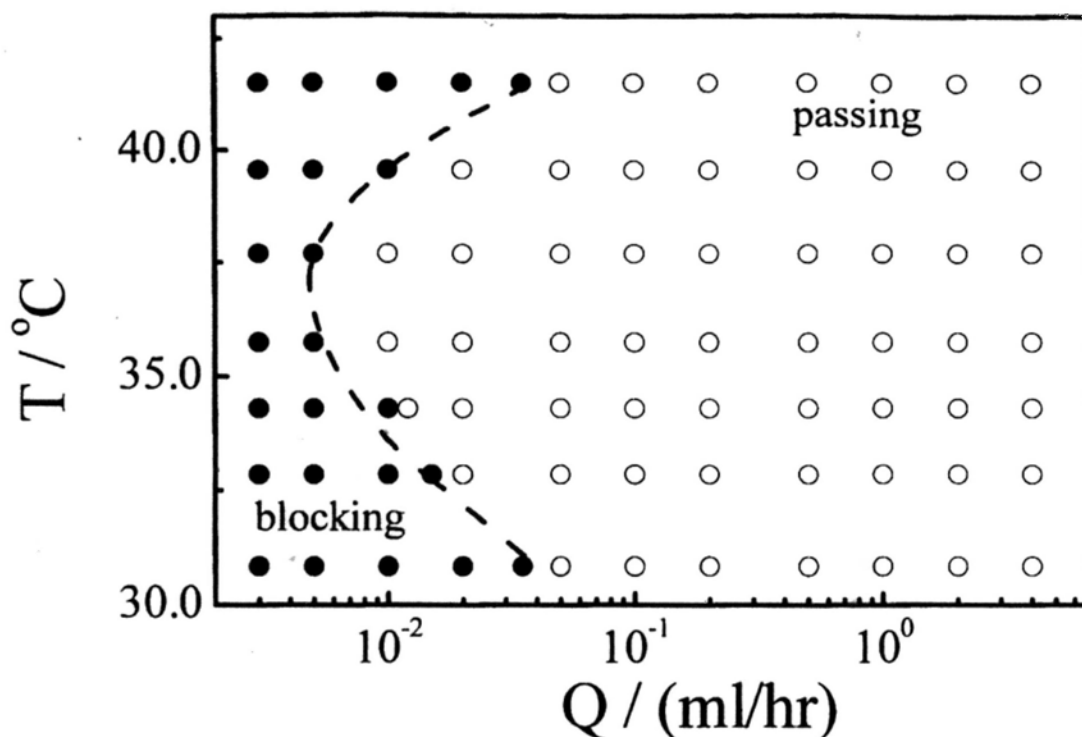
However, our measured q_c values are ~10-200 times smaller than $k_B T/(3\pi\eta)$ predicted.[1,2] Note that in the prediction the confinement force (F_c) equals ($k_B T/D^3)D^2$, i.e., $F_c = k_B T/D$, where $k_B T/D^3$ is the osmotic pressure generated by the random Brownian motion of the gravity center of the chain segments inside each blob.[25,26] In reality, each blob contains a swollen chain segment and is draining; namely, the hydrodynamic force [$F_h = 3\pi\eta(q/D^2)L_e$] on each blob should be much stronger than $3\pi\eta q/D$ because $L_e = \int_0^{l_b} \bar{v}\,dl = \frac{a}{\sqrt{3}}g_\xi > D$, where L_e is the effective length of the subchain segment inside each blob, $\bar{v}$ is the flow velocity, paralleling to the central line of the nanopore, l_b is the contour length of the chain segment, $a/\sqrt{3}$ is the average distance between any adjacent two monomers along the flow field,[19] $g_\xi = M_b/M_0$ is the monomer number in one blob, where M_b and M_0 are the molar masses of the blob and the segment, respectively. When $F_h = F_c$, q reaches its critical value, i.e.,

$$q_c = \frac{k_B T}{3\pi\eta}\left(\frac{D}{L_e}\right) \tag{4.2}$$

Qualitatively, it explains why our measured q_c values are much smaller than $k_B T/(3\pi\eta)$ because $L_e \gg D$. Quantitatively, we can estimate L_e assuming that each blob has a size of D. Using the scaling $D = kM_b^\upsilon$, we have $L_e = aM_b/\sqrt{3} M_0 = (a/\sqrt{3}M_0)k^{-1/\upsilon}D^{1/\upsilon}$, where υ is the Flory exponent and k is a constant for a given polymer solution. Equation 4.2 can be rewritten as

$$q_c = \frac{k_B T}{3\pi\eta}\left(\frac{\sqrt{3}M_0}{a}\right)\frac{D}{M_b} = \frac{\sqrt{3}k_B T}{3\pi\eta}\frac{M_0}{a}k^{\frac{1}{\upsilon}}D^{1-\frac{1}{\upsilon}} \tag{4.3}$$

It explains why $q_c/[k_B T/(3\pi\eta)]$ decreases with the temperature in the range $T \geq \Theta$ because M_b increases as the chain shrinks for a given pore size (D). Quantitatively, taking the theta state as a reference,[26] we have $k = 2.82 \times 10^{-9}$ cm and $\upsilon = 0.5$. Replacing $M_0 = 104$ g/mol, $D = 2 \times 10^{-6}$ cm and $\upsilon \approx 0.26$ nm $= 2.6 \times 10^{-8}$ cm, we have $q_c/[k_B T/(3\pi\eta)] \approx 9.2 \times 10^{-3}$, not too far away from those listed in Table 4.1.

Table 4.1 Solution-temperature dependence of critical macroscopic flow rate (Q_c), reduced critical microscopic flow rate ($q_c/(k_B T/\eta)$) and estimated hydrodynamic force (F_h) required to deform, stretch and pull long linear polystyrene chains in cyclohexane to pass through small pores (20 nm), where F_h is calculated using eq.4.4 (please refer the text for details) and the uncertainties of Q_c (or q_c) and F_h are $\pm5\%$ and $\pm10\%$, respectively.

T / °C	30.85	32.85	34.30	35.80	37.70	39.55	41.55
Q_c / 10^{-2} mL·hr^{-1}	4.25	1.50	1.10	0.60	0.75	1.75	4.25
$q_c/[k_B T/(3\pi\eta)]$ / 10^{-2}	4.32	1.47	0.99	0.56	0.72	1.52	3.56
F_h / fN	83	33	20	11	12	22	58

Following the same argument, we can estimate the hydrodynamic force on one blob by using

$$F_h = 3\pi\eta \frac{q_c}{D^2} L_e = \frac{\sqrt{3}\pi\eta a}{M_0} q_c k^{-\frac{1}{\upsilon}} D^{-2+\frac{1}{\upsilon}} \tag{4.4}$$

Recently, Melchionna et al[26] showed that under a strong squeeze force the chain could self-order into a multifolded state inside a small pore. Here the hydrodynamic force used is very weak and only overcome the entropic elasticity. Therefore, it is reasonable to assume that the chain inside the pore is still made of a string of blobs and the subchain inside each blob follows Gaussian statistics. On the other hand, υ is weakly dependent on the temperature in the range studied anyway. Using $T = \Theta$ (34.5 °C) as a reference point, we can estimate k and ν in the range $T \geq \Theta$ from Figure 4.2, wherein M is a constant, and then calculate the temperature dependence of F_h, as shown in Figure 4.4 and also listed in Table 4.1, where $\tau = (T - \Theta)/\Theta$.
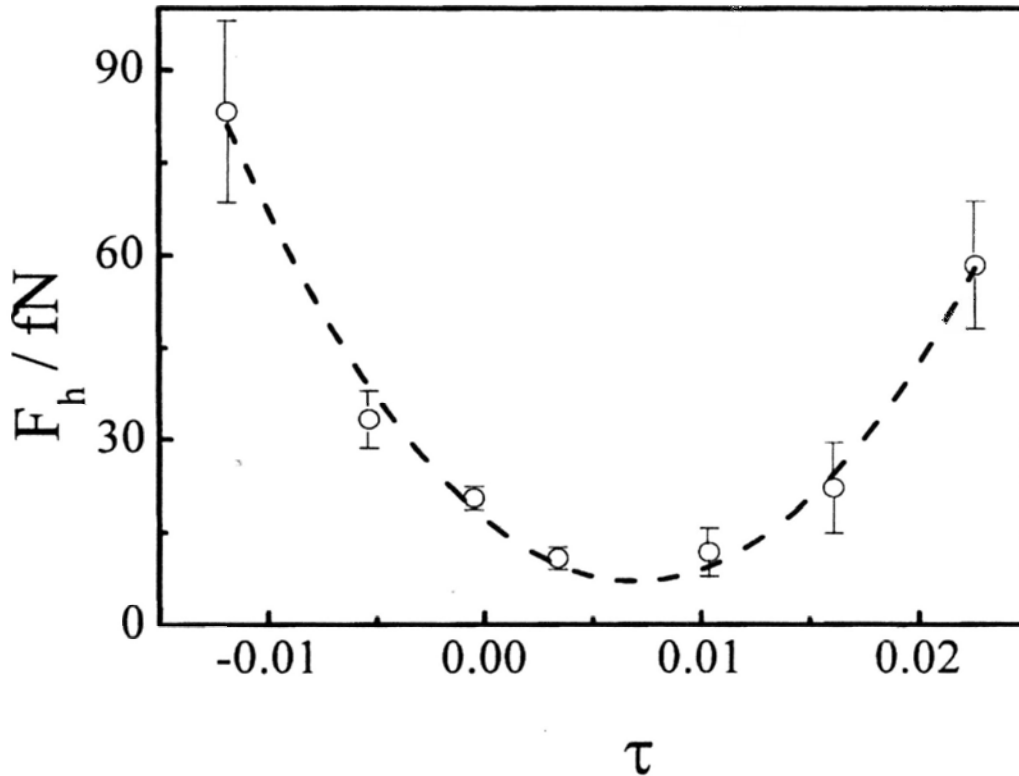
Figure 4.4 Solution temperature dependence of hydrodynamic force (F_h) needed to pull coiled linear polystyrene chains in cyclohexane through small pore (20 nm), where $\tau = (T - \Theta)/\Theta$, a reduced solution temperature and Θ is a solution temperature at which the second virial coefficient vanishes.

Figure 4.4 shows that $F_h = 5.8 \times 10^{-14}$ N at ~42 °C, not too far away from the calculated confinement force ($k_B T/D \sim 2.17 \times 10^{-13}$ N). Note that F_h reach es a minimum at ~36.5 °C, slightly away from the theta point ($\tau = 0$). This is not a

surprise because Θ is defined as the vanishing of the second viral coefficient (A_2), a pseudoideal state. Moreover, Θ is also a function of the chain length.[28] In an ideal solution, all the viral coefficients should approach zero, not only A_2. Therefore, the measurement of the temperature dependence of q_c might provide a better way to determine the true ideal point. The increase of F_h with the temperature in the range T > 36.5 °C is understandable because the entropic elasticity of a polymer chain is higher when the chain expands in a better solvent. On the other hand, one has to overcome some additional segment-segment attraction force when stretching a contracted chain in a poor solvent. This is why F_h increases as the temperature decreases in the range T < 36.5°C.

Noted that eq(4.3) shows that q_c should decreases as the pore size (D) increases, a complicate function of D, different from those previous predictions of the pore size independence.[1,2] To check such a discrepancy, we experimentally increased the pore size from 20 nm to 100 nm and found that q_c decreases from 1.85×10^{-14} to 1.98×10^{-15} mL/s and from 5.56×10^{-15} to 3.97×10^{-16} mL/s, respectively, at 41.6 and 34.3 °C. Equation 4.2 shows that $q_{c,20nm}/q_{c,100nm} \approx 3$ and 5, respectively, for $\upsilon = 0.6$ (athermal) and $\upsilon = 0.5$ (theta), qualitatively agreeing with our experimental results ($\upsilon \simeq 0.52$ at ~42 °C). On the other hand, eq 4.3 shows that $F_h \sim D^{-2+1/\upsilon}$. It means that at T = Θ (i.e., $\upsilon = 0.5$) F_h would be independent of the pore size. Table 4.2 shows that at the theta state F_h is indeed less dependent on D, qualitatively agreeing with eq 4.4.

Table 4.2. Pore size dependence of critical macroscopic flow rate (q_c) and estimated hydrodynamic force (F_h) required to deform, stretch and pull long linear polystyrene chains in cyclohexane to pass through small pores, where F_h is calculated using eq.4.4 and the uncertainties of Q_c (or q_c) and F_h are ±5% and ±10%, respectively.

Pore size		D = 20 nm	D = 100 nm
34.3 °C	q_c / (mL/s)	5.56×10^{-15}	3.97×10^{-16}
	F_h / N	2.0×10^{-14}	3.1×10^{-14}
41.6 °C	q_c / (mL/s)	1.85×10^{-14}	1.98×10^{-15}
	F_h / N	5.7×10^{-14}	1.3×10^{-13}

4.4 Conclusion

In summary, using the critical flow rate (q_c) obtained in the ultrafiltration of polymer chains through smaller pores, we have experimentally estimated the hydrodynamic force (F_h) required to overcome the weak entropic elastic force and stretch a linear chain into a string of blobs with a size comparable to the pore size (D). For linear polystyrene chains in cyclohexane at different solution temperatures, we reveal that the force required to stretch them is in the range 10-100 fN and q_c is indeed independent of the chain length, as predicted. Therefore, it is impossible to separate linear chains with different lengths by using a given membrane with some straight pores. However, our measured values of q_c are much smaller than $k_BT/(3\pi\eta)$ predicted by de Gennes and Pincus. Such a discrepancy is attributed to the improper assumption that each blob made of a subchain segment is a nondraining ball. After considering a possible full hydrodynamic draining and introducing the effective length of each blob along the flow direction (L_e), we are able to qualitatively explain why q_c is 20-140 times smaller than $k_BT/(3\pi\eta)$ and decreases as the pore becomes larger, especially in a good solvent. In comparison with other single-chain methods, such as a combination of tweezers and hydrodynamic force,[29] our method is less precise so that the results presented here are only semi-quantitative, but much cheaper, simpler and more user-friendly.

4.5 References and Notes

[1]   De Gennes, P. G. *J. Chem. Phys.* **1974**, *60*, 5030.

[2]   Pincus, P. *Macromolecules* **1976**, *9*, 386.

[3]   Rouse, P. E. *J. Chem. Phys.* **1953**, *21*, 1272.

[4]   Borisov, O. V.; Darinskii, A. A.; Zhulina, E. B. *Macromolecules* **1995**, *28*, 7180.

[5]   Colby, R. H.; Boris, D. C.; Krause, W. E.; Dou, S. *Rheol. Acta* **2007**, *46*, 569.

[6]   Jin, F.; Wu, C, *Phys. Rev. Letts.* **2006**, *96*, 237801.

[7]   Barrat, J. L.; Joanny, J. F. *Theory of Polyelectrolyte solutions*; **1996**.

[8]   Lemak, A.; Lepock, J. R.; Chen, J. Z. Y. *Proteins: Struct. Funct. Genet.* **2003**, *51*, 224.

[9]   Perkins, T. T.; Smith, D. E.; Chu, S. *Science* **1997**, *276*, 2016.

[10]   Benoit, H.; Doty, P. *J. Phys. Chem.* **1953**, *57*, 985.

[11]   Bohdanecky, M. *Macromolecules* **1983**, *16*, 1483.

[12]   Yamakawa, H.; Fujii, M. *Macromolecules* **1974**, *7*, 128.

[13]   Bednar, J.; Furrer, P.; Stasiak, A.; Dubochet, J.; Engelman, E. H.; Bates, A. D. *J. Mol. Biol.* **1994**, *235*, 825.

[14]   Frontali, C.; Dore, E.; Ferrauto, A.; Gratton, E.; Bettini, A.; Pozzan, M. R.; Valdevit, E. *Biopolymers* **1979**, *18*, 1353.

[15]   Gunari, N.; Schmidt, M.; Janshoff, A. *Macromolecules* **2006**, *39*, 2219.

[16]   Zhang, W.; Zou, S.; Wang ,C.; Zhang, X. *J. Phys. Chem. B* **2000**, *104*, 10258.

[17]   Butt, H. J.; Kappl, M.; Mueller, H.; Raiteri, R.; Meyer, W.; Rühe, J. *Langmuir* **1999**, *15*, 2559.

[18]   Smith, S. B. ; Finzi, L.; Bustamante, C. *Science* **1992**, *258*, 1122.

[19]   Teraoka, I. Eds. *Polymer Solutions: An Introduction to Physical Properties* John Wiley & Sons, InC.; New York, **2002**.

[20]   Berne, B. J.; Pecora, R. *Dynamic Light Scattering*: Vol. Plenum Press: New York, **1976**.

[21] Chu, B. *Laser Light Scattering*: 2nd ed.; Vol. Academic Press: New York, **1991**.

[22] Chu, B.; Ying, Q.; Grosberg, A. *Macromolecules* **1995**, *28*, 180.

[23] Li, J. F.; Li, W.; Hou, H.; Luo, S. Z.; Wu, C. *Macromolecules* **2008**, *41*, 901.

[24] De Gennes, P. G. *Adv. Polym. Sci.* **1999**, *138*, 91.

[25] Rubinsein, M.; Colby, R. H. *Polymer physics*; Oxford University press: London, UK, **2003**.

[26] Appelt, B.; Meyerhoff, G. *Macromolecules* **1980**, *13*, 657.

[27] Melchionna, S.; Bernaschi, M.; Fyta, M.; Kaxiras, E.; Succi, S. *Phys. Rev. E* **2009**, *79*, 030901.

[28] Saeki, S.; Kuwahara, N.; Konno, S.; Kaneko, M. *Macromolecules* **1973**, *6*, 246.

[29] Saleh, O.A.; McIntosh, D.B.; Pincus, P.; Ribeck, N. *Phys. Rev. Lett.* **2009**, *102*, 068301.

Chapter 5 Separation of linear and star chains by a nanopore

5.1 Introduction

The separation of polymer chains with different topologies but a similar hydrodynamic volume is still remained as a real, important and challenging problem in polymer research because we often face a mixture of polymer chains with different topologies due to the nature of some preparation methods. For example, there are usually two ways to prepare star chains with different arms; namely, the core first or the arm first.[1] In the core-first method, a multifunctional initiator is used to initiate polymerization of monomers. Such obtained star chains often have different arm numbers and lengths because not all of the initiating sites are simultaneously activated. In the arm-first method, linear polymer chains with a uniform length and an active end are first synthesized, often by anionic polymerization, and then they are coupled together with a multifunctional core. In order to make sure that each of the reactive sites on the core is attached with one arm, the number of linear chains must be much larger than that of active sites on the core. After such a coupling reaction, one inevitably has a mixture of linear and star chains. For star chains with few arms, their hydrodynamic volume is not much different from that of individual arms so that a conventional size exclusion chromatography (SEC) is not able to effectively and cleanly separate them. Previously, Meunier and his coworkers[2-4] tried to use different flow rates to separate polymer chains with different topologies by extruding a mixture of them through some monolithic columns packed with specially prepared polystyrene latex particles, which involves some unclear size exclusion mechanisms.

Recently, we experimentally confirmed a previous prediction; namely, there exist a critical flow rate ($q_{c,linear}$) for linear polymer chains to pass through a nanopore under an elongational flow filed[5,6] and such a critical flow rate is independent on the chain length but related to the pore diameter (D) as[7] $q_{c,linear} = \dfrac{k_B T}{3\pi\eta} k^{-1} D^{1-\frac{1}{\upsilon}}$, where k_B, T and η are the Boltzmann constant, the absolutely temperature, the solvent viscosity, respectively; k is a constant for a given polymer solution, but $1/2 \leq \upsilon \leq 3/5$, depending on the solvent quality.[8] It is energetically favored for star chains with f arms to crawl through a nanopore under an elongational flow by a symmetrical mode,

i.e., putting a half number of their arms forward. In such a mode,[9,10] there also exists a critical flow rate $q_{c,star} = q_{c,linear}(f/2)$. Note that linear chains are a special kind of star chains with f = 2. It is clear from a theoretical point of view that even for f = 3, $q_{c,star}$ is still 1.5 times higher than $q_{c,linear}$. Therefore, it is practically possible to separate linear and star chains by flushing a mixture of them through a nanopore with a properly chosen flow rate.

5.2 Experimental Section

To test such a possibility, we synthesized polystyrene (PS) linear and star chains (up to 41 arms) with different lengths by using divinylbenzene to couple living polystyl linear chains in solution. The details can be found elsewhere.[1,11,12] We further fractionate such prepared star chains into a series of narrowly distribution star chains with different numbers of arms.[13] The 3-arm star chains was previously synthesized by using chlorosilane as the coupling agent.[11] The molecular parameters, such as the weight-average molar mass (M_w), the polydispersity index (M_w/M_n) and average hydrodynamics radius ($<R_h>$) characterized by laser light scattering (LLS) of such obtained star chains as well as three linear chains used were summarized in Table 5.1.

Table 5.1. Summary of star, linear and reference polymer chains used in this study.

Polymers	f	$M_{w,arm}$ / (g mol^{-1})	$M_{w,star}$ / (g mol^{-1})	M_w/M_n	$<R_h>$ / nm
Reference	2	2.15×10^4	4.30×10^4	1.04	5
Linear-1	2	2.95×10^5	5.90×10^5	1.01	22
Linear-2	2	9.00×10^6	1.80×10^7	1.08	160
Star-3	3	2.10×10^5	6.30×10^5	1.08	32
Star-41	41	2.10×10^5	8.61×10^6	1.20	61

A modified commercial LLS spectrometer (ALV/DLS/SLS- 5022F) equipped with a multi-τ digital time correlator (ALV5000) and a cylindrical 22 mW UNIPHASE He-Ne laser (λ_0 = 632 nm) was used to characterize each solution before and after it

passes through the nanopores. The incident beam was vertically polarized with respect to the scattering plane. The details of the instrumentation and theory can be found elsewhere.[14] In static LLS, the excess absolute time-averaged scattered light intensity, known as the excess Rayleigh ratio $R_{vv}(\theta)$, of a very dilute polymer solution at an infinite small angle is proportional to the weight average molar mass (M_w). In dynamic LLS, the intensity-intensity time correlation function $(G^{(2)}(\tau))$ is measured. Each measured $G^{(2)}(\tau)$ is related to a normalized field-field autocorrelation function $|g^{(1)}(\tau)|$. The Laplace inversion of $g^{(1)}(\tau)$ leads to a line-width distribution $G(\Gamma)$ that can be converted to a hydrodynamic radius distribution $f(R_h)$ by the Stocks-Einstein equation.[14,15]

In our ultrafiltration experiments, a double layer membrane filter (Whatman, Anotop 10) was used. The top and bottom layers contain an equal number of 200 nm and 20 nm cylindrical pores, respectively; i.e., each large pore is on top of a small pore. Such a structure prevents any possible interference of the flow fields generated by different small pores at their entrances. Note that we purposely added a certain amount of short Reference PS chains with a size smaller than 20 nm in each solution. These short chains will pass the nanopore even without any flow so that they served as an internal reference. The concentrations of star, linear and reference chains (C_S, C_L and C_R) are properly chosen so that $<I_S>/<I_R> = C_S M_S/C_R M_R \sim 1$ and $<I_L>/<I_R> = C_L M_L/C_R M_R \sim 1$, where "$<I_S>$, $<I_L>$ and $<I_R>$" and "M_S, M_L and M_R" are the average scattered light intensity and the molar masses of star, linear and reference chains, respectively. In dynamic LLS, $<I_S>/<I_R>$ and $<I_L>/<I_R>$ are proportional to the area ratio of their corresponding peaks in $G(\Gamma)$. The scattered light intensity is proportional to the square of mass of a scattering subject. Therefore, the decrease of $<I_S>/<I_R>$ or $<I_L>/<I_R>$ sensitively reflects the retention of star or linear chains by the nanopore.[16] The solution temperature (T) and the flow rate (q) were precisely controlled by an incubator (Stuart Scientific, S160D) ($\pm$ 0.1 °C) and a syringe pump (Harvard Apparatus, PHD 2000), respectively.

5.3 Result and discussion

Figure 5.1 shows how Star-3 and Linear-1 chains in a mixture are separated by different flow rates. When the flow rate is 5.56×10^{-12} mL s^{-1}, higher than $q_{c,star}$(5.43×10^{-14} mL s^{-1} for Star-3), we observed two peaks, as shown in Figure 5.1a, very

similar to those before the extrusion, indicting that both Star-3 and Linear-1 chains have passed through the nanopore under such a flow. Note that Star-3 and Linear-1 chains have a similar average hydrodynamic size so that they appear as one peak in $f(R_h)$. As the flow rate decreases to 2.78×10^{-14} mL s^{-1}, lower than $q_{c,star}$(Star-3) but higher than $q_{c,linear}$(1.94×10^{-14} mL s^{-1}), Figure 5.1b shows that the peak located at ~25 nm shrinks, revealing, in principle, that Star-3 chains in the solution mixture are retained, but we are not really sure about it. This is why we put a question mark on it. Figure 5.1c shows that further decrease of the flow rate to 2.78×10^{-15} mL s^{-1}, lower than $q_{c,linear}$, only one peak related to Reference chains appears after the extrusion, clearly demonstrating that both Star-3 and Linear-1 chains are not able to pass through the nanopore under this condition.
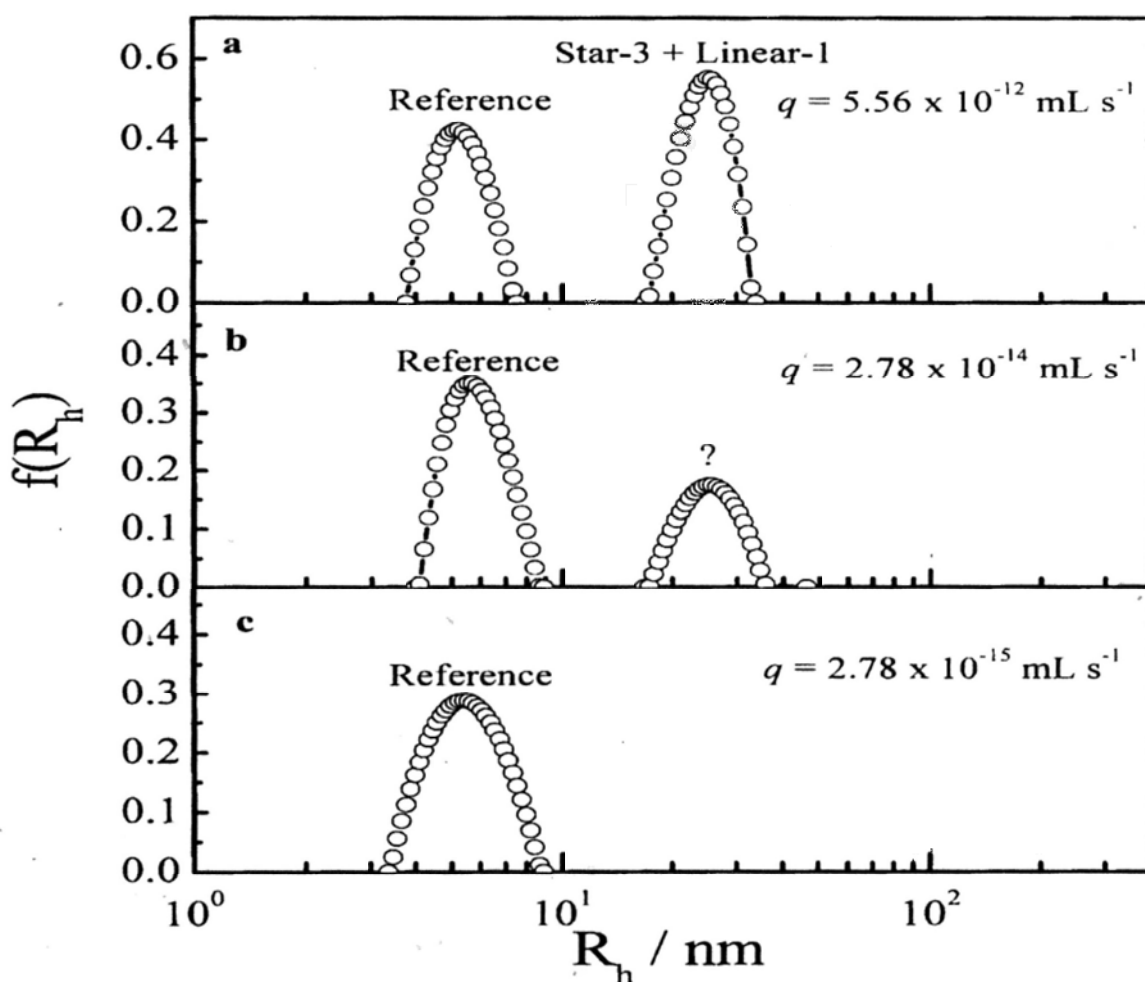

Figure 5.1 Hydrodynamic radius distribution of a mixture of Reference, Linear-1 and Star-3 chains in toluene at T = 25°C after the solution is extruded through nanopores under different elongational flow rates, where $C_{Reference} = 1.20 \times 10^{-2}$ g/mL, $C_{Linear-1} = 2.50 \times 10^{-4}$ g/mL and $C_{Star-3} = 3.80 \times 10^{-4}$ g/mL, respectively.
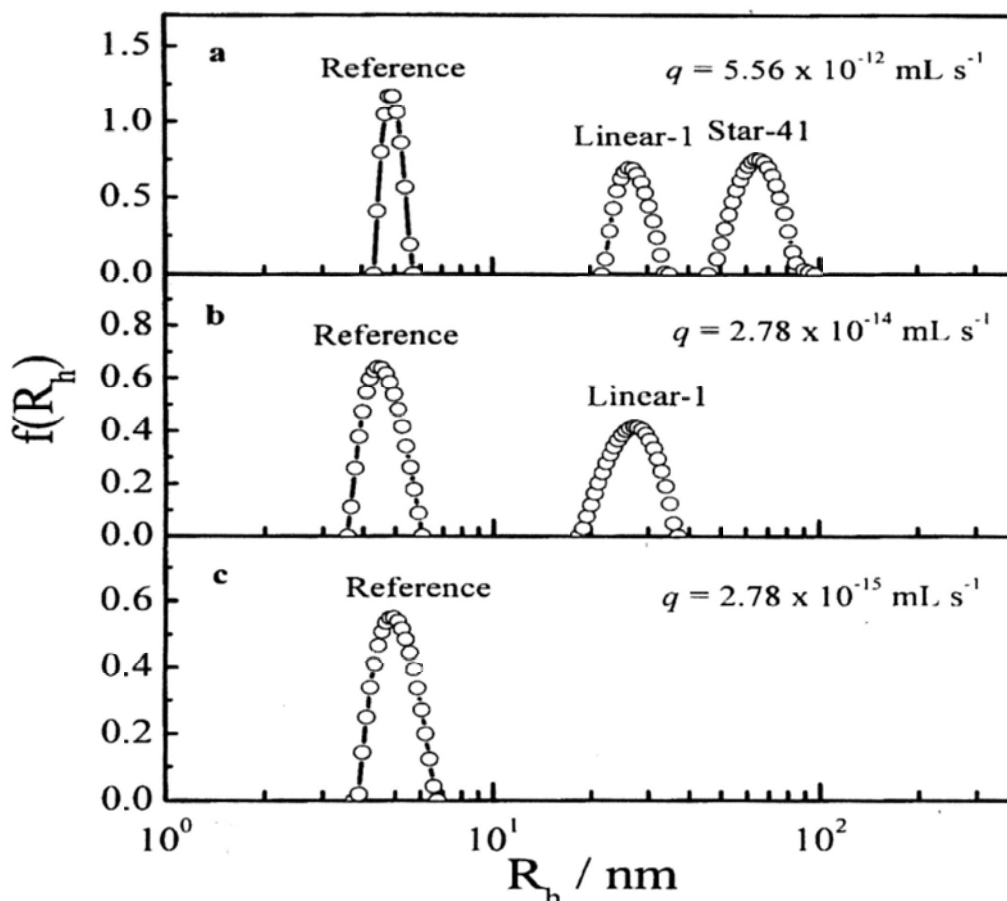
Figure 5.2 Hydrodynamic radius distribution of a mixture of Reference, Linear-11 and Star-41 chains in toluene at T = 25°C after the solution is extruded through nanopores under different elongational flow rates, where $C_{Reference} = 2.00 \times 10^{-2}$ g/mL, $C_{Linear-1} = 8.00 \times 10^{-4}$ g/mL and $C_{Star-41} = 1.00 \times 10^{-4}$ g/mL, respectively.

In order to prove that at $q = 2.78 \times 10^{-14}$ mL s^{-1}, only linear chains have passed through the nanopore, we further mixed much bigger Star-41 chains with Linear-1 chains so that we can resolve them in $f(R_h)$. Figure 5.2a shows two well-separated peaks, respectively, located at ~25 nm and ~60 nm, when the flow rate is much higher than both $q_{c,star}$ and $q_{c,linear}$, very similar to those before the extrusion. This is expected because both Star-41 and Linear-1 chains have passed through the nanopore under this condition. When the flow rate is decreased to the range $q_{c,linear} < q < q_{c,star}$(Star-41), Figure 5.2b shows that the peak associated to Star-41 completely disappears, presumably, retained by the filter. It clearly shows that we are able to effectively and cleanly separate Star-41 and Linear-1 chains by using a properly chosen flow rate. As expected, further decrease of the flow rate to $q < q_{c,linear}$, the peak associated to Linear-1 chains also vanishes (Figure 5.2c). Therefore, we are not

only able to separate star and linear chains by a properly chosen flow rate, but also able to fractionate them by gradually increasing q.
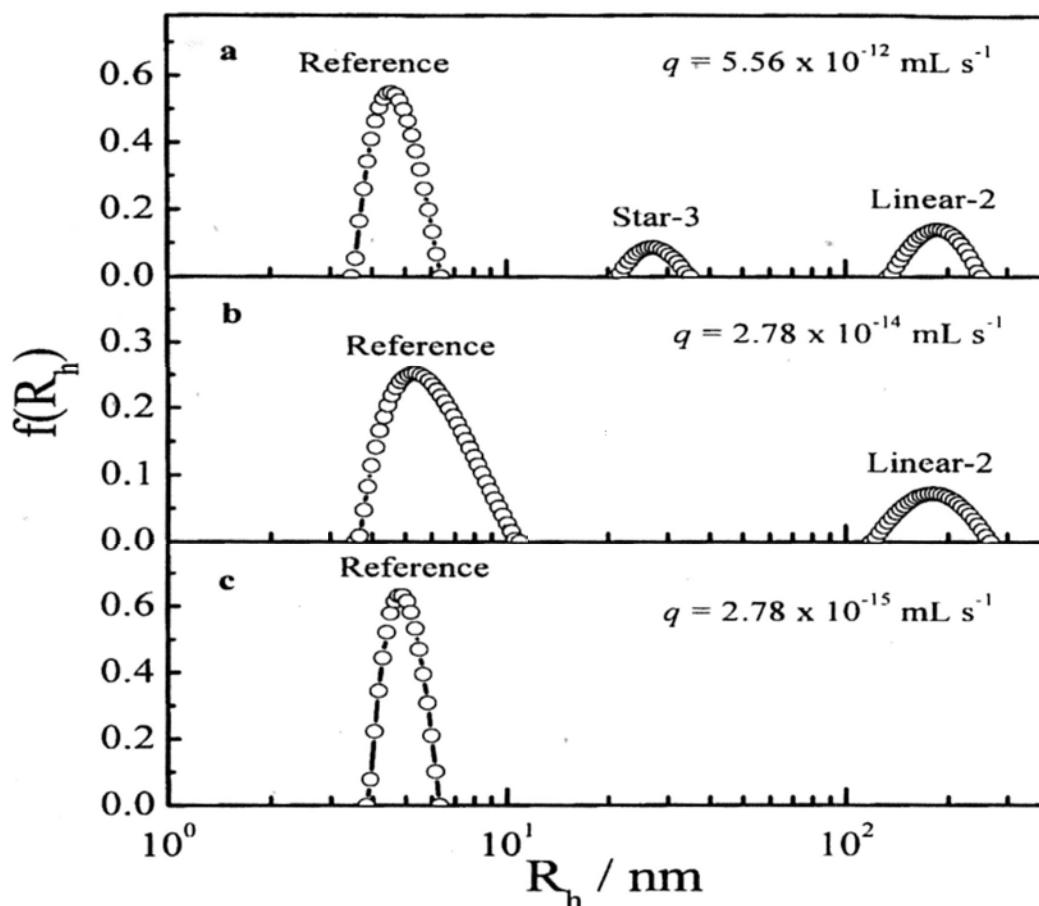

Figure 5.3 Hydrodynamic radius distribution of a mixture of Reference, Linear-2 and Star-3 chains in toluene at T = 25°C after the solution is extruded through nanopores under different elongational flow rates, where $C_{Reference} = 1.80 \times 10^{-2}$ g/mL, $C_{Linear-3} = 8.00 \times 10^{-6}$ g/mL and $C_{Star-3} = 2.50 \times 10^{-4}$ g/mL, respectively.

An attentive reader might say "Of cause, this is just a size effect, not related to the chain topology, because Star-41 chains are much bigger than Linear-1 chains." To prove that such a separation is indeed due to the topology, not the size, of polymer chains, we have further mixed smaller Star-3 chains with relatively bigger Linear-2 chains. As expected, both Linear-2 and Star-3 chains are able to pass through the nanopore when q is higher than both $q_{c,star}$ and $q_{c,linear}$, appearing as two distinguished additional peaks in Figure 5.3a. The decrease of the flow rate into the range $q_{c,linear} < q < q_{c,star}$(Star-3) results in the block of Star-3 chains, as shown in Figure 5.3b, even though they are smaller than Linear-2 chains, clearly demonstrating that the

separation of polymer chains in our experiment is due to different chain topologies, not their sizes. As expected, Figure 5.3c shows that when the flow is sufficiently low, both Star-3 and Linear-2 chains are retained. It is worth-noting that for the convenience of discussion, we have shown the results in an decreasing order of the flow rate. In a real separation/fractionation experiment, we increase q step-by-step so that linear chains pass first and then followed by star chains.

5.4 Conclusion

In summary, we have clearly demonstrated that under an elongational flow: 1) polymer chains with different topologies are able to "crawl" through a much smaller pore only when the flow rate (q) is higher than their corresponding critical values (q_c), independent on their sizes; and 2) one can effectively and cleanly separate and fractionate star and linear polymer chains in terms of different chain topologies, not their sizes, when the flow rate is properly chosen; namely, $q_{c,star} < q < q_{c,linear}$. Further, such a novel method can be further developed to separate and fractionate a mixture of polymer chains with different topologies, especially a mixture of linear chains with other topological chains, such as ring and branched chains as long as we know their corresponding critical flow rates. For a mixture of branched chains with different sizes or star chains with different numbers of arms, we expect that one can separate and fractionate them by gradually increase the flow rate in a step-by-step fashion.

5.5 References and Notes

[1] Hadjichristidis, N.; Pitsikalis, M.; Pispas, S.; Iatrou, H. *Chem. Rev.* **2001**, 101, 3747.

[2] Meunier, D. M.; Smith, P. B. *Macromolecules* **2005**, 38, 5313.

[3] Meunier, D. M.; Stokich Jr. T. M.; Gillespie, D.; Smith, P. B. *Macromol. Symp.* **2007**, 257, 56.

[4] Edam, R.; Meunier, D. M.; Mes, E. P. C.; Van Damme, F. A.; Schoenmakers, P. J. *J. Chromatogr. A.* **2008**, 1201, 208.

[5] De Gennes, P. G. *J. Chem. Phys.* **1974**, 60, 5030.

[6] Pincus, P. *Macromolecules* **1976**, 9, 386.

[7] Ge, H.; Jin, F.; Li, J. F.; Wu, C. *Macromolecules* **2009**, 42, 4400.

[8] Teraoka, I. Eds. *Polymer Solutions: An Introduction to Physical Properties* John Wiley & Sons, InC.; New York, **2002**.

[9] Brochard-Wyart, F.; De Gennes, P. G. *C. R. Acad. Sci. ser II.* **1996**, 323, 473.

[10] De Gennes, P. G. *Adv. Polym. Sci.* **1999**, *138*, 91.

[11] Lee, H. J.; Lee, K.; Choi, N. *J. Polym. Sci., Part A: Polym. Chem.* **2005**, 43, 870.

[12] Hadjichristidis, N.; Iatrou, H.; Pispas, S.; Pitsikalis, M. *J. Polym. Sci. Part A: Polym. Chem.* **2000**, 38, 3211.

[13] Zhou, S. Q.; Fan, S. Y.; Au-yeung, S. T. F.; Wu, C. *Polymer* **1995**, 36, 1341.

[14] Chu, B. *Laser Light Scattering*: 2nd ed.; Vol. Academic Press: New York, **1991**.

[15] Berne, B. J.; Pecora, R. *Dynamic Light Scattering*: Vol. Plenum Press: New York, **1976**.

[16] Jin, F.; Wu, C, *Phys. Rev. Letts.* **2006**, 96, 237801.

Chapter 6
How do star chains pass through a nanopore under a flow?

6.1 Introduction

de Gennes and Pincus predicted that the critical (minimum) flow rate ($q_{c,1}$) for a linear chain to pass through a nanopore is independent on both the chain length and the pore size,[1,2] i.e., $q_{c,1} = k_BT/(3\pi\eta)$, where k_B, T and η are the Boltzmann constant, the absolutely temperature and viscosity, respectively. Our previously study showed that the chain length indeed has no effect on $q_{c,1}$,[3] but $q_{c,1}$ decreases as the pore size increases. In addition, the measured $q_{c,1}$ is ~10-200 time smaller than the predicted ones, depending on the solvent quality and the pore size. Such discrepancies are attributed to an over-simplified assumption in theory; namely, each blob (the subchain confined inside the nanopore) is a hard sphere so that its experienced hydrodynamic force along the flow direction is linearly proportional to the pore diameter (D). In reality, the hydrodynamic force (F_h) experienced by the subchain should be related to its effective length (L_e) along the flow direction, i.e., the integration of all segments inside each subchain along the flow direction, $F_h \propto L_e = \int_0^{l_b} \bar{v}dl$, where $\bar{v}$ is the flow velocity, parallel to the central line of the nanopore and l_b is the contour length of the subchain. Assuming that the subchain inside each blob takes a random Gaussian coil conformation, the average of the projection of each segment with a length of l_s along the flow direction is $l_s/\sqrt{3}$. Therefore, $L_e = l_b/\sqrt{3} = kD^{1/\upsilon} > D$, k is a scaling constant and $1/2 \le \upsilon \le 3/5$, depending on the solvent quality.[4] In this way, F_h is not a linear function of D so that $q_{c,1}$ should be modified as:[3]

$$q_{c,1} = \frac{k_BT}{3\pi\eta}(D/L_e) = \frac{k_BT}{3\pi\eta}k^{-1}D^{1-\frac{1}{\upsilon}} \qquad (6.1)$$

Eq (6.1) clearly shows that it is impossible to use the ultrafiltration of linear polymer chains through a nanopore to separate them with different lengths. The dependence of $q_{c,1}$ on the pore size, was experimentally verified.[3]

In contrast to linear chains, the ultrafiltration of polymers with some complicated

structure, such as star and branched configurations, through a nanopore is more intricate. In theory, a regular star polymer with f number of uniform arms joined at a central point might be the simplest case.[5] In 1996, de Gennes and Brochard-Wyart[6,7] formulated how such a star chain passes through a nanopore under an elongational flow field. They showed that the critical (minimum) flow rate ($q_{c,star}$) depends not only on the total number of arms, but also on the number of forwarded arms (f_{in}) squeezed into the nanopore. In their theory, $q_{c,star}$ is related to the arm length when $f_{in} < f/2$, where they assumed that each forwarded arm inside the nanopore is fully stretched under the flow field, i.e., by the hydrodynamic force.

Such predictions and their speculated applications have existed for years,[6-8] but never been experimentally verified. This is partially because this kind of experimental studies involves a combination of delicate polymer synthesis and precise physical characterization. Namely, 1) star polymers should be narrowly distributed in terms of both the arm number and length; 2) the hydrodynamic radius of stars must be larger than the pore diameter, i.e., each arm must be sufficiently long (over 10^3 monomers); and 3) the preparation of a proper nanopore structure so that the flow at its entrance is close to elongational without any rotational component.[7] Recently, using high-vacuum anionic polymerization,[9] we have overcome difficulties in the preparation of star chains with different arm numbers and lengths. Armed with these well-defined star polymers and using our previously established ultrafiltration method, we have finally experimentally studied how star chains pass through a nanopore.

6.2 Experimental Section

6.2.1 Sample preparations

Polystyrene (PS) linear and star chains (up to 41 arms) with different lengths, as summarized in Table 6.1, were synthesized using a combination of high-vacuum anionic polymerization and a coupling method of using divinylbenzene (DVB).[9-11] Namely, using high-vacuum anionic polymerizaition, we first prepared narrowly distributed linear PS living chains with an active anionic end by initiating styrene (St, from Aldrich) with n-Butyllithium (n-BuLi, 1.5M in cyclohexane, from Aldrich) in cyclohexane at ~30 °C. Further, these linear chains are coupled together to form star chains when a required amount of DVB molecules were added into the

solution of living polystyl anions. The ratio of [DVB]:[anions] was kept at 0.7:1. All the chemicals were purified before the polymerization. The details can be found elsewhere.[9,11] The coupling reaction between linear polystyl anions and DVB was lasted for 1-7 days, depending on the arm length. The longer the arm length was, the longer the coupling reaction time would be. Further addition of the same amount of DVB resulted in star chains with more arms. Such a step-by-step addition of DVB finally led to a series of star chains with different arm numbers but an identical arm length.[10] Note that such prepared star chains are broadly distributed in the arm number. Therefore, we further fractionated them by the following procedure;[12] 1) dissolving these star chains in 1,4-dioxane at 80 °C with a concentration of 0.03 g/mL; 2) adding ethanol dropwise until the solution just became slightly milky; 3) letting the solution standing at the room temperature for few weeks so that a small fraction of star chains with the highest number of arms precipitated out of the solution.; and 4) Repeating Steps 2 and 3 to obtain narrowly distributed star chains with different arms. The 3-arm star chains (M_{w_arm} = 2.1 x 10^5 g/mol, M_w/M_n = 1.08) was previously synthesized by using chlorosilane as the coupling agent.[9] The weight-average molar mass (M_w) and polydispersity index (M_w/M_n) of such obtained star chains were characterized by laser light scattering (LLS), also as summarized in Table 6.1.

Table 6.1. Arm number (f), length ($M_{w,arm}$), weight molar mass ($M_{w,star}$), polydispersity index (M_w/M_n) and average hydrodynamic radius ($<R_h>$) of polystyrene star and linear chains in toluene.

Code	f	$M_{w,arm}$/ (g mol^{-1})	$M_{w,star}$ / (g mol^{-1})	M_w/M_n	$<R_h>$ / nm
Star-41	41	2.10 x 10^5	8.61 x 10^6	1.20	61
Star-6A	6	1.30 x 10^5	7.80 x 10^5	1.18	28
Star-6B	6	2.10 x 10^5	1.26 x 10^6	1.20	41
Star-6C	6	3.50 x 10^5	2.10 x 10^6	1.20	56
Star-3	3	2.10 x 10^5	6.30 x 10^5	1.08	32
Star-2 (linear chain)	2	5.90 x 10^5	5.90 x 10^5	1.01	22

6.2.2. Laser Light Scattering (LLS)

A modified commercial LLS spectrometer (ALV/ DLS/SLS-5022F) equipped with a multi-τ digital time correlator (ALV5000) and a cylindrical 22 mW UNIPHASE He-Ne laser (λ_0 = 632 nm) was used. The incident beam was vertically polarized with respect to the scattering plane. The details of the LLS instrumentation and theory can be found elsewhere.[13]

In dynamic LLS, the intensity-intensity time correlation function ($G^{(2)}(\tau)$) of each polymer solution was measured before and after the ultrafiltration. $G^{(2)}(\tau)$ is related to the normalized field-field autocorrelation function $|g^{(1)}(\tau)|$. The Laplace inversion of each $g^{(1)}(\tau)$ leads to a line-width distribution $G(\Gamma)$ that can be further converted to a hydrodynamic radius distribution $f(R_h)$ by using the Stocks-Einstein equation.[13,14]

Briefly, in static LLS, the excess absolute time-averaged scattered light intensity, known as the excess Rayleigh ratio $R_{vv}(\theta)$, of a dilute polymer solution at concentration C (g/mL) is related to the weight average molar mass M_w, the root-mean square radius of gyration $<R_g^2>^{1/2}$, and the scattering vector k_s as

$$\frac{KC}{R_{vv}(\theta)} \approx \frac{1}{M_w}(1+\frac{1}{3}<R_g^2>h^2)+2A_2C \qquad (6.2)$$

where $K = 4\pi^2 n^2(dn/dC)^2/(N_A\lambda_0^4)$ and $h = (4\pi n/\lambda_0)\sin(\theta/2)$ with N_A, dn/dC, n, θ and λ_0 being the Avogadro number, the specific refractive index increment, the solvent refractive index, the scattering angle and the wavelength of the light in vacuum, respectively; and A_2 is the second virial coefficient. For PS in cyclohexane at 34.5 °C and in toluene at 25 °C, dn/dC = 0.171 and 0.109 mL/g, respectively.

6.2.3. Ultrafiltration

In our ultrafiltration experiments, a double layer membrane filter (Whatman, Anotop 10) was used. The top and bottom layers contain an equal number of 200 nm and 20 nm cylindrical pores, respectively; i.e., each large pore is on top of a small pore. Such a structure prevents any possible interference of the flow fields generated by different small pores at their entrances. In each solution, we added a certain amount of short linear chains with a size smaller than the pore diameter. These short linear

chains will pass the nanopore even without any flow so that they served as an internal standard. The concentrations of large star and short linear chains (C_L and C_S) are properly chosen so that $<I_L>/<I_S> = C_L M_L / C_S M_S \sim 1$, where M_L and M_S are the molar masses of large star and short linear chains, respectively. Note that in dynamic LLS, $<I_L>/<I_S>$ equals the area ratio of their corresponding peaks in $G(\Gamma)$. Since the nanopore has no retention on short linear chains, the decrease of $<I_L>/<I_S>$ must be related to the retention of large star chains. On the other hand, in static LLS, we can measure the total time-average scattered light intensity ($<I_{tot}> = <I_L> + <I_S>$). A combination of static and dynamic LLS measurements enables us to determine $<I_L>$ and $<I_S>$ and then the relative retention $[(C_0 - C)/C_0]$ of larger star chains under different flow rates (q).[15] In each ultrafiltration experiment, the solution temperature and q were controlled by an incubator (Stuart Scientific, S160D) ($\pm$ 0.1 °C) and a syringe pump (Harvard Apparatus, PHD 2000), respectively.

6.3 Result and discussion

Figure 6.1 shows the flow rate (q) dependent relative retention of 6-arm star chains with different arm lengths in toluene. There is no obvious difference in "$[(C_0 - C)/C_0]$ vs q" among these different 6-arm star chains. As discussed in introduction, no arm-length dependence of $q_{c,star}$ should only occur in the symmetrical mode;[6] namely, $f_{in} = f/2$. It has to be stated that de Gennes and Brochard-Wyart[6] assumed that when in the region of $1 \leq f_{in} < f/2$, each arm inside the nanopore is fully stretched so that its effective length along the flow direction is related to the contour length of each arm. In this way, star chains with shorter arms require a higher flow rate to pull the backwarded f_{out} arms through the nanopore because the hydrodynamic force on each arm F_h is proportional to both the arm length and the flow rate. Apparently, if de Gennes and Brochard-Wyart were right, Figure 6.1 would indicate that these 6-arm star chains would only pass through the nanopore via the symmetrical mode, namely, $f_{in} = f/2$.
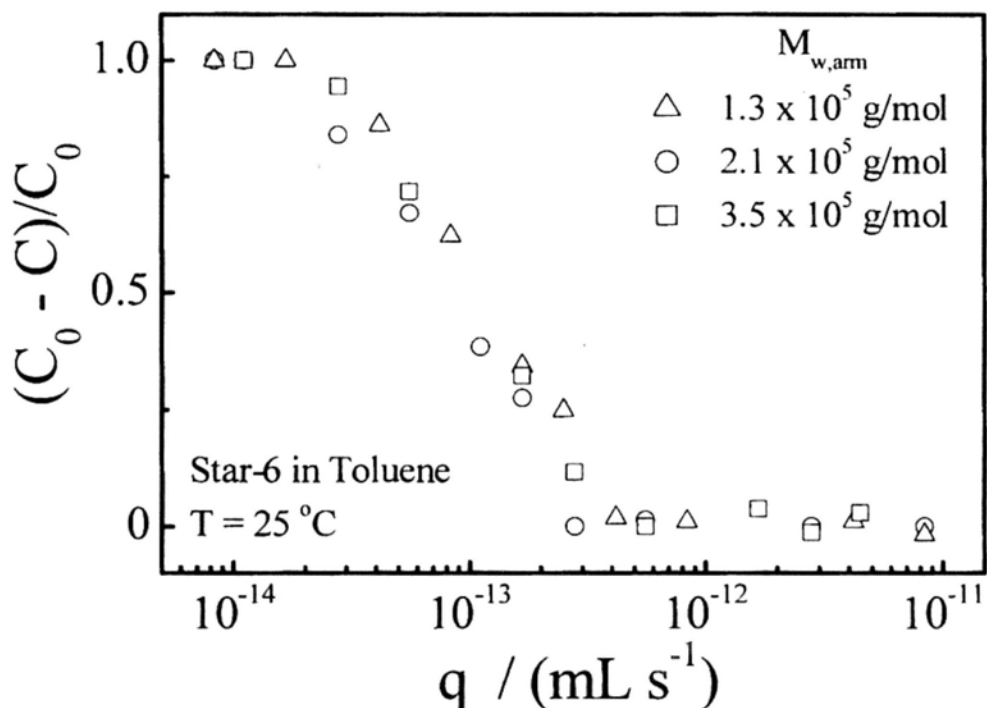
Figure 6.1 Flow rate (q) dependence of relative retention [$(C_0 - C)/C_0$] of star chains with six arms but different arm lengths in toluene, where C_0 and C are the polymer concentrations before and after the ultrafiltration.

Figure 6.2 shows that the relative retention of star chains decreases as the flow rate increases. The change is apparently not as abrupt as the first-order coil-to-stretch transition of linear polymer chains observed before[3,15]. It should be noted that here the x-axis is in a logarithmic scale. The transition is actually sharp except for star chains with 41 arms. For Star-41, f_{in} can, in principle, vary from 1 to 41 and each f_{in} leads to one different $q_{c,star}$, which might explain why the change of " relative retention vs q " is not as sharp as those for Star-6 and Star-3.
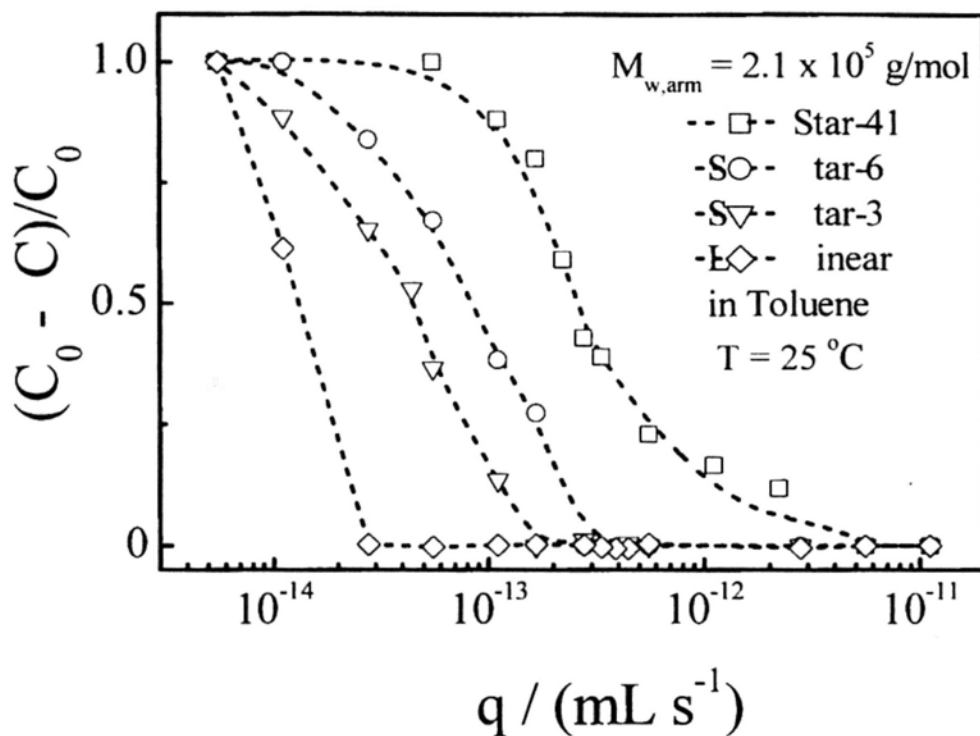
Figure 6.2. Flow rate (q) dependence of relative retention [$(C_0 - C)/C_0$] of star chains with different arm numbers but an identical arm length in toluene, where the weight-average molar mass ($M_{w,arm}$) of each arm is 2.1×10^5 g/mol.

Figure 6.3 shows a better view of a typical variation of the relative retention with q for Star-41 (by differentiation of relative retention to flow rate, i.e., $d[(C_0 - C)/C_0]/dq$)), where we define two critical flow rates ($q_{c,star,s}$ and $q_{c,star,p}$) marked as the starting and peaking positions. For Star-41, $q_{c,star,s} = 2.40 \times 10^{-12}$ mL·s^{-1} and $q_{c,star,p} = 5.14 \times 10^{-13}$ mL·s^{-1}. These measured critical flow rates are different from those predicted by de Gennes and Brochard-Wyart.[6] Therefore, we have to rethink about whether there is something wrong in their assumption and theoretical treatments.
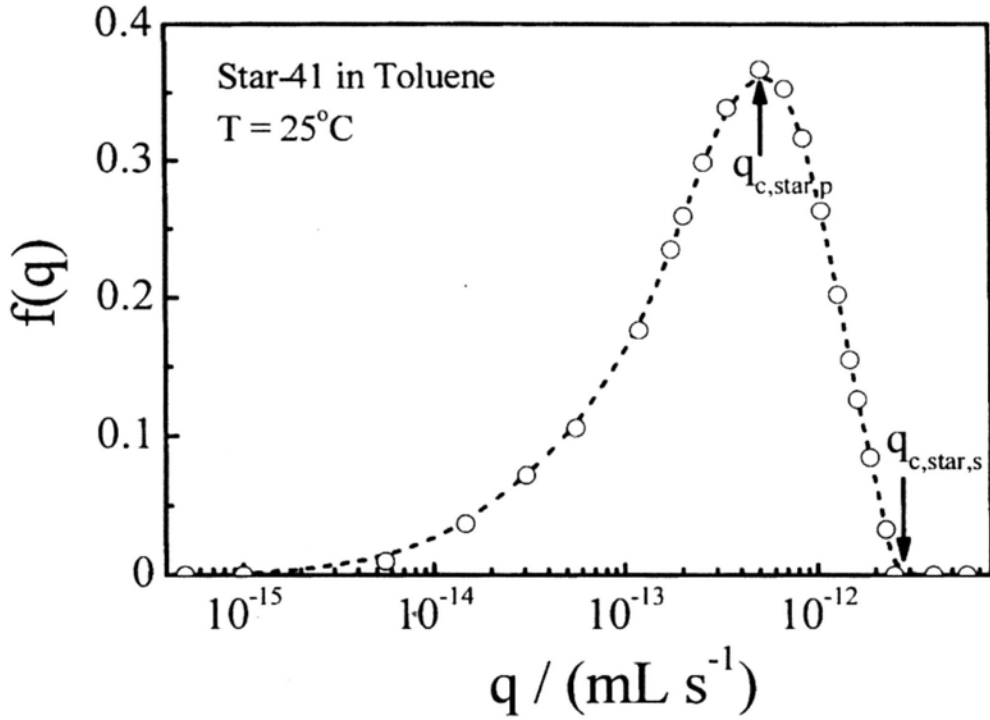
Figure 6.3. Differentiation of relative retention to flow rate, $d[(C_0 - C)/C_0]/dq$, for star chains with 41 arms, where $q_{c,star,s}$ and $q_{c,star,p}$ define the starting and peaking points of retention, respectively.

Figure 6.4 schematically illustrate two different situations: $1 \leq f_{in} \leq f/2$ and $f/2 \leq f_{in} \leq f$, depending on whether more arms are forwarded or backwarded when each star chain enters the nanopore. When $f/2 \leq f_{in} \leq f$, we only need to consider under which flow rate f_{in} arms can enter the nanopore with a diameter (D), not to worry about the backwarded arms because $f_{out} < f_{in}$. Imaging that under the flow, f_{in} arms just filled up the pore, each arm inside is made of n_b blobs and each blob has a diameter of ξ_{in}, we have $\xi_{in}^2 f_{in} = D^2$, as shown in Figure 6.4. Thermodynamically, the force to confine each blob is $k_B T/\xi_{in}$ so that the total confinement force (F_c) is $(k_B T/\xi_{in}) n_b f_{in}$. On the other hand, the hydrodynamic force on each blob is $3\pi\eta l_e(q/D^2)$ and the total hydrodynamic force (F_h) is $3\pi\eta l_e(q/D^2)n_b f_{in}$, where l_e is the effective length of each blob along the flow direction. The condition of $F_h = F_c$ leads to the critical flow rate for $f/2 \leq f_{in} \leq f$,

$$q_{c,star}(f/2 \leq f_{in} \leq f) = \frac{k_B T}{3\pi\eta} f_{in} \frac{\xi_{in}}{l_e} \qquad (6.3)$$
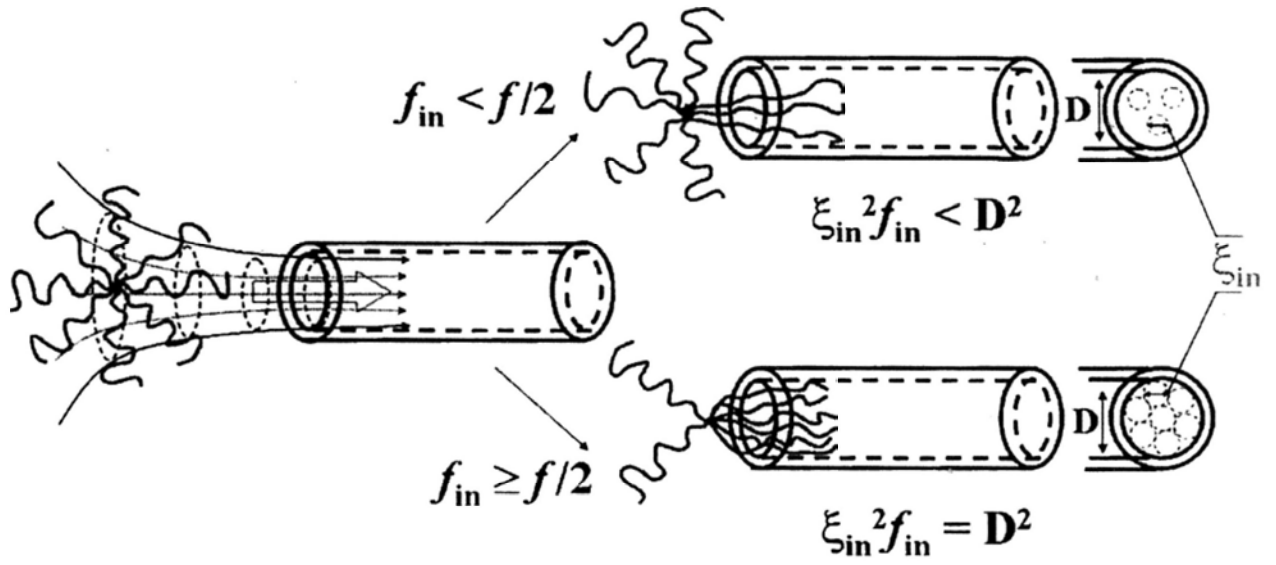
98

Figure 6.4. Schematic of how a star chain enters a nanopore under two different situations; namely, $f \geq f_{in} \geq f/2$ and $f/2 \geq f_{in} \geq 1$.

An attentive reader can find that in the above discussion we only need to consider under which flow rate the first blob of each arm can enter the nanopore because the second and rest blobs just follow the first blob. When $1 \leq f_{in} \leq f/2$, we have to consider how many number of arms are outside of the nanopore, as shown in Figure 6.4. Note that $f_{out} = f - f_{in}$. Obviously, $q_{c,star}$ calculated in eq (6.3) can only pull f_{in} arms in, not sufficient to pull f_{out} arms into the nanopore because $f_{out} > f_{in}$. Therefore, one has to increase q to stretch each arm inside the nanopore further, i.e., ξ_{in} decreases at the same time. In this way, $\xi_{in}^2 f_{in}$ becomes less than D^2, as also schematically shown in Figure (6.4). The decrease of ξ_{in} leads to the increase of the force required to confine each blob. Therefore, when

$$3\pi\eta \frac{q}{D^2} l_e f_{in} = \frac{k_B T}{\xi_{in}} f_{in} = \frac{k_B T}{\xi_{out}} f_{out} ,$$ the hydrodynamic force is just sufficient to pull the

outside backwarded arms into and through the nanopore, wherein $\xi_{out}^2 f_{out} = D^2$, just filled the nanopore. Therefore, we have

$$q_{c,star}(1 \leq f_{in} \leq f/2) = \frac{k_B T}{3\pi\eta} \frac{f_{out}^3}{f_{in}^2} \frac{\xi_{in}}{l_e} \qquad (6.4)$$

If each blob is treated as a hard sphere, i.e., $l_e = \xi_{in}$, eqs (6.3) and (6.4) become

$$q_{c,star}(f/2 \leq f_{in} \leq f) = \frac{k_B T}{3\pi\eta} f_{in} \qquad (6.5a)$$

99

$$q_{c,star}(1 \le f_{in} \le f/2) = \frac{k_B T}{3\pi\eta} \frac{(f - f_{in})^3}{f_{in}^2} \qquad (6.5b)$$

Our revised formulas reveal that $q_{c,star}$ is independent on the arm length no matter what f_{in} is. Note that eq. (6.5a) is identical to that in ref 6 in which de Gennes and Brochard-Wyart mistakenly wrote it $\propto f_{in}^2$ instead of f_{in}. The continuous lines in Figure 6.5 shows how $q_{c,star}$ changes with f_{in} for star chains with different arm numbers on the basis of eqs (6.5a) and (6.5b). It is clear that $q_{c,star}$ linearly increases with f_{in} when $f/2 \le f_{in} \le f$, but dramatically increases as f_{in} decreases when $f_{in} << f/2$. The minimum is located at $f_{in} = f/2$, different from the optimal f_{in} predicted by de Gennes and Brochard-Wyart.[6] Physically, this is reasonable because the decrease of f_{in} reduces the overall hydrodynamic force on the forwarded arms inside the nanopore, and at the same time, increases the force required to confine those backwarded arms still outside the nanopore. As discussed in Introduction for linear chains, we can treat the subchain inside each blob as a random Gaussian coil so that $l_e = k\xi_{in}^{1/\upsilon}$. Therefore, eq 6.5 can be rewritten as

$$q_c(f/2 \le f_{in} \le f) = q_{c,1} f_{in}^{\frac{1}{2}(1+\frac{1}{\upsilon})} \qquad (6.6a)$$

$$q_c(1 \le f_{in} \le f/2) = q_{c,1} \frac{(f - f_{in})^{\frac{3}{2}(1+\frac{1}{\upsilon})}}{f_{in}^{1+\frac{1}{\upsilon}}} \qquad (6.6b)$$

where $q_{c,1}$ is defined by eq (6.1). Eqs (6.6a) and (6.6b) also shows that $q_{c,star}$ is only related to both f_{in} and f and independent on the arm length, independent on f_{in}, agreeing with experimental results in Figure 6.1. Note that linear chains are a special kind of star chains with $f = 2$ and $f_{in} = 1$. Under this special condition, $q_{c,star}$ in eqs (6.6a) and (6.6b) returns to $q_{c,1}$, as expected. Figure 6.5 also shows how $q_{c,star}$ vary with f_{in} for each given with f and υ. Further, we can estimate f_{in} from our measured values of $q_{c,star}/q_{c,1}$ on the basis of eqs (6.5) and (6.6). The results are summarized in Table 6.2.

For Star-41, $q_{c,star,p}/q_{c,1} \sim 26$, not too far away from the minimum point ($f_{in} = f/2$) calculated from eqs (6.5) and (6.6), but lower than that calculated from eqs (6.6). The difference between eqs (6.5) and (6.6) is whether we should treat each blob as a hard sphere. When a half number of arms of a Star-41 chain is squeezed into a nanopore with a diameter of 20 nm, each arm must be highly stretched and ξ_{in} is only 4-5 nm. Note that the estimated diameter of a polystyrene chain is ~1.2 nm. Therefore, each

blob can be viewed as a hard ball filled with the segments of the subchain without draining, which explains why its $q_{c,star,p}/q_{c,1}$ is close to those calculated from eq (6.5). Also note that for Star-41, f_{in} is larger than 13, which is understandable because $q_{c,star}$ increases sharply when f_{in} is low for star chains with a high number of arms.

Table 6.2. Experimental determined values of reduced critical flow rate ($q_{c,star}/q_{c,1}$) and corresponding f_{in} calculated on the basis of eqs 6.5 and 6.6, where $q_{c,1}$ is the critical flow rate for linear chains .

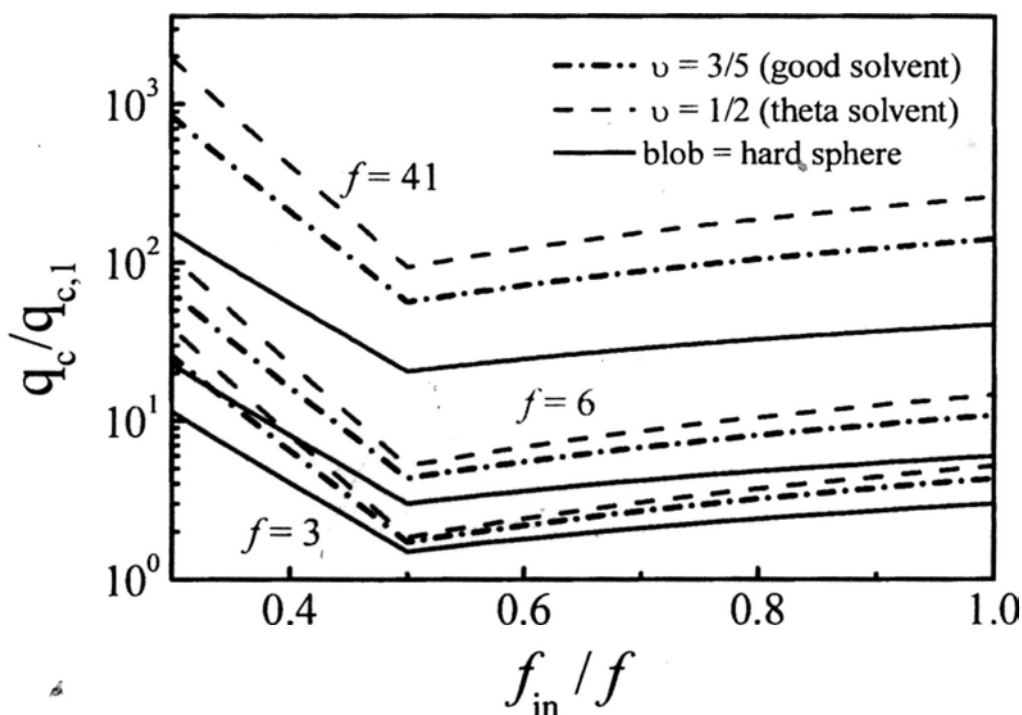| Code	Measured $q_{c,star}/q_{c,1}$	f_{in}	
		Eqs (6.5a) and (6.5b)	Eqs (6.6a) and (6.6b)
Star-41	26.5 – 128.9	13 ~ 41	18 ~ 38
Star-6	6.3 – 21.8	2 ~ 6	2 ~ 6
Star-3	2.8 – 14.4	1 ~ 3	1 ~ 3

Figure 6.5 Forwarded arm number (f_{in}) dependence of reduced critical flow rate ($q_{c,star}/q_{c,1}$) of star chains with different arm numbers but an identical arm length, calculated on the basis of eqs 6.5 and 6.6, respectively.

On the other hand, For Star-6 and Star-3, we found that $q_{c,star,p}/q_{c,l} = 6.3$ and 2.8 respectively, slightly higher than the minimum points (3 and 1-2) calculated based on eqs (6.5), but more close to 4 and 2 estimated from eqs (6.6). It indicates that for star chains with a less number of arms, eqs (6.6) is a better choice because the subchain inside each blob is much less confined; namely, it is not necessary to fully stretch each arm to pull the outside backwarded arms into the nanopore. Also note that a comparison of $q_{c,star}/q_{c,l}$ and eqs (6.6) shows that $2 \leq f_{in}$ (Star-6) ≤ 6 and $1 \leq f_{in}$ (Star-3) ≤ 3, revealing that star chains with a less number of arms can enter the nanopore in different ways even its mostly preferred way is $f_{in} \sim f/2$.

Further, we studied the effect of the arm conformation on $q_{c,star}$ by dissolving polystyrene star chains in cyclohexane in which each arm contracts as the solution temperature decreases below its theta temperature (~34.5 °C), as shown in Figure 6. It should be noted that both the average radius of gyration ($<R_g>$) and hydrodynamic radius ($<R_h>$) of Star-41 chains decrease with the solution temperature, but the change is much smaller than that of linear PS chains within the same temperature range, [5,16] presumably because 41 arms are crowed within a small space and the excluded volume prevents their collapse even in a poor solvent (lower temperatures). It should be noted that in the temperature range studied there is no change in the scattered light intensity, implying that there is no interchain association.
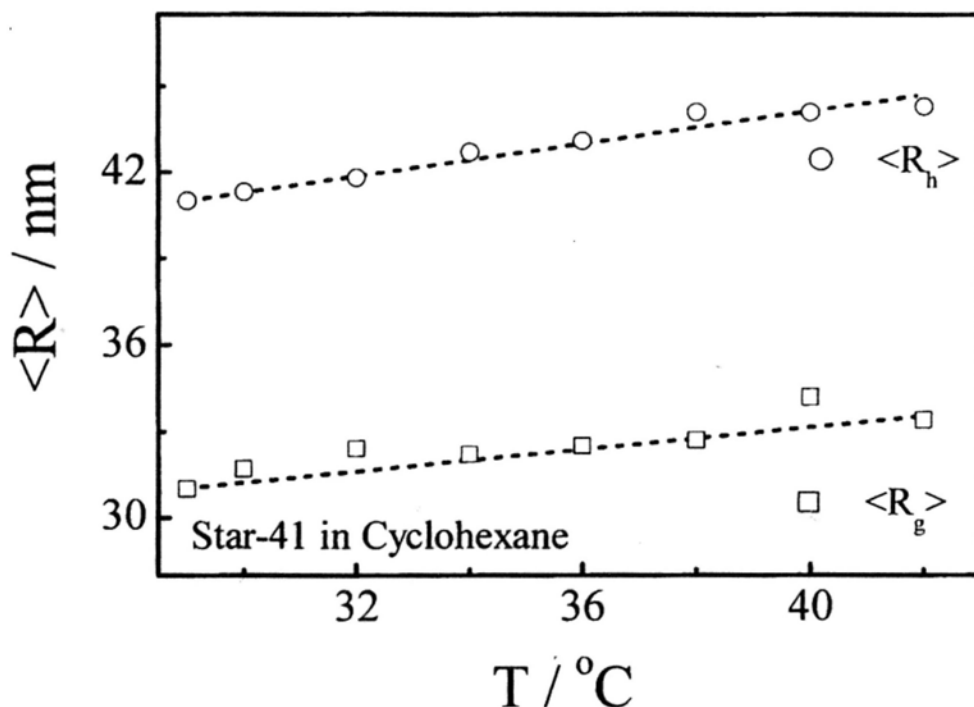

Figure 6.6 Solution temperature dependence of average radius of gyration ($<R_g>$)

and average hydrodynamic radius ($<R_h>$) of star chains with 41 arms in cyclohexane.

It has been previously suggested that the temperature at which q_c reaches its minimum could be attributed to the true theta solvent,[3] which was based of a reasonable assumption that polymer chains at the theta solvent are softest and mostly deformable. Namely, in a good solvent, the chain is highly swollen so that a stronger hydrodynamic force is required to stretch it into a string of blobs and confine each blob inside the nanopore due to its entropic elasticity; while in a poor solvent, the segment-segment attraction is stronger than the segment-solvent interaction so that a stronger hydrodynamic force is needed to overcome the enthalpy-originated force.
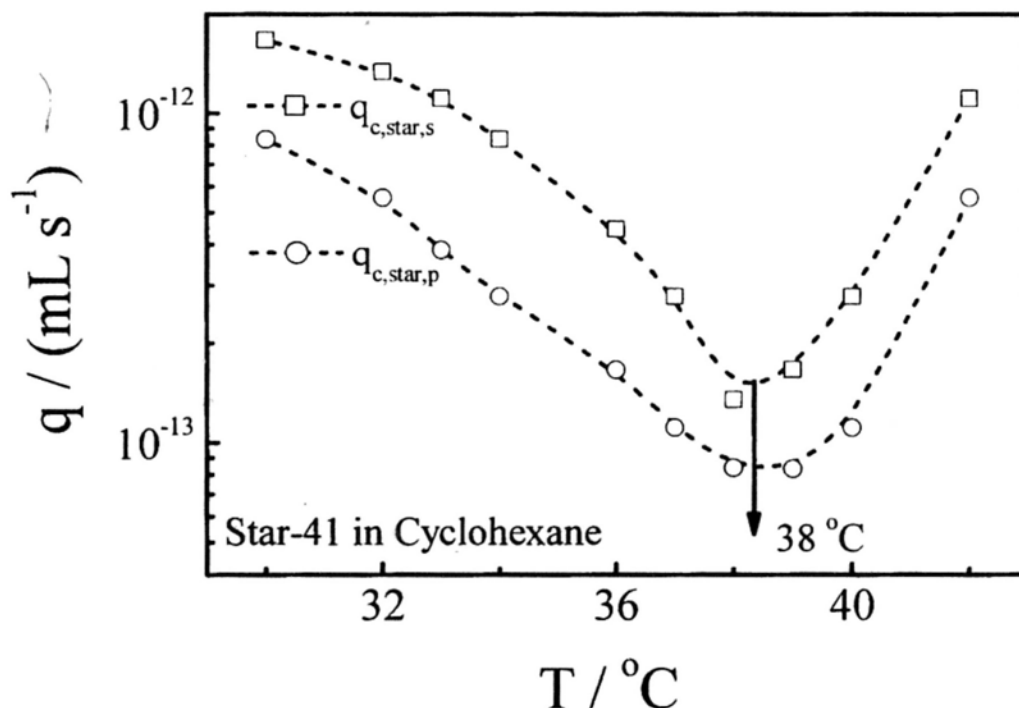

Figure 6.7 Solution temperature dependence of $q_{c,star,s}$ and $q_{c,star,,p}$ of star chains with 41 arms in cyclohexane.

Figure 6.7 shows the temperature dependence of $q_{c,star,s}$ and $q_{c,star,p}$ of Star-41 in cyclohexane at different flow rates. In spite that there is no much change in both $<R_g>$ and $<R_h>$, $q_{c,star}$ varies a lot in the same temperature range because the collapse of a star chain at lower temperatures is hindered by the excluded volumes of different arms but the hydrodynamic force experienced inside the nanopore is related to the properties of individual arms, similar to that of linear chains free in solution. For Star-41, the minimum of q_c is located at ~38 °C, few degrees higher than that of linear polystyrene chains.[17] Such a difference has been previously reported for star

103

and branched chains, especially when the arm number is high and the arm or branch is long,[18-20] presumably because the star and branching configurations increase the distance between segments so that the inter-segment attraction becomes stronger.

6.4 Conclusion

The ultrafiltration of star chains with different arm numbers and lengths reveals that the critical (minimum) flow rate ($q_{c,star}$), at which the chains start to pass a nanopore, is independent on the arm length but strongly influenced by the numbers of total arms and forwarded arms that initially enter the nanopore (f and f_{in}), contrary to a previous prediction made by de Gennes and Brochard-Wyart in 90s in which there exists an optimum number of f_{in} between 1 and $f/2$. Our revision of their theory shows that such a discrepancy is attributed to their assumption that each forwarded arm inside the nanopore is fully stretched by the flow when $f_{in} < f - f_{out}$. In our revised formulation, the passing of a star chain through a nanopore depends on whether $f_{in} \leq f/2$ or $f_{in} \geq f/2$. In the case of $f_{in} \geq f/2$, $q_{c,star}$ linearly increases with f_{in}, fairly slow; but when $f_{in} \leq f/2$, $q_{c,star} \sim (f - f_{in})^3 / f_{in}^2$, dramatically drops as f_{in} increases, especially when f is high. The minimum of $q_{c,star}$ is exactly located at $f_{in} = f/2$, independent on the arm number and length. Our experimental results confirm that most of star chains indeed pass through the nanopore with f_{in} around $f/2$, especially when f is high, not involving the fully stretched forward arms. Further, our study of star chains with 41 arms in cyclohexane at different temperatures reveals that there is a minimum $q_{c,star}$ located at ~38 °C, slightly higher than the theta temperature, which demonstrates that as in the case of linear chains, the ultrafiltration of star chains in a dilute solution through a nanopore provides a better and convenient way to determine the theta temperature. This study has laid a foundation for further applications of using the ultrafiltration to separate and characterize star chains with different arm numbers. Our results also have some implications in the design of non-viral polymeric carriers with different architectures for transporting drugs or genes into or through some organs, such as kidney and liver.

6.5 References and Notes

[1] De Gennes, P. G. *J. Chem. Phys.* **1974**, 60, 5030.

[2] Pincus, P. *Macromolecules* **1976**, 9, 386.

[3] Ge, H.; Jin, F.; Li, J. F.; Wu, C. *Macromolecules* **2009**, 42, 4400.

[4] Teraoka, I. Eds. *Polymer Solutions: An Introduction to Physical Properties* John Wiley & Sons, InC.; New York, **2002**.

[5] Daoud, M.; Cotton, J. P. *J. Physique* **1982**, 43, 531.

[6] Brochard-Wyart, F.; De Gennes, P. G. *C. R. Acad. Sci. ser II.* **1996**, 323, 473.

[7] De Gennes, P. G. *Adv. Polym. Sci.* **1999**, *138*, 91.

[8] Meunier, D. M.; Smith, P. B. *Macromolecules* **2005**, 38, 5313.

[9] Hadjichristidis, N.; Pitsikalis, M.; Pispas, S.; Iatrou, H. *Chem. Rev.* **2001**, 101, 3747.

[10] Lee, H. J.; Lee, K.; Choi, N. *J. Polym. Sci., Part A: Polym. Chem.* **2005**, 43, 870.

[11] Hadjichristidis, N.; Iatrou, H.; Pispas, S.; Pitsikalis, M. *J. Polym. Sci. Part A: Polym. Chem.* **2000**, 38, 3211.

[12] Zhou, S. Q.; Fan, S. Y.; Au-yeung, S. T. F.; Wu, C. *Polymer* **1995**, 36, 1341.

[13] Chu, B. *Laser Light Scattering*: 2nd ed.; Vol. Academic Press: New York, **1991**.

[14] Berne, B. J.; Pecora, R. *Dynamic Light Scattering*: Vol. Plenum Press: New York, **1976**.

[15] Jin, F.; Wu, C, *Phys. Rev. Letts.* **2006**, 96, 237801.

[16] Appelt, B.; Meyerhoff, G. *Macromolecules* **1980**, 13, 657

[17] Chu, B.; Ying, Q.; Grosberg, A. Y. *Macromolecules* **1995**, *28*, 180.

[18] Papanagopoulos, D.; Dondos, A. *Eur. Polym. J.* **2004**, 40, 2305.

[19] Ganazzoli, F.; Allegra, G. *Macromolecules* **1990**, 23, 262.

[20] Dondos, A.; Papanagopoulos, D. *Polymer* **1997**, 38, 6255.